

# Materials Advances



Accepted Manuscript

This article can be cited before page numbers have been issued, to do this please use: D. Muringaniza, L. Zulu, L. G. Marazani, P. Tshuma and G. Mehlana, *Mater. Adv.*, 2025, DOI: 10.1039/D5MA01105A.



This is an Accepted Manuscript, which has been through the Royal Society of Chemistry peer review process and has been accepted for publication.

Accepted Manuscripts are published online shortly after acceptance, before technical editing, formatting and proof reading. Using this free service, authors can make their results available to the community, in citable form, before we publish the edited article. We will replace this Accepted Manuscript with the edited and formatted Advance Article as soon as it is available.

You can find more information about Accepted Manuscripts in the <u>Information for Authors</u>.

Please note that technical editing may introduce minor changes to the text and/or graphics, which may alter content. The journal's standard <u>Terms & Conditions</u> and the <u>Ethical guidelines</u> still apply. In no event shall the Royal Society of Chemistry be held responsible for any errors or omissions in this Accepted Manuscript or any consequences arising from the use of any information it contains.



Recent Progress in Synthesis and Applications of Monolith Toda Andrica Online Applications of Monolith Toda Advanced Continuous Cont

**Metal-Organic Frameworks** 

Donald Muringaniza, Laurencia Zulu, Linia Gedi Marazani, Piwai Tshuma and Gift Mehlana.\*

Department of Chemical Sciences, Faculty of Science and Technology, Midlands State

University, P Bag 9055 Senga Road Gweru, Zimbabwe.

Email: mehlanag@staff.msu.ac.zw

**ABSTRACT** 

Monolithic MOFs have so far exhibited significant advantages in various industrial applications such as catalysis, sensing, separation, and gas storage. Compared to their powder counterparts, they have been exceptional in terms of mechanical strength, stability, and improved handling. This addresses the critical challenges with powder MOFs in real-world industrial applications. Despite the notable developments in the synthesis of monolith MOFs, challenges related to their functional optimization and large-scale production are still being encountered. This review presents the synthetic methodologies that have been used to prepare monolithic MOFs. Characterisation techniques are also presented with the hardness test being used to distinguish between a monolith and a powdered MOF. Owing to their tunable structures, flexibility, and unique physicochemical properties, monolithic MOFs are increasingly being adopted in diverse industrial sectors, including catalysis, environmental remediation, energy storage, and sensing. Their ongoing development is poised to play a

pivotal role in advancing sustainable and high-performance technologies.

INTRODUCTION

Open Access Article. Published on 08 listopadu 2025. Downloaded on 13.11.2025 7:46:18.

This article is licensed under a Creative Commons Attribution 3.0 Unported Licence.

The field of metal organic frameworks (MOFs) is a rapidly evolving area of materials science of materials activities of metal in the structures, comprised of metal ions or clusters coupled by organic ligands, have received significant scientific attention due to their outstanding architectural diversity and exceptional functional qualities. MOFs possess several remarkable characteristics: precisely engineerable porous networks, high catalytic activity, and remarkable structural stability. The porous networks can be tailored at the molecular level, enabling control over material properties, while the catalytic activity and stability make them promising for applications under challenging conditions. MOFs have emerged as attractive candidates for advanced technologies such as targeted drug delivery systems, gas storage, sensing and selective molecular separation because of their modular nature which facilitates systematic design and modification. The potential of MOFs to address diverse scientific and industrial challenges becomes inherently important as analytical and synthetic technologies continue to advance, thereby placing MOFs at the forefront of contemporary material research and technological innovation. At 14,15

However, the physical and chemical characteristics of MOF powders pose significant practical challenges, with the main issue being pronounced handling difficulties.<sup>16</sup> Applications like catalysis, gas separation, and energy storage require materials that possess controllable mechanical strength, uniform particle size, consistent geometry, and predictable microscopic morphology. MOF powders often lack these fundamental properties, thereby restricting their industrial applications.<sup>17, 18</sup> Additionally, MOF powders are prone to aggregation, are fragile, and present challenges in accurate dosing and maintaining consistency during operations. <sup>19</sup>

These multifaceted limitations necessitate pre-processing techniques, such as pelletization, immobilization on support matrices, or advanced morphological engineering, to transform

these promising materials from laboratory curiosities into viable technological, solutions dicte online capable of meeting stringent industrial performance criteria. <sup>20</sup> It is within this context that the development of monolithic MOF materials has emerged as a powerful solution to address the challenges inherent to their powdered counterparts. <sup>21, 22</sup>

Monolithic MOFs are defined as macroscopically continuous, self-supporting solid materials composed of a MOF or its composite, which possess structural integrity and can be handled without the need for an additional binder or support matrix. They are hierarchically structured materials that integrate a continuous porous network across multiple length scales, from micro-(<2 nm) and meso- (2-50 nm) to macropores (>50 nm). <sup>23</sup> This nature gives them rigidity, stability, and a high density, and their porosity can be engineered for a wide range of applications. <sup>24</sup>

The transition from loose powders to monolithic architectures resolves several critical limitations: Their cohesive, solid form makes them easy to manipulate and integrate into devices, and they can be readily recovered for reuse. <sup>25–27</sup> A key advantage is their engineered hierarchical pore system, <sup>24</sup> which preserves the essential microporosity of the parent MOF (ensuring high surface area and selectivity) while incorporating meso- and macropores that drastically enhance mass transfer, <sup>28</sup> leading to excellent permeability and powerful separation capabilities suitable for applications like chromatographic columns.<sup>29</sup> Furthermore, monoliths exhibit significantly superior mechanical properties (e.g., enhanced hardness and Young's modulus), providing critical resistance to attrition. <sup>30</sup> Finally, by eliminating interparticle voids, monolithic MOFs achieve a much higher bulk density, which often translates to superior volumetric performance (e.g., gas storage per volume), <sup>31,32,33</sup> a key metric for practical applications where space is a constraint.

The rapid evolution of monolithic MOFs is marked by key developments in synthetic, strategies and conceptual advances. **Figure 1** outlines this progress timeline, highlighting pioneering works that have demonstrated the potential of monolithic MOFs in creating hierarchically porous, mechanically robust, and application-ready structures. The field has progressed from early shaping methods to advanced manufacturing techniques like 3D printing and sophisticated templating approaches, leading to increasingly complex and high-performance monolithic structures for multifunctional applications.

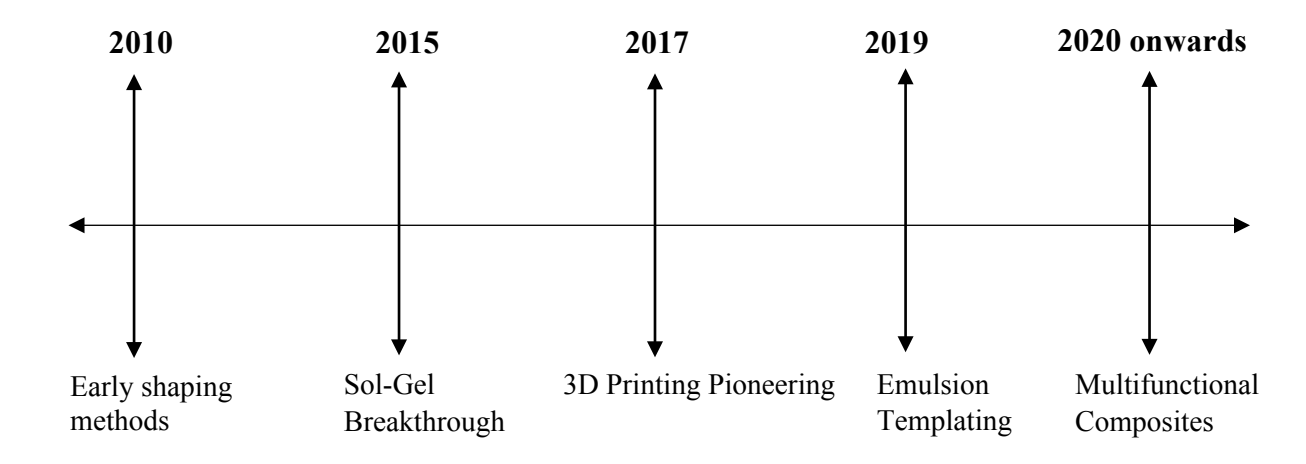


Figure 1: Timeline of key developments in the synthesis and application of monolithic MOFs

This review focuses on these advancements in monolithic MOFs, highlighting their importance due to enhanced structural stability and handling compared to powdered MOFs. Key synthetic methods, particularly sol-gel processes and 3D printing, are discussed for their ability to create materials with customized geometries and functionalities. We further examine the characterisation techniques and industrial applications of monolithic MOFs in gas storage, catalytic processes, water treatment, sensing, and drug delivery. Moving beyond pure monolithic MOF systems, the review also explores the design and utility of multifunctional composites. Finally, the review presents current trends, ongoing challenges, and future directions in the field, with a specific emphasis on emerging applications and their potential to meet complex technological needs across various sectors.

Open Access Article. Published on 08 listopadu 2025. Downloaded on 13.11.2025 7:46:18.

View Article Online DOI: 10.1039/D5MA01105A

#### MONOLITHIC MOF SYNTHESIS METHODS

## **Sol-Gel Synthesis**

Sol-gel synthesis is a versatile and widely used method for creating monolithic materials with defined shapes and porous, continuous structures. The process involves the transition from a liquid colloidal suspension (sol) into a solid, interconnected network (gel). This is typically initiated by distributing metal-organic framework (MOF) precursors in a solvent to form a stable sol system. <sup>34,35</sup>A key indicator of the gelation process is a sharp increase in the solution's viscosity.

The formation of the monolith is governed by several critical stages: supersaturation, nucleation, growth, and Ostwald ripening. These stages collectively determine the final material's size, morphology, and properties. Supersaturation often occurs as precursors undergo hydrolysis and condensation reactions, forming small clusters. These clusters then develop into stable nuclei through homogeneous (throughout the solution) or heterogeneous (on surfaces) nucleation. Subsequent growth occurs as more material deposits onto these nuclei. Finally, during Ostwald ripening, larger, more stable particles grow at the expense of smaller ones, further densifying the structure. <sup>30,36,37</sup>As shown in **Figure 2**, the high concentration reaction (HCR) method utilizes a base, triethylamine (NEt<sub>3</sub>), to deprotonate the organic linker. This accelerates the formation of metal-organic clusters, creating a high density of nucleation sites. The resulting nanoparticles are sufficiently small to form a gel. Upon drying at room temperature, this gel network solidifies into a monolithic structure. <sup>38</sup>

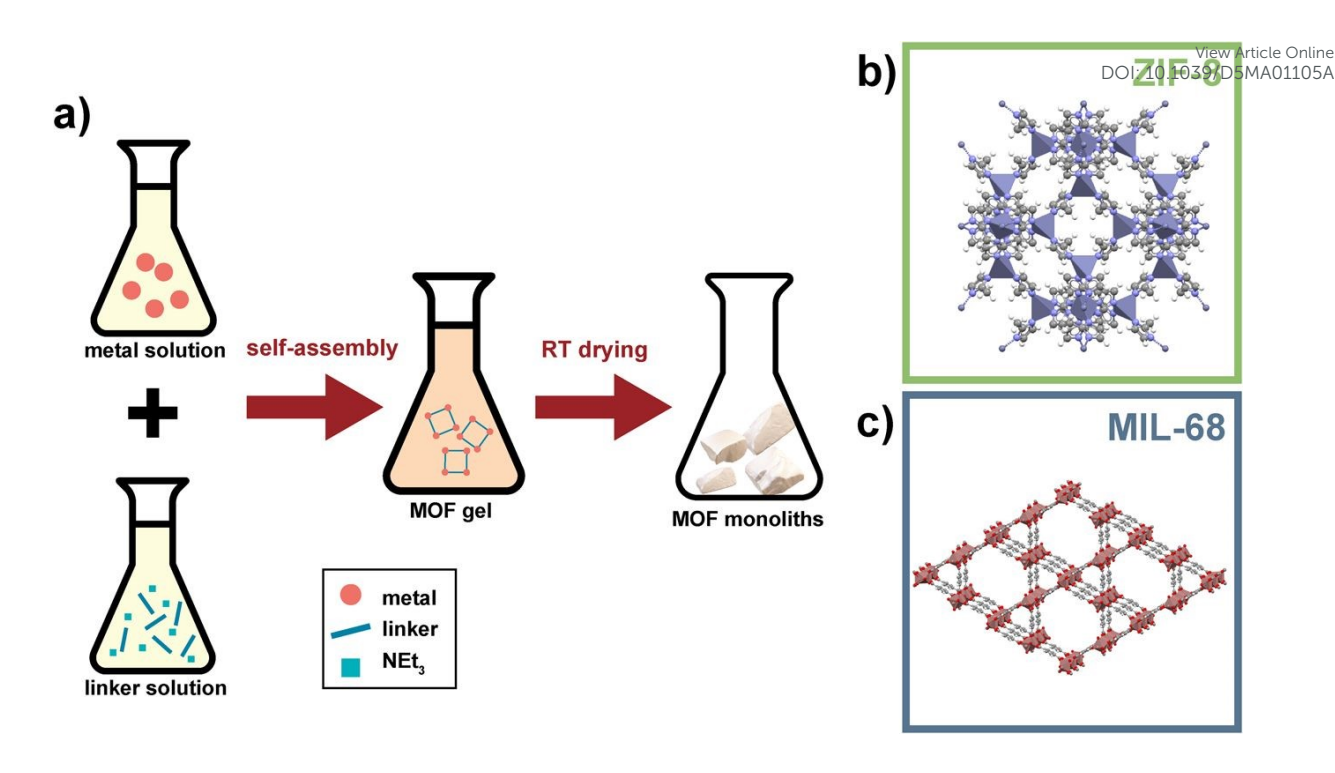


**Figure 2:** An illustration of the Sol-gel synthesis of ZIF-8 and MIL-68 monolith MOF. <sup>38</sup> Note that in some instances after self-assembly centrifugation is applied prior to drying. Reproduced from reference **38**, with permission from the Royal Society of Chemistry.

This is also demonstrated in the work of Tian *et al.*, <sup>30</sup> who synthesized monolithic HKUST-1 (monoHKUST-1) via a sol-gel process. Their work exemplifies how precise control over nucleation and growth conditions yields a densely packed, robust monolith. The synthesis began with the formation of approximately 51 nm primary nanoparticles. A subsequent mild drying process at room temperature promoted epitaxial growth at the particle interfaces, effectively using the MOF itself as a binder to create a continuous monolith without external additives or high-pressure compaction. In contrast, rapid drying at elevated temperatures resulted in a powdered material with interparticle voids and lower density.

The advantages of this approach are multifaceted. For instance, the achieved bulk density of monoHKUST-1 (1.06 g cm<sup>-3</sup>) significantly exceeded that of hand-packed powder and even the theoretical crystal density. This high density directly contributed to superior mechanical

properties, with a hardness of 460 MPa and a Young's modulus of 9.3 GPa. Concurrently and the continuous material exhibited a exceptional volumetric methane storage capacity of 259 cm³ (STP) cm⁻³ at 65 bar and 298 K, nearly meeting the U.S. DOE target, without sacrificing adsorption kinetics.

In their study, He *et al*.³9 developed a sophisticated synthesis route to create monolithic MOF-801, representing a significant advancement of the sol-gel method that combined sol-gel phase separation with a subsequent acid-heat treatment as illustrated in **Figure 3**.

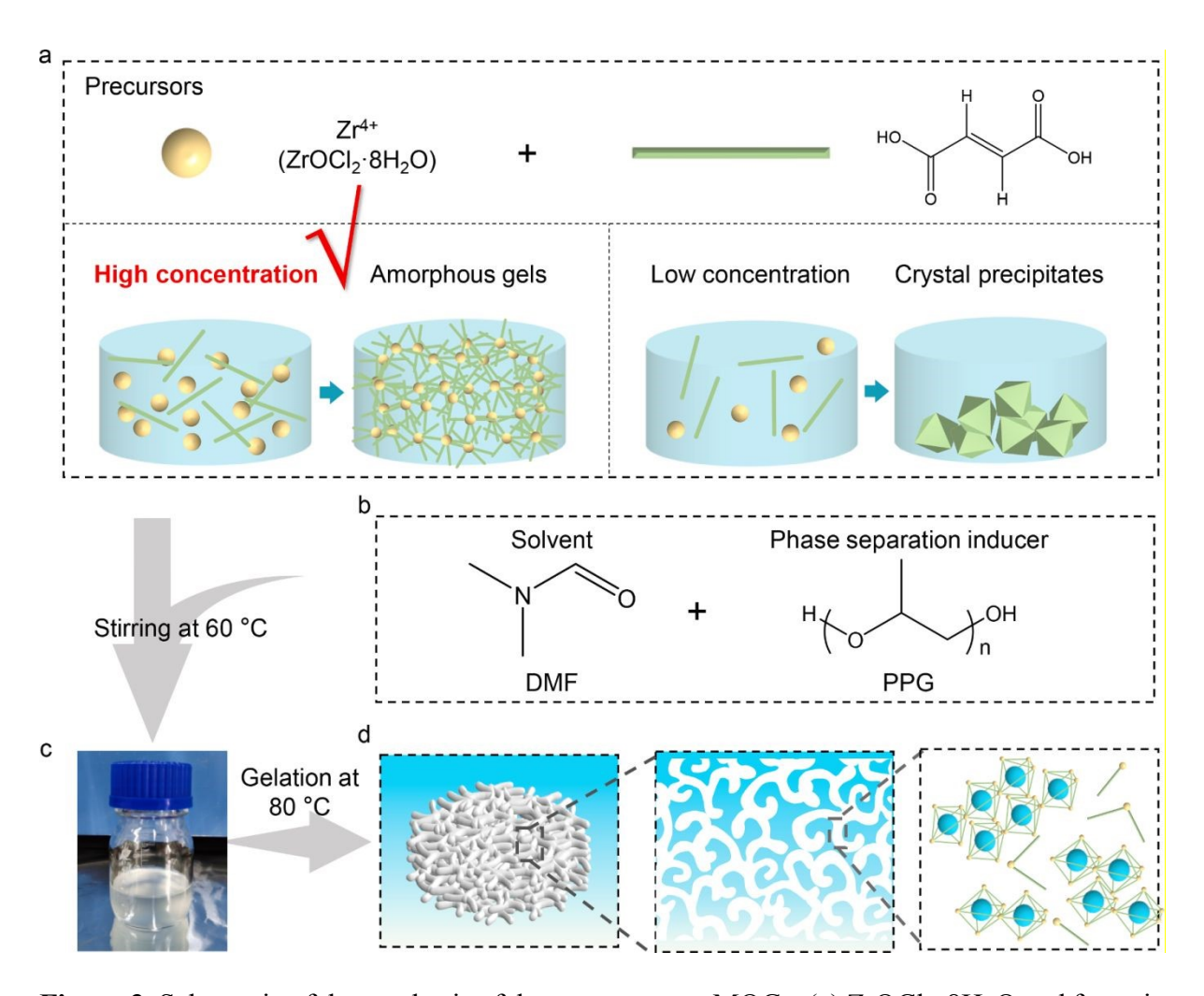


**Figure 3**: Schematic of the synthesis of the macroporous MOGs. (a) ZrOCl<sub>2</sub>·8H<sub>2</sub>O and fumaric acid precursors in DMF; (b) Introduction of PPG as a phase separation inducer; (c) Formation of a homogeneous emulsion after stirring at 60 °C; (d) Formation of macroporous MOGs after gelation at 80 °C accompanied by phase separation.<sup>39</sup> Reproduced from reference **39**. Copyright (2023) Elsevier B. V.

The process began by dissolving zirconyl chloride and fumaric acid in DMF before adding poly(propylene glycol) (PPG) as a phase separation inducer. This mixture was stirred at 60 °C to form a homogeneous emulsion, which was then transferred to a mold and heated at 80 °C for gelation and aging. During this step, phase separation occurred, where the DMF phase formed continuous MOF skeletons and the PPG phase created continuous macroporous channels, which were later washed away. A critical acid-heat post-treatment using formic acid was then employed to enhance the crystallinity and micropore volume. This innovative method yielded a robust, centimetre-scale monolith with a hierarchically porous structure, exhibiting a high porosity of 59.7%, a superior specific surface area of 977.8 m<sup>2</sup> g<sup>-1</sup>, and a micropore volume of 0.234 cm<sup>3</sup> g<sup>-1</sup>. Crucially, the monolith also possessed excellent mechanical strength, with a compressive Young's modulus of up to 61.3 MPa, enabling its practical use in scaled-up applications.

This article is licensed under a Creative Commons Attribution 3.0 Unported Licence.

Open Access Article. Published on 08 listopadu 2025. Downloaded on 13.11.2025 7:46:18.

Beyond this example, the sol-gel process offers remarkable simplicity and cost-effectiveness while delivering products of high purity and versatility. <sup>40, 41</sup> It allows for the creation of various product forms, including fibres and aerogels, and is particularly suited for producing materials with enhanced physical properties. The solution-phase nature of the process provides detailed control over the material's structure through adjustable variables during the early stages of its formation and network development. <sup>42</sup> However, challenges remain, including scalability, the risk of cracking during drying if not properly handled, and potential diffusion limitations due to the dense monolithic structure. **Table 1** provides a summary of selected monolithic MOFs monoliths via sol-gel synthesis, along with their applications, advantages, and disadvantages.

**Table 1:** Summary of selected monolith MOF prepared using the sol-gel, including their View Article Online application, advantages and disadvantages.

Monolith MOF Examples	Application	Advantages	Disadvantages
ZIF-8 and ZIF-67	Toluene vapour adsorption <sup>43</sup>	- Simple, ambient temperature synthesis -High surface area (e.g., 1450-1732 m²/g for ZIF-8) and hierarchical porosity <sup>43, 44, 45</sup> - Narrow particle size distribution (e.g., 55 nm). <sup>44</sup> -High vapour capacity <sup>45</sup>	-Can Require longer aging time (e.g., 96-120 hrs) 44 - Potential pore blockage.
HKUST-1	-Hydrogen storage. <sup>31</sup> Methane uptake <sup>32</sup>	-Enhanced mechanical stability (Hardness: of 460 MPa, Young Modulus: 3 GPa). <sup>32</sup> -High volumetric storage capacities <sup>31, 32</sup> (e.g., 259 cm <sup>3</sup> (STP) cm <sup>-3</sup> for CH <sub>4</sub> at 65 bar; 10.1g L <sup>-1</sup> for H <sub>2</sub> at 100 bar.) -Improved handling.	-Scale up challenges Susceptible to cracking during drying if not properly handled.
MIL-101	CO <sub>2</sub> adsorption, methylene dye removal from water	- Easier handling and integration into systems - High thermal stability (stable up to 300 °C) -Reduces pressure drop in fixed-bed reactors, facilitating scale up.	-Requires multi step solvothermal synthesis with tight control of solvent composition and temperature, icreasing process costLimited adaptability for post-synthetic functionalisation due to rigid chromium terephthalate frameworkSusceptible to cracking during drying or activation because of capillary stress in the dense monolithic matrixDense framework may impede desorption kinetics, making regeneration slower and less energy-efficient after multiple adsorption cycles.
UiO-66 <sup>33</sup>	Gas storage <sup>33</sup>	-Cohesive solid form simplifies packaging and reactor loading.	-Scaling up limited by the need for uniform gelation and solvent exchange, which can cause structural

		- High bulk density with preserved porosity and surface area (BET ~1000-1200 m <sup>2</sup> g <sup>-1</sup> )	inhomogeneity in larger View Art cle O batchesSynthesis requires careful control of washing solvents and drying conditions to avoid framework collapse and residual solvent contamination Susceptible to cracking during solvent removal due to capillary stress in dense monolithic matrices.
MOF 801	Atmospheric water harvesting. <sup>39</sup>	<ul> <li>Robust hierarchical porosity (BET: 977.8 m²g⁻¹, micropore volume: 0.234 cm³g⁻¹)</li> <li>High water uptake from air under low humidity (≥ 0.2 g·g⁻¹ at 30% RH)</li> <li>Fabrication of centimetre scale monolith demonstrated.</li> <li>High structural stability under cycling</li> <li>Suitable for passive water harvesting applications.</li> </ul>	- Synthesis requires multistep sol-gel and phase-separation control with post-synthetic acid treatment to enhance crystallinity, increasing process complexity.  - Relatively higher material cost due to use of zirconium precursors (e.g., ZrOCl <sub>2</sub> ·8H <sub>2</sub> 0) and formic acid treatment reagents.  - Performance consistency depends on optimising solvent ratio, gelation temperature (68-80 °C), and aging time to achieve uniform pore structure.

# **3D Printing**

3D printing enables control over structure, geometry, and porosity, making it a valuable technique for creating tailored MOF materials.<sup>47</sup> The process allows for the fabrication of complex structures without expensive retooling and with less waste than traditional methods.

48 3D-printed monoliths are usually created by synthesizing MOF particles or utilizing commercial MOF powders, which are then mixed into a paste that includes a binder, co-binder, solvents, and plasticizer. A general schematic of the 3D printing technique for deriving carboxylate MOFS is shown in **Figure 4**, which outlines the key steps from ink formulation

This article is licensed under a Creative Commons Attribution 3.0 Unported Licence

Open Access Article. Published on 08 listopadu 2025. Downloaded on 13.11.2025 7:46:18.

and printing to the necessary post-processing treatments required to achieve a function and printing to the necessary post-processing treatments required to achieve a function and printing to the necessary post-processing treatments required to achieve a function and printing to the necessary post-processing treatments required to achieve a function and printing to the necessary post-processing treatments required to achieve a function and printing to the necessary post-processing treatments required to achieve a function and printing to the necessary post-processing treatments required to achieve a function and printing to the necessary post-processing treatments required to achieve a function and printing to the necessary post-processing treatments required to achieve a function and printing the necessary post-processing treatments are not achieve a function and printing treatments are not achieve a function and printing treatments are not achieve and achieve a function achieve a function achieve and achieve a function achieve a function achieve and achieve a function achieve a function achieve and achieve a function achieve achieve and achieve achieve achieve and achieve achie

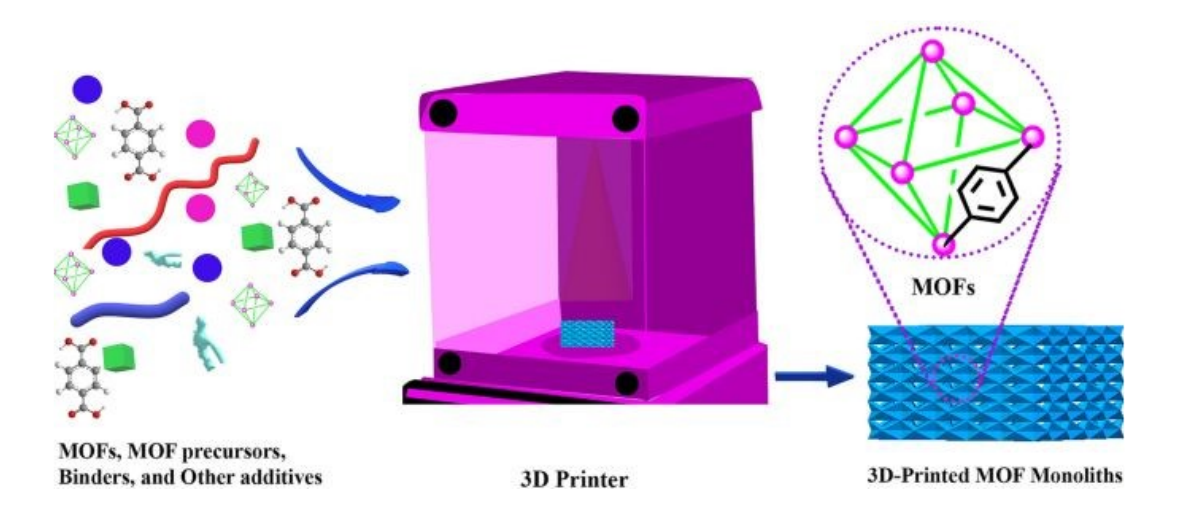


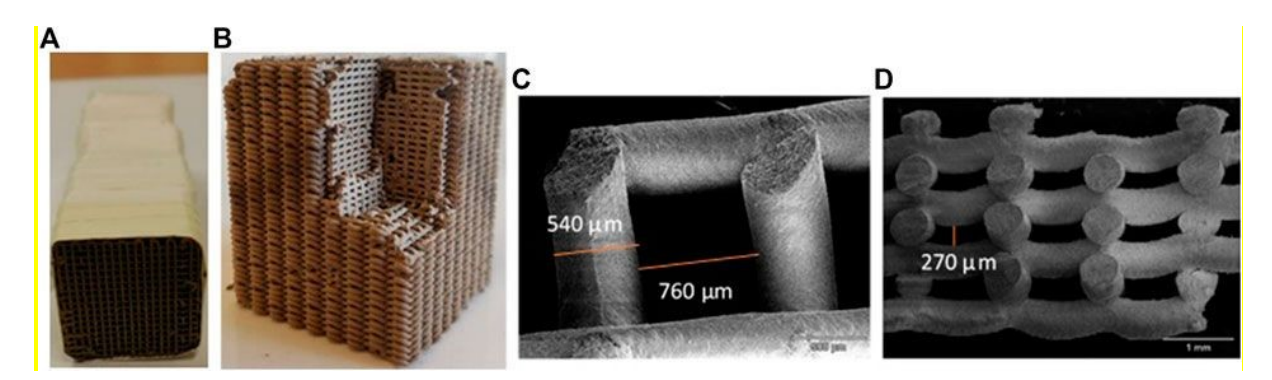
**Figure 4:** 3D printing pathway of carboxylate derived MOFs.<sup>49</sup> Reproduced from reference 49, with permission from Springer.

The following sections will explore the primary strategies employed in 3D printing MOF monoliths, including Direct Ink Writing (DIW), seed-assisted *in situ* growth, matrix incorporation, selective laser sintering (SLS), digital light processing (DLP), and template-assisted methods.

## **Direct Ink Writing**

Direct Ink Writing (DIW), a form of 3D printing, is a technique that offers high precision and versatility. It is a simple, flexible and cheap technique whereby a paste or ink is ejected layer-by-layer through a fine nozzle. <sup>50</sup> A critical requirement of the process in that the active material must be made into an ink with ideal viscosity and must also be able to flow through a nozzle continuously and then solidify quickly to preserve its shape. <sup>48</sup> Once formulated, the prepared ink is typically rolled at room temperature for 1 to 2 days during the binding process to ensure proper interaction between the various components and achieve the desired results. During the densification step, the prepared ink is slowly heated to a temperature range of 40-

The feasibility of fabricating ZIF-8 monoliths via DIW was demonstrated by Verougstraete *et al.*<sup>53</sup> providing a clear example of the 3D printing fibre deposition method, as shown in **Figure 5**. ZIF-8 powder (66.7 wt%), bentonite (16.7 wt%) and methylcellulose (16.7 wt%) were mixed with water to form a printable paste. This was followed by activation under Argon at 450 °C, to remove the methylcellulose binder, yielding a final composition of 80 wt% ZIF-8 and 20 wt% bentonite.



This article is licensed under a Creative Commons Attribution 3.0 Unported Licence

Open Access Article. Published on 08 listopadu 2025. Downloaded on 13.11.2025 7:46:18.

**Figure 5**: 3D printed ZIF-8 monolith. A) Monolith used for breakthrough experiments. Several pieces were stacked and held together with Teflon tape. (B) Side view showing the presence of channels in the radial direction. (C) Scanning electron microscopy-picture of the top-view of the monolith. (D) Scanning electron microscopy-picture of side view visualizing the radial gaps present in the structure.<sup>53</sup> Reproduced with permission from reference **53**, under the terms of the Creative Commons Attribution License (CC BY).

Building upon this foundational work, Claessens *et al.* <sup>54</sup> subsequently employed a similar DIW approach to fabricate ZIF-8 monoliths for biobutanol recovery. Their study provided a detailed analysis of how printing parameters dictate monolith architecture and, consequently, separation efficiency. Using a paste of ZIF-8, bentonite, and methylcellulose, they produced monoliths with 600 µm and 250 µm nozzles. After thermal treatment, the monoliths exhibited a dark-brown colour due to binder degradation. As shown in **Figure 6**, SEM analysis revealed the 600

μm monolith had a fibre thickness of 540 μm and open side channels (260 μm), while the fictorial management (<60 μm). This structural difference, clearly visible in the figure, caused flow maldistribution in the smaller monolith, leading to broader breakthrough profiles, whereas the larger monolith demonstrated superior performance with high butanol capacity (0.2 g/g) and selectivity.

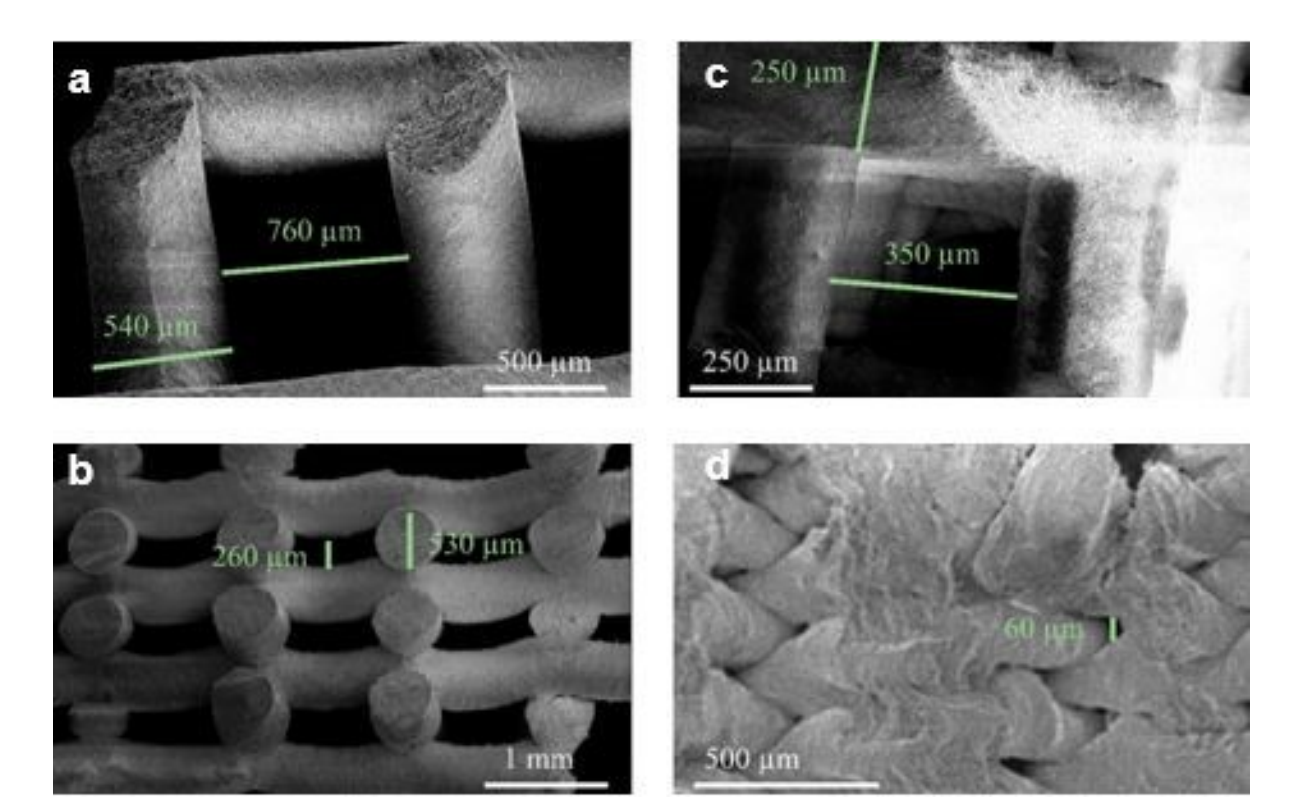


**Figure 6:** SEM images of 3D printed 600 μm monolith (a, b) and 250 μm monolith (c-d) <sup>54</sup> Reprinted with permission from reference **54**. Copyright (2020), American Chemical Society.

Beyond ZIF-8, the DIW technique has been successfully applied to other MOFs. For instance, Lim *et al.* <sup>48</sup> successfully fabricated a self-standing HKUST-1 monolith using the DIW strategy as illustrated in **Figure 7**. Their key innovation was formulating a printable colloidal gel from only HKUST-1 nanoparticles and ethanol, entirely omitting the need for a binder, which demonstrated excellent printability and rheological properties. The figure shows photos of the HKUST-1 gel and various 3D-printed structures, SEM images of the filament and

nanoparticles, and rheological data proving the ink's shear-thinning behaviour and solid madical continuous gel properties. Crucially, the process preserved the MOF's original pore volume, resulting in a monolith with a high specific surface area (1134 m<sup>2</sup> g<sup>-1</sup>) and significant methane uptake of 64 cm<sup>3</sup> (STP) cm<sup>-3</sup> at 65 bar.

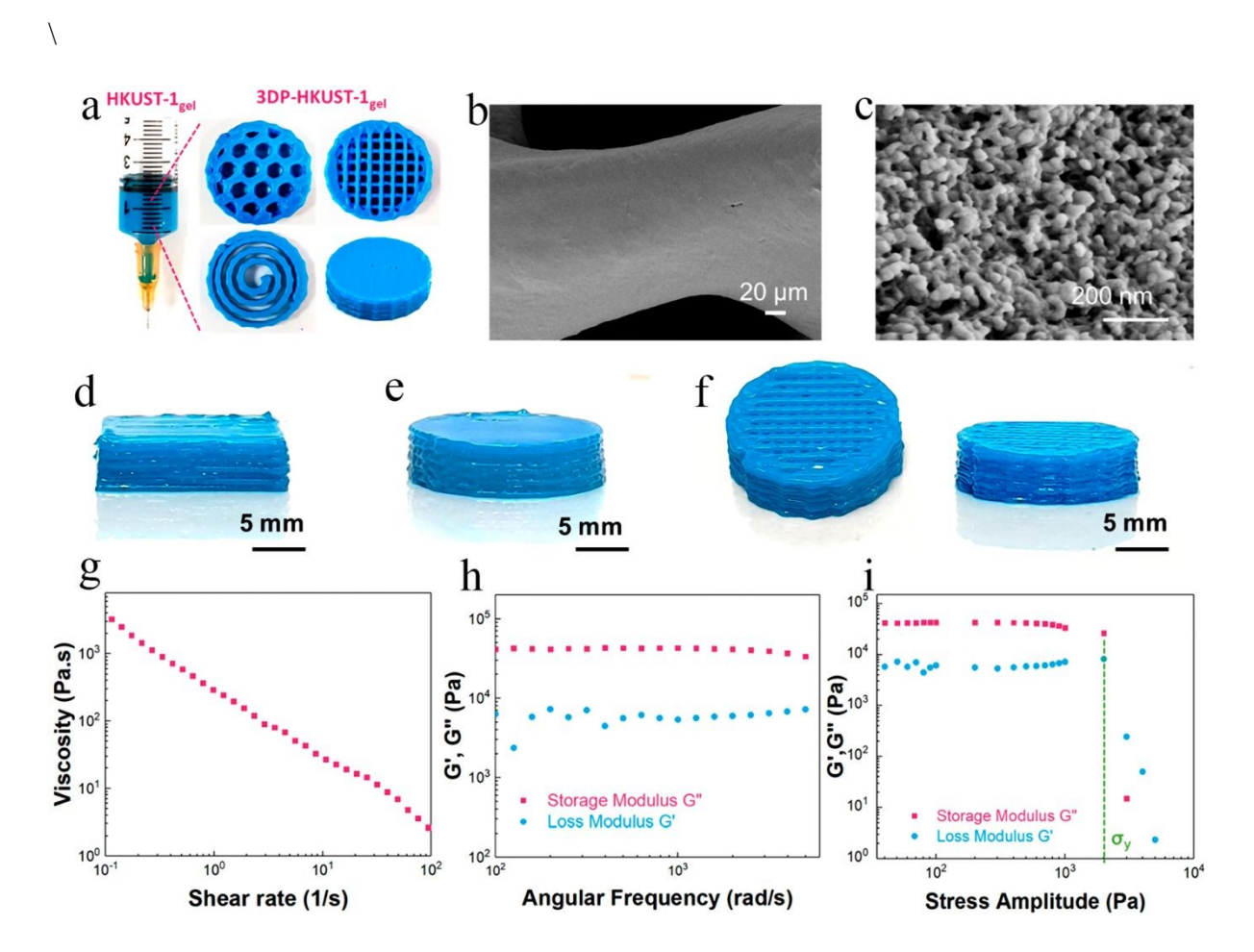


**Figure 7:** Characterization of the HKUST-1 gel and 3D-printed monoliths, including (a) photos of the gel and printed structures, (b-c) SEM images of a filament and its nanoparticles, (d-f) photos of monoliths with different geometries, and (g-i) rheological profiles of the ink. <sup>48</sup> Reprinted with permission from reference **48**. Copyright (2020), ResearchGate GmbH.

Bouzga *et al.*<sup>55</sup> developed 3D-printed UTSA-16 monoliths using a non-aqueous ink formulation. The ink, tailored with boehmite and hydroxypropyl cellulose as rheology modifiers, exhibited optimal printability and enhanced the dispersion of UTSA-16 nanoparticles within the monolithic structure. The study demonstrated that the resulting 3D-

printed monoliths function as efficient CO<sub>2</sub> adsorbents, exhibiting high uptake capacity and its printed monoliths function as efficient CO<sub>2</sub> adsorbents, exhibiting high uptake capacity and its printed monoliths function as efficient CO<sub>2</sub> adsorbents, exhibiting high uptake capacity and its printed monoliths function as efficient CO<sub>2</sub> adsorbents, exhibiting high uptake capacity and its printed monoliths function as efficient CO<sub>2</sub> adsorbents, exhibiting high uptake capacity and its printed monoliths function as efficient CO<sub>2</sub> adsorbents, exhibiting high uptake capacity and its printed monoliths function as efficient CO<sub>2</sub> adsorbents, exhibiting high uptake capacity and its printed monoliths function as efficient CO<sub>2</sub> adsorbents, exhibiting high uptake capacity and its printed monoliths function as efficient CO<sub>2</sub> adsorbents, exhibiting high uptake capacity and its printed monoliths function as efficient CO<sub>2</sub> adsorbents, exhibiting high uptake capacity and its printed monoliths function as efficient CO<sub>2</sub> adsorbents, exhibiting high uptake capacity and its printed monoliths function as efficient conditions. This stability was attributed to the hydroxypropyl cellulose component, which effectively shields the MOF centres from water molecules.

In a related study, Lawson *et al.* <sup>56</sup> developed 3D-printed monoliths from amine-functionalized MIL-101 for CO<sub>2</sub> capture in enclosed environments. They employed a DIW technique using two strategies: pre-impregnation (where the MIL-101 powder was first impregnated with polyethylenimine (PEI) or polyethylenimine (TEPA) and then printed) and post-impregnation (where the monolith was printed first and then functionalized). The study concluded that the pre-impregnation approach was superior, yielding higher amine loadings and CO<sub>2</sub> capacities (1.6 mmol/g for TEPA and 1.4 mmol/g for PEI at 3000 ppm) due to successful amine grafting within the pores during paste densification. However, despite their high capacity, the adsorption kinetics were slow, leading to the conclusion that future work must focus on tuning the monolith dimensions to optimize CO<sub>2</sub> diffusion.

Monolith MOFs synthesised via 3D technology have the following advantages: (1) Interconnected channels are formed which facilitates the transfer of heat and mass during operation conditions, (2) MOFs can be used in large-scale practical applications, (3) 3D printing enables the incorporation of different materials within a single structure, allowing for multifunctional applications, (4) Allows for the creation of complex and customized shapes that meet specific application requirements <sup>49</sup> and finally (5) the creation of complex structural networks while generating minimum waste.<sup>57</sup>

The main challenge with 3D-printed MOF monoliths is that they typically have lower specific surface areas and pore volumes than their powdered equivalents. This problem occurs due to several factors like, the need for high temperatures and pressure during the printing process

This article is licensed under a Creative Commons Attribution 3.0 Unported Licence

Open Access Article. Published on 08 listopadu 2025. Downloaded on 13.11.2025 7:46:18.

which makes the MOFs deform, the presence of additives in the paste can result in several in the paste can result in the paste can result in several in the paste can result in the p

## **Template-Assisted Synthesis of Monolithic MOFs**

The inherent microporosity of MOFs, while ideal for molecularly selective applications, imposes significant mass transfer limitations in processes requiring high flow rates or involving viscous media. To overcome this, template-assisted synthesis has emerged as a powerful strategy to engineer hierarchical pore systems within scalable, monolithic structures.<sup>34</sup> By using dynamic soft templates, this approach creates well-defined macropores that facilitate convective flow, which are seamlessly integrated with the intrinsic micro- and mesopores of the MOF to combine efficient mass transport with high surface area and selectivity. This versatile pathway enables the rational design of MOF monoliths with enhanced functionality for demanding applications in catalysis, adsorption, and separation.

A foundational approach to creating hierarchical MOFs is the bottom-up, direct templating of mesoporosity during crystal growth. Do *et al.* <sup>59</sup> pioneered this concept by using amphiphilic block copolymers as structure-directing agents to synthesize mesostructured MIL-53(AI), designated L-MOF. Instead of using a solid scaffold, they employed soft templates in the form of block copolymers (Pluronic P123 and F127). Under solvothermal conditions, these surfactants self-assemble into micelles. The MOF precursors (for MIL-53(AI)) then crystallize around these micellar templates. Subsequent removal of the polymer leaves behind a material whose walls are made of microporous MIL-53(AI) crystals. The successful creation of intrinsic mesoporosity was confirmed by N<sub>2</sub> physisorption (**Figure 8**). The Type IV isotherm with distinct hysteresis steps (**Figure 8A**) provided definitive evidence of mesopores, while the corresponding pore size distribution (**Figure 8B**) revealed a trimodal system comprising the native micropores alongside two mesopore networks: a wormhole-like system (~4 nm) and

larger channels (5.4–7.6 nm) templated by the block copolymers. This exemplifies the direction of a MOF with hierarchical porosity, ideal for catalysis involving bulky molecules.

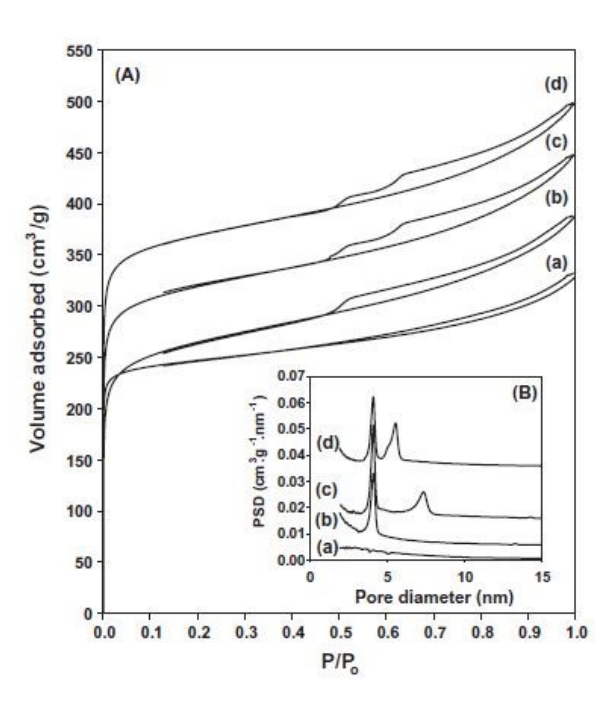


**Figure 8:** Pore structure analysis of mesostructured MOFs. Mesopore structures analysis of mesostructured MOFs: (A)  $N_2$  adsorption-desorption isotherms at 77 K for (a) MIL-53(Al), (b) L-MOF(0), (c) L-MOF(1), and (d) L-MOF(2); (B) Pore size distribution for (a) MIL-53(Al), (b) L-MOF(0), (c) L-MOF(1), and (d) L-MOF(2). <sup>59</sup>

While the approach by Do *et al.* <sup>59</sup> exemplifies the templating of internal porosity within a MOF crystal, the challenge of assembling MOFs into macroscopic, handleable objects still remains. To advance the concept of soft templating to a larger scale, Sun *et al.*<sup>20</sup> demonstrated how a dynamic emulsion template could be used not only to structure porosity but to shape an entire monolithic device. Their strategy utilized a Pickering high internal phase emulsion (HIPE), where ZIF-8 nanoparticles acted as the sole stabilizer for oil droplets dispersed in a water phase containing molecular MOF precursors. As illustrated in **Scheme 1**, the process begins with ZIF-8 nanoparticles stabilizing droplets of cyclohexane (the internal phase) within an aqueous solution containing ZIF-8 precursors. A key innovation was the subsequent in situ growth of additional ZIF-8 within the continuous phase, which acts as a natural "cement" to bond the nanoparticle stabilizers together without any foreign polymeric binder.

Toluene
Malononitrile
Benzaldehyde
Benzylidene malononitrile

ZIF-8 monoliths
Toluene, 25°C

Toluene, 25°C

**Scheme 1**: Knoevenagel Reaction of Benzaldehyde with Malononitrile in Toluene Using the 3D ZIF-8 Monolith as a Flowthrough Catalyst.<sup>20</sup> Reprinted with permission from reference **20** Copyright (2021), American Chemical Society.

After synthesis, the emulsion is freeze-dried to remove the liquid oil template, leaving behind a solid, monolithic structure. The resulting morphology, revealed in the SEM images of **Figure 9**, shows a highly interconnected macroporous network that is a direct inverse replica of the original emulsion droplets, while the walls consist of microporous ZIF-8. This unique structure endowed the monolith with exceptional performance in dual applications: it served as an extremely efficient flow-through catalyst, achieving complete conversion in a Knoevenagel reaction within 130 seconds, and as a rapid oil absorbent, reaching absorption equilibrium for hydrocarbons in less than 5 seconds due to its open, permeable architecture.

This article is licensed under a Creative Commons Attribution 3.0 Unported Licence

Open Access Article. Published on 08 listopadu 2025. Downloaded on 13.11.2025 7:46:18.

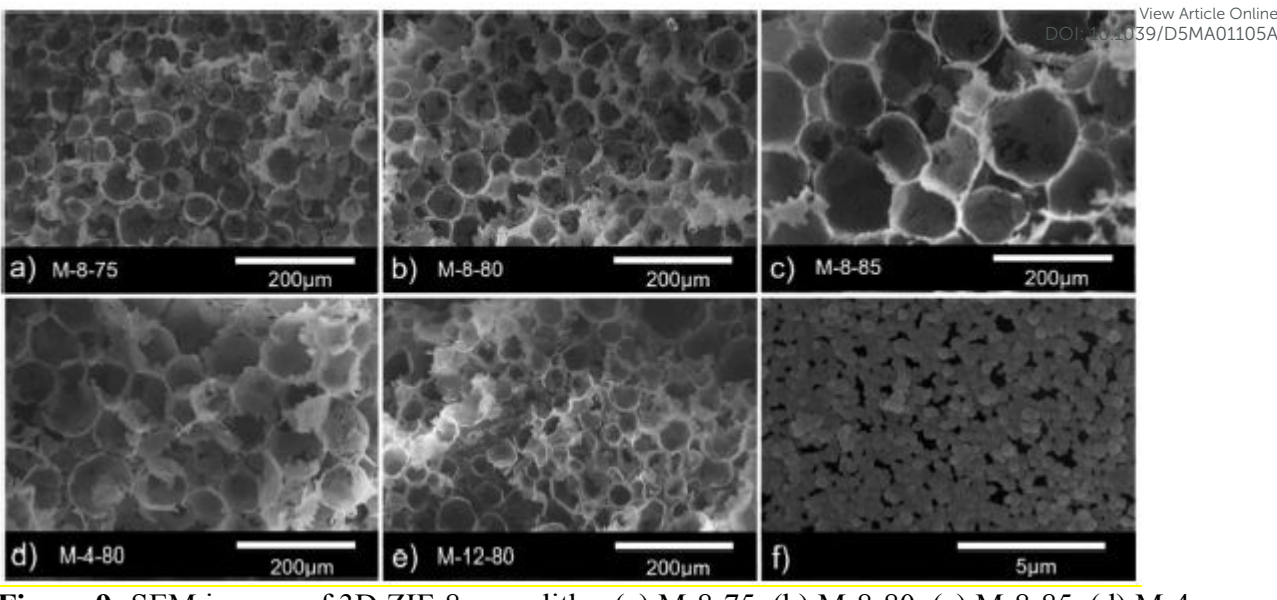


**Figure 9:** SEM images of 3D ZIF-8 monoliths: (a) M-8-75, (b) M-8-80, (c) M-8-85, (d) M-4-80, (e) M-12-80, and (f) surface of the void wall of M-8-80. <sup>20</sup> Reprinted with permission from reference **20** Copyright (2021), American Chemical Society.

The synergy between these two approaches illustrates the power and versatility of dynamic soft templating for structuring MOFs across multiple length scales. The work of Do *et al.*<sup>59</sup> illustrates an intrinsic strategy, templating mesopores within the MOF crystal to enhance molecular diffusion. To complement this work, Sun *et al.*<sup>20</sup> demonstrate an extrinsic assembly strategy, templating macropores between crystals to create a functional monolith. Both methods effectively decouple molecular selectivity from mass transport, providing valuable blueprints for designing hierarchical MOF architectures tailored to specific applications.

#### Seed assisted in-situ growth

The seed-assisted in situ growth strategy is analogous to the Direct Ink Writing (DIW) technique in its initial stage, as it also begins with the formulation of a printable ink containing solvents, inert binders, and plasticizers. However, a key distinction is that the structured monoliths produced do not require a large amount of the active MOF material to be functional. Instead, the 3D-printed substrate itself acts as a nucleation site, containing metal oxides or

MOF precursors that enable the coordination and growth of an active MOF layer after a printing Atticle Online densifying step. 49

This strategy has been effectively applied to the interfacial synthesis of MOF-74 onto 3D-printed monoliths, as demonstrated by Lawson *et al.*<sup>60</sup> The process began by printing MOF-74 nanoparticles into a dope of a Torlon polymer solution. Although the crystalline structure of these initial MOF particles was degraded during the subsequent solvent extraction process, they successfully served as growth seeds. When these monoliths were exposed to MOF precursors in a secondary solvothermal synthesis step, new MOF-74 crystals grew from the seeds, resulting in the fabrication of monoliths with a high MOF loading of 40 wt%.

As illustrated in **Figure 10**, this two-step approach, direct printing of seeds followed by secondary growth enables the formation of a dense, continuous MOF film on the polymer scaffold. This approach effectively created chemically active monoliths with significantly enhanced CO<sub>2</sub> adsorption capacity, increasing from 0.5 mmol/g for the directly printed monolith to 2.5 mmol/g after secondary growth and improved mass transfer kinetics due to the formation of a thin, continuous MOF film on the surface. However, it was noted to be relatively time-consuming and produced extra waste, making it less suitable for large-scale production.

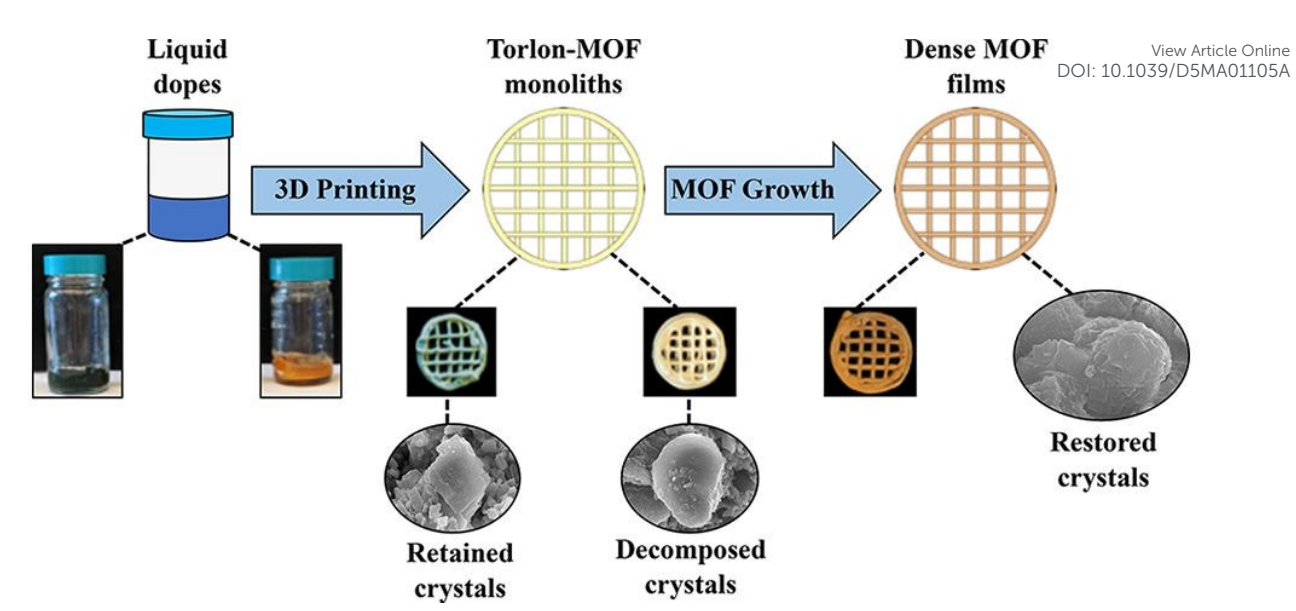


**Figure 10.** Schematic representation of the two-step strategy for fabricating polymer-MOF monoliths: (Step 1) Direct ink writing of a polymer dope containing MOF particles, which act as seeds, and (Step 2) Secondary growth via solvothermal synthesis to form a dense, continuous MOF film on the monolithic scaffold. <sup>60</sup> Reprinted with permission from Reference **60** Copyright (2019), American Chemical Society.

#### **Matrix** incorporation

The matrix incorporation strategy involves dispersing pre-synthesized, chemically active MOF particles as a filler within an inert polymeric stabilizer or binder. This method is primarily used to overcome the rheological limitations of pure MOF inks, enhance the mechanical properties of the final structure, and modulate its hierarchical porosity.

A foundational example of this approach is the work by Kreider *et al.*<sup>61</sup> They were among the first to employ this strategy to fabricate 3D-printed MOF monoliths by creating composites of acrylonitrile butadiene styrene (ABS) and MOF-5. The process involved the solvent casting of an ABS mixture containing 10 wt% MOF-5 particles to produce a liquid-phase dope with suitable printability. This ink was then used to print structures with various geometries as illustrated in **Figure 11**.

However, a significant limitation was identified, the MOF content could not exceed 10 wt% without the ink exhibiting shear-thickening behaviour, rendering it unprintable. Furthermore,

This article is licensed under a Creative Commons Attribution 3.0 Unported Licence

Open Access Article. Published on 08 listopadu 2025. Downloaded on 13.11.2025 7:46:18.

the high temperatures and pressures involved in the thermoplastic processing, combined with item of the presence of the polymer matrix, typically lead to a reduction in the specific surface area and accessible pore volume compared to the pure MOF powder. Despite this partial degradation, the study confirmed that the MOF-5 particles retained their functionality for applications like hydrogen storage.

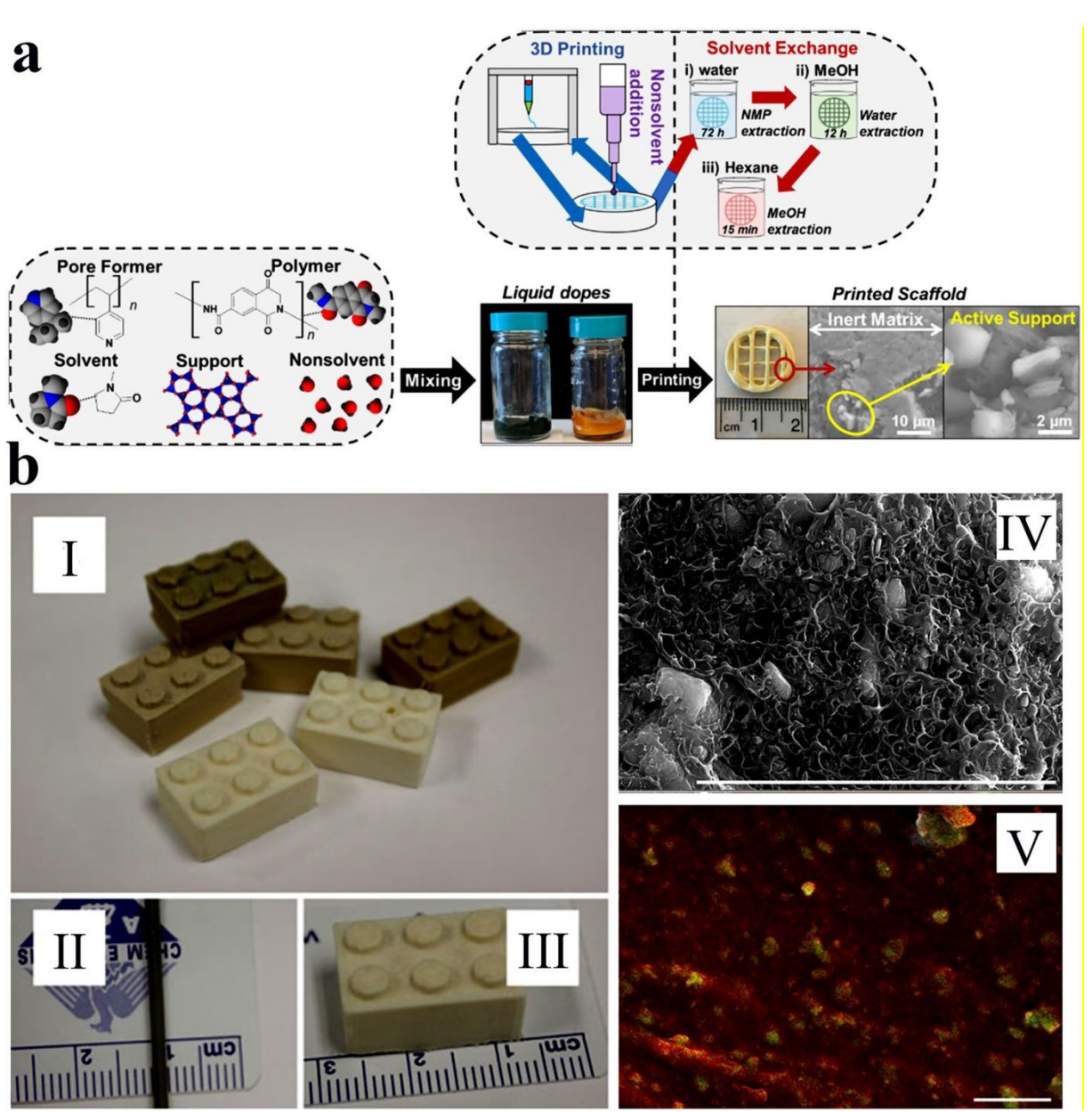


**Figure 11**: a) Schematic representation for the 3D-printed monolith MOF monolith via the matrix incorporation strategy. b) Photoimages of the ABS-MOF-5 filament and the 3D-printed structures: (I) 3D-printed block, (II) filament utilized in the printing process, (III) 3D-printed structure shows scale with corresponding (IV) SEM and (V) zinc maps.<sup>61</sup> Reprinted with permission from reference **61**. Copyright (2021), American Chemical Society.

This article is licensed under a Creative Commons Attribution 3.0 Unported Licence

Open Access Article. Published on 08 listopadu 2025. Downloaded on 13.11.2025 7:46:18.

View Article Online

DOI: 10.1039/D5MA01105A

Selective laser sintering (SLS) strategy involves using a program-controlled laser beam to sinter powdered materials, such as thermoplastic polymers, layer-by-layer into a 3D solid structure.<sup>49</sup> A key advantage of this method is that the operating conditions can be finely tuned to only partially melt the polymer powders, creating a porous, solid monolith with micro-voids between the sintered particles. When MOF nanoparticles are mixed with the polymer powder, these micro-voids form open channels that improve the exposure of the MOF fillers to the external environment, allowing fluids to pass through the monolith. A series of polymer-based MOF mixed matrix films (MMFs) have been prepared by Li et al.<sup>62</sup> utilizing thermoplastic polyamide 12 (PA12) powder as the printable polymer matrix and five kinds of powdered MOFs, MOF-801, ZIF-67, ZIF-8, HKUST-1, and NH<sub>2</sub>-MIL-101(Al) as the porous fillers (Figure 12a). In their study, single-layer MMFs with a lacing structure were printed to evaluate their mechanical properties, BET surface area, and performance. The resulting films were flexible, free-standing, and could be shaped or folded, indicating excellent mechanical stability. The NH<sub>2</sub>-MIL-101(Al)-PA12 MMF, with the smallest pore size, was identified as an efficient adsorbent for methylene blue (MB) dye removal, showing high adsorption capacity and kinetics. The reusability was demonstrated through cyclic adsorption/desorption tests, where the adsorbent maintained an 83% removal efficiency after five consecutive cycles (Figure 12b), highlighting its durability and potential for practical water treatment applications.

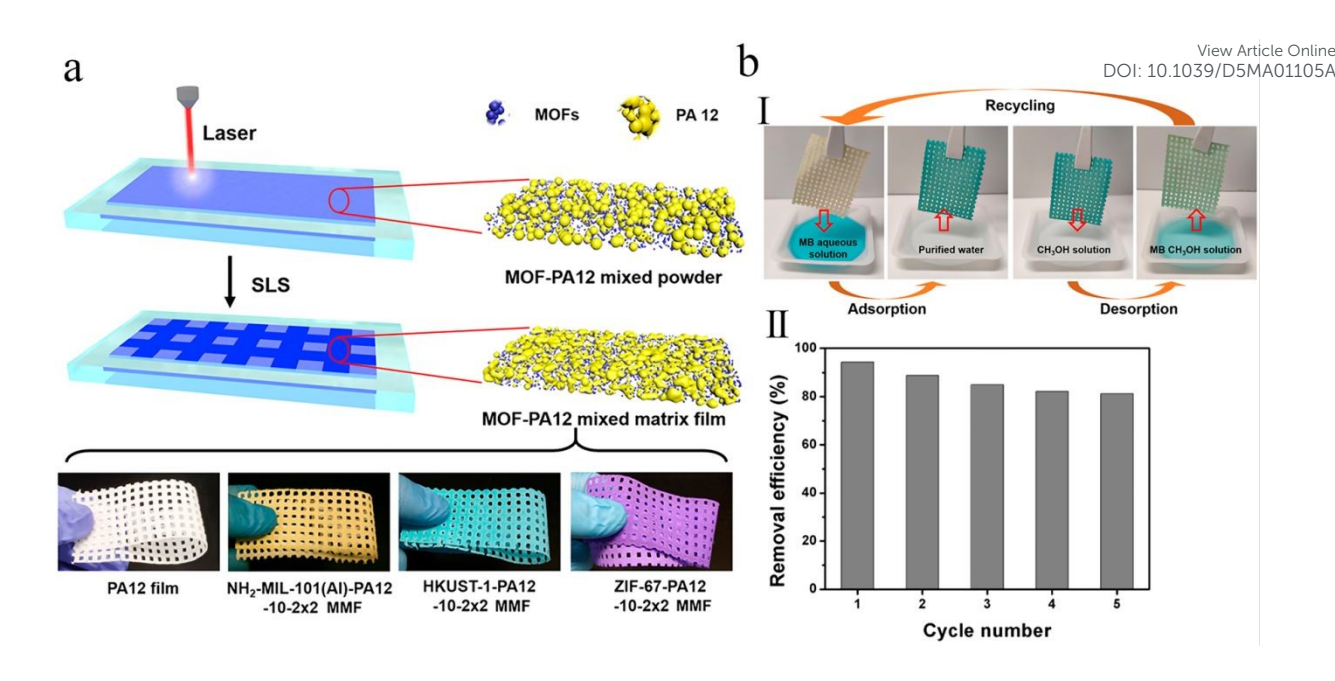


**Figure 12:** Fabrication and performance of 3D-printed MOF-PA12 mixed matrix films (MMFs): a) Schematic of the manufacturing process and photographs of PA12 and MOF-PA12 MMFs with various MOF fillers; b) Recyclability assessment of the NH<sub>2</sub>-MIL-101(Al)-PA12 MMF, including (I) visual documentation of the adsorption-desorption cycles and (II) quantitative methylene blue (MB) removal efficiency over five consecutive cycles.<sup>62</sup> Reproduced from reference **62**, under the terms of Creative Commons (CC BY) licence Copyright 2019, American Chemical Society.

#### **Digital Light processing**

Digital light processing (DLP) approach generally involves localized photopolymerization of monomers or oligomers with appropriate photoinitiators. This technique uses photoinduced cross-linking to solidify liquid resins on locally illuminated regions, replicating a 3D structure sequentially in a layer-by-layer manner. This enables rapid prototyping and provides precise control over layer thickness and resolution, which is crucial for fabricating functional MOF-based devices.<sup>63</sup>

This method was used by Halevi *et al.* <sup>64</sup> to fabricate flexible and complex 3D monoliths containing HKUST-1 nanoparticles, as shown in **Figure 13**. The images demonstrate the printing process, the intricate designs achieved, and the material's flexibility. Crucially, the

This article is licensed under a Creative Commons Attribution 3.0 Unported Licence.

Open Access Article. Published on 08 listopadu 2025. Downloaded on 13.11.2025 7:46:18.

graph reveals that while the adsorption capacity of the 3D-printed monolith matched that while the adsorption capacity of the 3D-printed monolith matched that while online pure HKUST-1 powder initially, the printed structure proved superior over time by preventing the dye release caused by the hydrolysis and decomposition that degraded the pure powder.

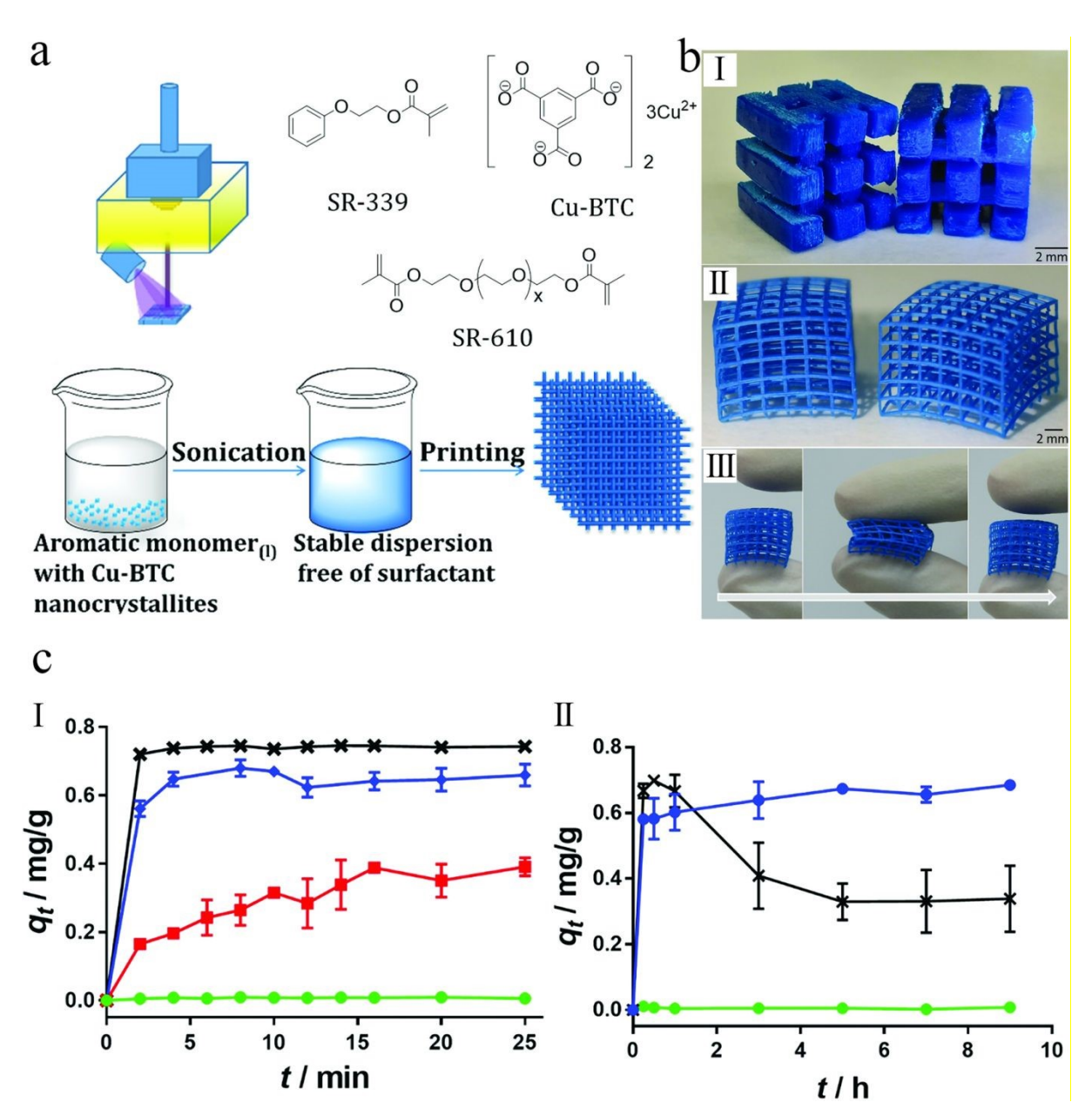


**Figure 13.** Digital Light Processing (DLP) of HKUST-1 composites: a) schematic of the DLP strategy and material chemistries, b) photographs of the resulting flexible 3D-printed monoliths, and c) evaluation of their methylene blue (MB) adsorption performance over time.<sup>64</sup> Reproduced from reference **64**, under the terms of Creative Commons (CC BY) licence.

The diverse 3D printing strategies for fabricating MOF monoliths offer distinct advantages and dictional face specific limitations, making them suitable for different applications. **Table 2** provides a comparative overview of the primary techniques, summarizing their key benefits, challenges, and typical use cases to guide the selection of an appropriate method.

**Table 2:** 3D printing methods for monolithic MOFs including their advantages, disadvantages and applications.

3D	Advantages	Disadvantages	Application	Examples
printing				
strategies  Direct ink writing	-Simple and flexible processOperating at room temperature. <sup>48</sup> -Compatible with diverse range of MOFs (e.g., HKUST, ZIF-8, UiO-66, MIL-101) -Moderate to high production rate (faster than seed-assisted, slower than LDP).	-Clogging of printing nozzlePotential deformation of MOFs due to high pressure during processing. 58 -Laborious, multi-step ink preparation (e.g., 1 to 2 days of rolling and densification). 51, 52 -Can be brittle, depending on binderParticle agglomeration in high MOF loadingsRequires rheological modifiers (e.g bentonite, cellulose). 50, 53 -Low resolution compared to light based techniquesRequire post-processing (e.g thermal activation). 53	Methane uptake <sup>48</sup> - CO <sub>2</sub> /CH <sub>4</sub> , CO <sub>2</sub> /N <sub>2</sub> and CO <sub>2</sub> /H <sub>2</sub> separation <sup>54</sup> , <sup>65</sup> , <sup>66</sup> CO <sub>2</sub> , N <sub>2</sub> , CH <sub>4</sub> and H <sub>2</sub> 0 uptake <sup>55</sup> - Butanol recovery <sup>54</sup> - CO <sub>2</sub> capture <sup>56</sup>	HKUST-1 <sup>48</sup> UTSA-16(Co) <sup>54, 55</sup> MOF-74(Ni) <sup>65</sup> ZIF-8 <sup>54,66</sup> UiO-66 <sup>51</sup> MIL-101 <sup>56</sup>
Seed- assisted in situ growth	-Forms a dense, continuous MOF film on the printed scaffoldGood interaction between MOFs and matricesUniform distribution of MOFs within the matricesSignificantly enhances CO <sub>2</sub> capacity (from 0.5 to 2.5 mmolg <sup>-1</sup> ) and improves mass transfer kinetics.	-Not suitable for high MOF loadings (typically < 50 wt%)60 -Poor crystallinity of MOF phases -Multi-step process leading to long fabrication times -Generate liquid waste; not ideal for scale-up.	CO <sub>2</sub> adsorption <sup>60</sup>	MOF-74 <sup>60</sup>
Matrix incorporatio n	-Effective dispersion of MOF particles within the polymer matrixInk exhibits suitable viscoelasticity for printing.	-Not suitable for high MOF loadings (e.g., limited to ~10 wt% in some cases). <sup>61</sup> -Possibility of partial decomposition of the	- Hydrogen storage <sup>61</sup> -CO <sub>2</sub> uptake <sup>60</sup>	- MOF-5 <sup>61</sup> - MOF-74 <sup>60</sup>

	-Relies on inexpensive polymer matrices like acrylonitrile butadiene styrene (ABS)Fabricating MOF monoliths via a simple solvent-casting process.	MOF crystals and pore blockageBatch process with limited throughput.		View Article DOI: 10.1039/D5MAC
Selective laser sintering	-High resolution and good control over physical characteristicsFormation of micropores between MOF and polymer powders, improving exposure. 62	-Limited range of applicable materialsLimited by small build chambers, resulting in lower throughputHigh processing temperatures (> 100 °C) can degrade some MOFs. 62 - Poor interaction between MOF and matrices.	- Water adsorption, purification <sup>62</sup> - CO <sub>2</sub> conversion <sup>67</sup>	MOF-801, ZIF- 67, ZIF-8, HKUST -1, <sup>62</sup> ZIF 8 <sup>67</sup>
Digital light processing	- High resolution and very fast layer-by-leyer curingGood control over thickness and monolith formationEnables rapid fabrication of complexhigh resolution 3D monolith.	-Limited to photosensitive resin -Needing photo initiators -Needing a light sourceCan result in reduced mechanical properties for some composites.	-Adsorption of methylene blue dye <sup>64</sup> -CO <sub>2</sub> /CH <sub>4</sub> separation <sup>63</sup>	- HKUST-1 <sup>64</sup> -MIL-53(Fe)-NH <sub>2</sub> <sup>63</sup>
Template- assisted synthesis	-It is a more versatile technique as it offers a chance to achieve more diverse structures (e.g., macroporous networks)Templating results in control over the chemical reactivity of guests.	-Limited template availability. -Template removal challenging, often requiring calcination, or solvent extraction.	- Oil-water separation and Knoevenagel reaction <sup>20</sup>	- ZIF-8 <sup>20</sup> - MIL-53(Al) <sup>68</sup>

#### CHARACTERIZATION OF MONOLITH BASED MOFS

Several techniques have been employed to understand the structural, thermal, and functional properties of monolithic-based MOFs. These include, but are not limited to, powder X-ray diffraction (PXRD) for assessing crystallinity and phase purity, Fourier-transform infrared spectroscopy (FTIR) for analyzing chemical bonding and functional groups, thermogravimetric analysis (TGA) for evaluating thermal stability and compositional changes, scanning electron and Transmission electron microscopy (SEM and TEM) for morphological analyses, and gas sorption measurements for determining porosity and surface area. A good understanding of

monolith MOF properties will allow for their rational design and optimization in specific online applications such as catalysis, gas storage, sensing, separation, and drug delivery. This knowledge also provides insights into their structural integrity, chemical resilience, and performance under various operational conditions.

### **Powder X-Ray Diffraction (PXRD)**

PXRD is a critical tool for identifying the crystallinity and structural integrity of MOFs. <sup>47,69</sup> PXRD gives detail on phase purity of materials, which is necessary to guarantee the mechanical stability and reliable use of monolithic MOFs. The PXRD profiles of monoliths and powders can exhibit distinct variations due to differences in crystal orientation and sample morphology. Powder samples consist of many small crystallites oriented randomly. This ensures that all crystal planes are statistically represented during diffraction, and this usually produces sharp, intense and well-defined peaks. These peaks are also easily compared with simulated or database patterns. In monolithic samples (especially dense, compacted, or shaped samples), however, the crystals may be aligned in specific directions, leading to non-random orientation. This results in intensity variations, some peaks may be enhanced, suppressed, broadened or even missing. This makes it best for checking bulk crystallinity and phase retention after monolith fabrication, but not always quantitative for crystallographic detail.

Furthermore, PXRD analysis is able to unmask a lot about the material for example, the degree of crystallinity within the monolith is indicated by the PXRD pattern's strong, distinct diffraction peaks. To The broadening of these peaks in some monoliths, may indicate the existence of an amorphous material, which could affect its mechanical stability and functionality. However, in monolithic UiO-66, significant peak broadening has been identified and this was attributed to the nanocrystallites causing nano-convergence of diffraction peaks. Additionally, PXRD is also used to identify any phase transitions or structural

Open Access Article. Published on 08 listopadu 2025. Downloaded on 13.11.2025 7:46:18.

This article is licensed under a Creative Commons Attribution 3.0 Unported Licence.

alterations<sup>70</sup> that may occur in the monolithic MOF due to external factors, such as mechanical diction of the monolithic stress, temperature, or exposure to different environments.<sup>72</sup> The preservation of the monolithic MOF's original crystalline structure is essential for its long-term stability and dependable operation, and researchers may verify this by tracking the PXRD patterns over time or under various circumstances.

Over the years there has been a marked advancement in the development of new and more advanced techniques which has made material analysis easy, notable examples include High-resolution PXRD and Synchrotron radiation PXRD.<sup>73,74</sup>These techniques provide detailed information on the crystalline structure, including unit cell parameters, atomic positions, and the presence of minor impurities or defects.<sup>75</sup> By utilizing PXRD as a reliable and comprehensive characterization tool, researchers can confidently validate the crystallinity and structural integrity of monolithic MOFs,<sup>76</sup> ensuring that these materials meet the stringent requirements for their intended applications,<sup>76</sup> such as gas storage,<sup>80</sup> catalysis or separation processes.<sup>81</sup> The insights gained from PXRD analysis, coupled with other characterization methods, play a crucial role in the development and optimization of high-performance monolithic MOF materials.<sup>28,82</sup>

However, it must be noted that while PXRD provides valuable information on the crystallinity and phase purity of MOFs, it does not always distinguish if a MOF is powdered or monolithic. Takahashi *et al.* <sup>83</sup> used powder X-ray diffraction (XRD) characterisation to verify the crystallinity of HKUST-1 structures. The resulting pattern, presented in **Figure 14**, indicated the presence of the target MOF but was dominated by crystalline material of Cu<sub>2</sub>(OH)<sub>3</sub>NO<sub>3</sub> and Cu(NH<sub>3</sub>)<sub>4</sub>(NO<sub>3</sub>)<sub>4</sub> phases.

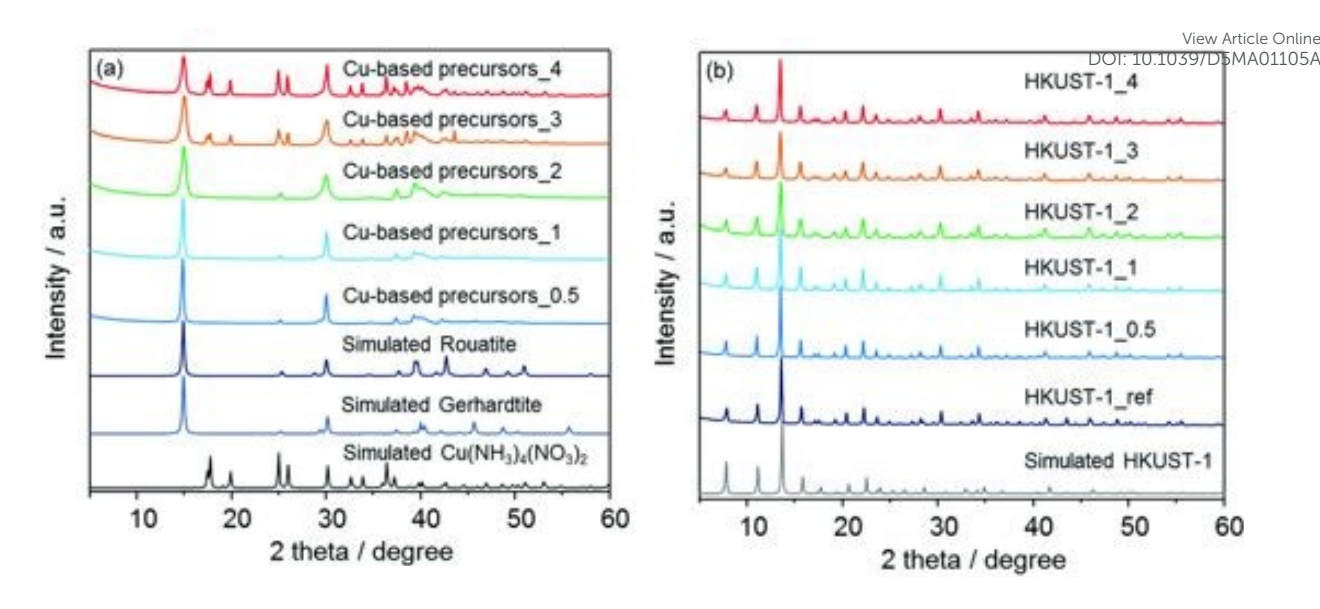


**Figure 11**: XRD analysis of Copper based monoliths.<sup>83</sup> (a) the solvent insoluble Cu-based precursors (Cu-based precursors *X*) with simulated patterns for Cu<sub>2</sub>(OH)<sub>3</sub>NO<sub>3</sub> (rouaite and gerhardite) and Cu(NH<sub>3</sub>)<sub>4</sub>(NO<sub>3</sub>)<sub>2</sub> and (b) corresponding HKUST-1-**X** with HKUST-1 reference and simulated pattern for HKUST-1.<sup>83</sup> Reproduced from Reference **83**, with permission from the Royal Society of Chemistry.

#### Scanning Electron Microscopy (SEM) Analysis

Scanning Electron Microscopy is a fundamental tool for comprehensive characterisation of monolithic MOFs, offering unprecedented insights into their structural, morphological, and compositional characteristics.<sup>84,85</sup> The measurements allow for the analysis of both pore structure and overall morphology. <sup>86,87</sup> Due to its high-resolution imaging capabilities, SEM enables researchers to meticulously examine the intricate microstructure of MOFs, revealing critical details about crystal morphology, surface topology, and potential structural defects that might significantly impact material performance. <sup>85,88,89</sup>

The profound impact of synthesis conditions on morphology is eloquently illustrated in the work of Hunter-Sellars *et al.*, as shown in **Figure 15** <sup>41</sup> The well-defined, faceted crystals of conventional ZIF-8 and ZIF-67 powders provide a stark contrast to the structures formed by monolithic synthesis. The transition to a monolithic form via a ligand-assisted sol-gel method using n-butylamine (NB) as a modulator result in a dramatic morphological change. For

This article is licensed under a Creative Commons Attribution 3.0 Unported Licence.

Open Access Article. Published on 08 listopadu 2025. Downloaded on 13.11.2025 7:46:18.

instance, ZIF-67 (NB) consists of densely packed, much smaller nanoparticles that appredicte Online agglomerated with what is assumed to be amorphous material. This evolution is even more pronounced when a mixture of modulators (n-butylamine and 1-methylimidazole, ML) is used. The resulting ZIF-8 (ML) and ZIF-67 (ML) monoliths lack any distinct or well-defined particles altogether, an observation that aligns with PXRD data indicating a severe loss of crystallinity. This suppression of crystal growth is attributed to monodentate linkages formed between metal ions and the modulating ligands, which inhibit the formation of long-range crystalline order.

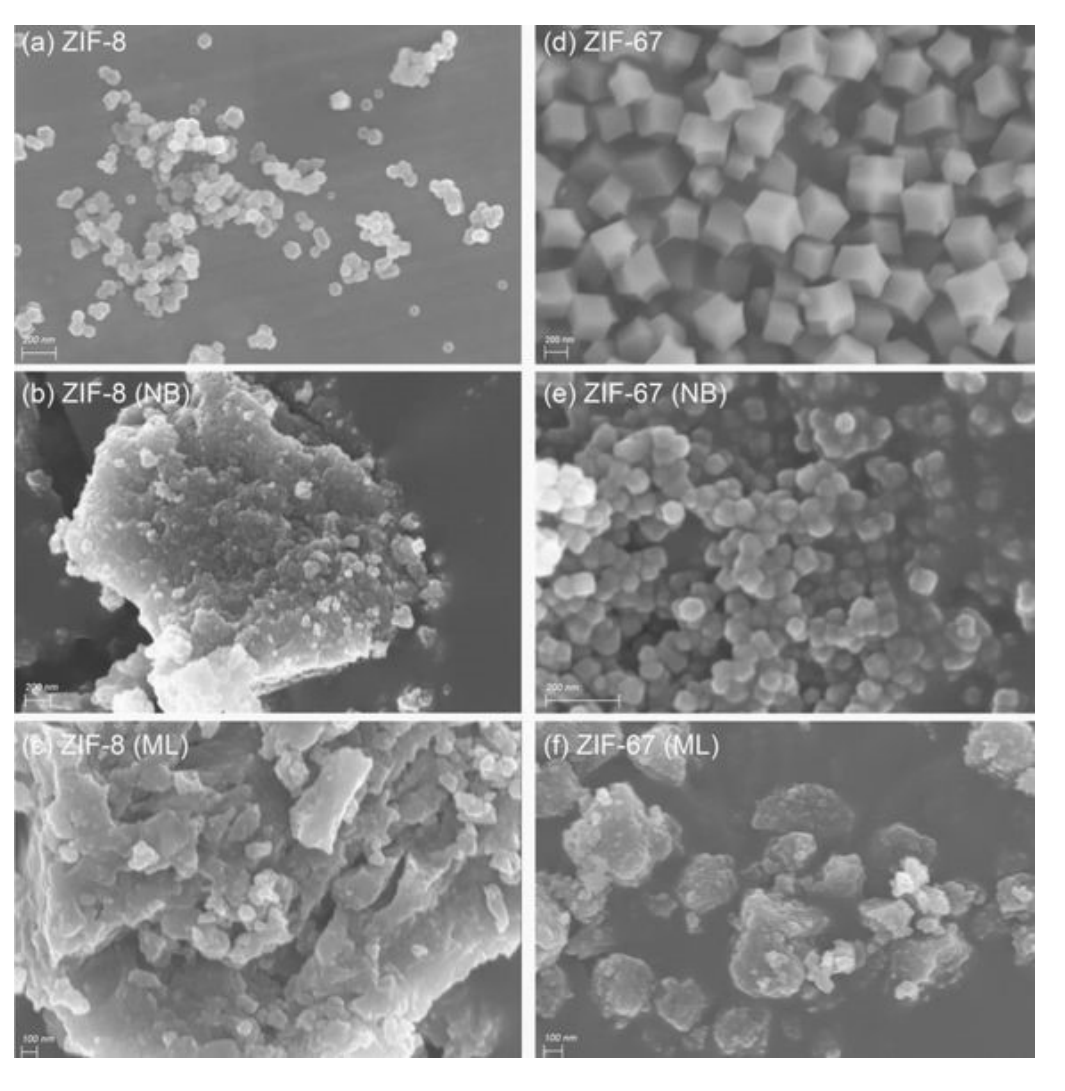


**Figure 12:** Image showing SEM images of monolithic ZIF-MOF family. (a) ZIF-8, (b) ZIF-8 (NB), (c) ZIF-8 (ML), (d) ZIF-67 (e) ZIF-67 (NB) and (f) ZIF-67 (ML). <sup>41</sup> NB stands for n-

Beyond revealing this microstructural evolution, SEM, when coupled with Energy-Dispersive X-ray Spectroscopy (EDS), allows for the mapping of elemental composition across the monolith's surface. This is crucial for confirming the homogeneous distribution of metal nodes and organic linkers, ensuring the chemical integrity of the monolith and the absence of phase segregation.

#### **Transmission Electron Microscopy (TEM)**

This article is licensed under a Creative Commons Attribution 3.0 Unported Licence

Open Access Article. Published on 08 listopadu 2025. Downloaded on 13.11.2025 7:46:18.

TEM is a critical characterization tool in the study of MOFs, offering nanoscale insights that complement other techniques such as PXRD, BET surface area analysis, and SEM. In monolithic MOFs, where the morphology, internal nanoparticle arrangement, and nanoparticle interactions are key to performance, TEM allows researchers to directly observe the size, shape, and dispersion of these nanoparticles that aggregate into the final monolithic structure. It has been proven through TEM that monoliths of Al-BDC and UiO-66 are comprised of nanoparticles of sizes that are around 10 nm.<sup>33,90</sup> One of the most important contributions of TEM to monolithic MOF research is its ability to reveal how synthesis parameters such as solvent choice, concentration, or aging time directly influence the nucleation and final morphology of colloidal precursors.

A study by Pathak *et al.*<sup>44</sup> powerfully illustrates this, using TEM to deconvolute the effects of solvent system and temperature on ZIF-8 monolith MOF formation. Their TEM analysis, summarised in **Figure 16**, was pivotal in explaining why certain synthesis yielded powdered (pZIF-8) and other monoliths (mZIF-8-R, mZIF-8- $\Delta$ ). The images reveal that synthesis in pure water resulted in very large particles which hinder the dense packing required for monolithicity. Conversely, the optimised 15% v/v EtOH-H<sub>2</sub>O solvent system produced significantly smaller, uniform primary nanocrystallites, with mean size of 55  $\pm$  10 nm for mZIF-8- $\Delta$ . This precise

This article is licensed under a Creative Commons Attribution 3.0 Unported Licence.

Open Access Article. Published on 08 listopadu 2025. Downloaded on 13.11.2025 7:46:18.

control over particle size was identified as the key factor enabling the particles to agglomy maddite online into coherent, robust monolith rather than a powder.

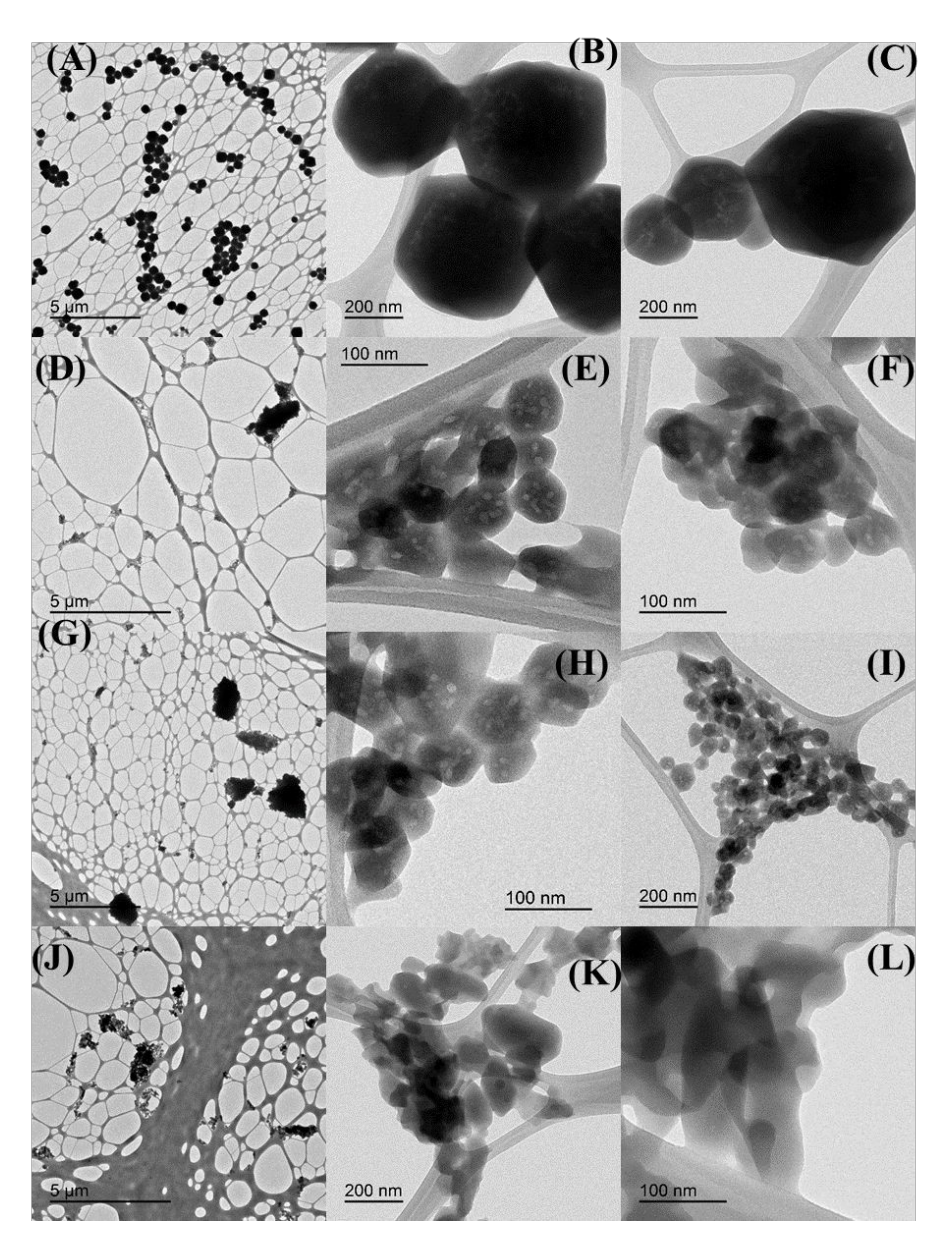


**Figure 16:** Representative TEM images of MOFs after the complete drying of gel followed by activation in a vacuum oven. pZIF-8 (A, B, C), mZIF-8-R (D, E, F), mZIF-8-Δ (G, H, I) and mZIF-8-CS (J, K, L). Scale bars; 5 nm (A, D, G, J), 200 nm (B, C, I, K) and 100 nm (E, F, H, L).<sup>44</sup> Reproduced with permission from reference **44** under the terms of the Creative Commons (CC BY) license.

Furthermore, the study used TEM to track the reaction progress in situ. Aliquots taken from the reaction mixture at various times showed that primary particles formed rapidly but required extended periods (96-120 hours) to achieve their final, well-defined state. This TEM evidence

directly supported the conclusion that the solvent mixture's primary effect was to drastically additionally slow down the reaction kinetics and colloidal aggregation. This ability to visually corroborate kinetic data makes TEM an indispensable tool for understanding the complex sol-gel process that underpin monolithic MOF formation.

TEM also enables the detailed examination of structural features that are difficult to detect using other techniques. These include the interfaces between aggregated nanoparticles, mesoporous interparticle spaces, the presence of defects or amorphous regions, and the degree of fusion or continuity within the monolith. 90 Such information is essential for understanding how microstructural features affect macroscopic properties like mechanical strength, gas permeability, or catalytic activity.

In addition, it is particularly useful for characterizing hybrid or composite monoliths, where MOFs are combined with polymers, carbon materials, or other functional components. It can resolve the nanoscale interfaces between phases and provide insights into compatibility, dispersion, and potential phase separation. These factors are critical when designing monoliths for real-world applications such as gas separation membranes, adsorbents, or catalytic reactors.

#### **Porosity and Surface Area Analysis**

The applications of MOFs in gas storage, separation and heterogeneous catalysis fundamentally relies on their extraordinary intrinsic porosity and massive surface areas, properties that often surpass those of traditional porous materials like zeolites and activated carbons. This porosity is a direct consequence of their modular, crystalline architecture, where metal nodes are connected by organic linkers to form well-defined cages and channels. Precise characterization of these textural properties is therefore a critical endeavour that links synthetic design and molecular-scale structure directly to application performance.

The most established technique for this purpose is gas physisorption, most commonly of Rolling Rollin

However, a significant challenge arises when transitioning from laboratory powder to industrial application, which necessitates shaping the MOF into robust, handleable forms such as pellets or monoliths. Conventional techniques like pelletization under high mechanical pressure often incur a catastrophic loss of surface area and porosity. This makes the development of shaping methods that preserve porosity a key research focus. <sup>93</sup>

For instance, Pathak *et al.*<sup>44</sup> demonstrated that monolithic ZIF-8 (mZIF-8) possesses a hierarchical pore structure combining micro- and mesoporosity, which is a significant advancement over conventional powdered ZIF-8 (pZIF-8). While the powder form is exclusively microporous (Type-I isotherm, BET ~1450 m²/g), the monoliths exhibit a Type-IV isotherm with a distinct hysteresis loop, confirming the introduction of mesopores with a mean size of 16 nm. Crucially, despite this architectural change, the optimal monolith (mZIF-8-Δ) retained a high BET surface area of 1421 m²/g. The key distinction lies in the density and volumetric performance; the monolith's much higher bulk density (0.76 g cm⁻³ vs. 0.35 g cm⁻³ for the powder) results in a far superior volumetric surface area (1080 m²cm⁻³ vs. 508 m² cm⁻³), making it far more practical for real-world applications where space is a constraint, without sacrificing its adsorptive capacity.

This article is licensed under a Creative Commons Attribution 3.0 Unported Licence.

Open Access Article. Published on 08 listopadu 2025. Downloaded on 13.11.2025 7:46:18.

This principle of creating hierarchical structures within monoliths is further advanced in monoliths work of Thakkar *et al.*,<sup>47</sup> who utilized 3D printing to structure MOF-74(Ni) and UTSA-16(Co). The results, summarized in **Figure 17**, reveal significant structural insights: The pure MOF powders exhibited classic Type I isotherms, confirming their purely microporous nature with high BET surface areas (1180 m²/g for MOF-74(Ni) and 727 m²/g for UTSA-16(Co)). In contrast, the 3D-printed monoliths, particularly UTSA-16(Co), displayed a Type IV isotherm with a distinct hysteresis loop, confirming the successful introduction of mesoporosity during the printing process. While the incorporation of non-porous binders led to a reduction in gravimetric surface area and micropore volume, the highest-loaded monoliths retained substantial values (737 m²/g and 0.32 cm³/g for MOF-74(Ni); 568 m²/g and 0.23 cm³/g for UTSA-16(Co)). The UTSA-16(Co) monolith also exhibited an additional mesopore volume of 0.06 cm³/g with a mean size of 25 nm.

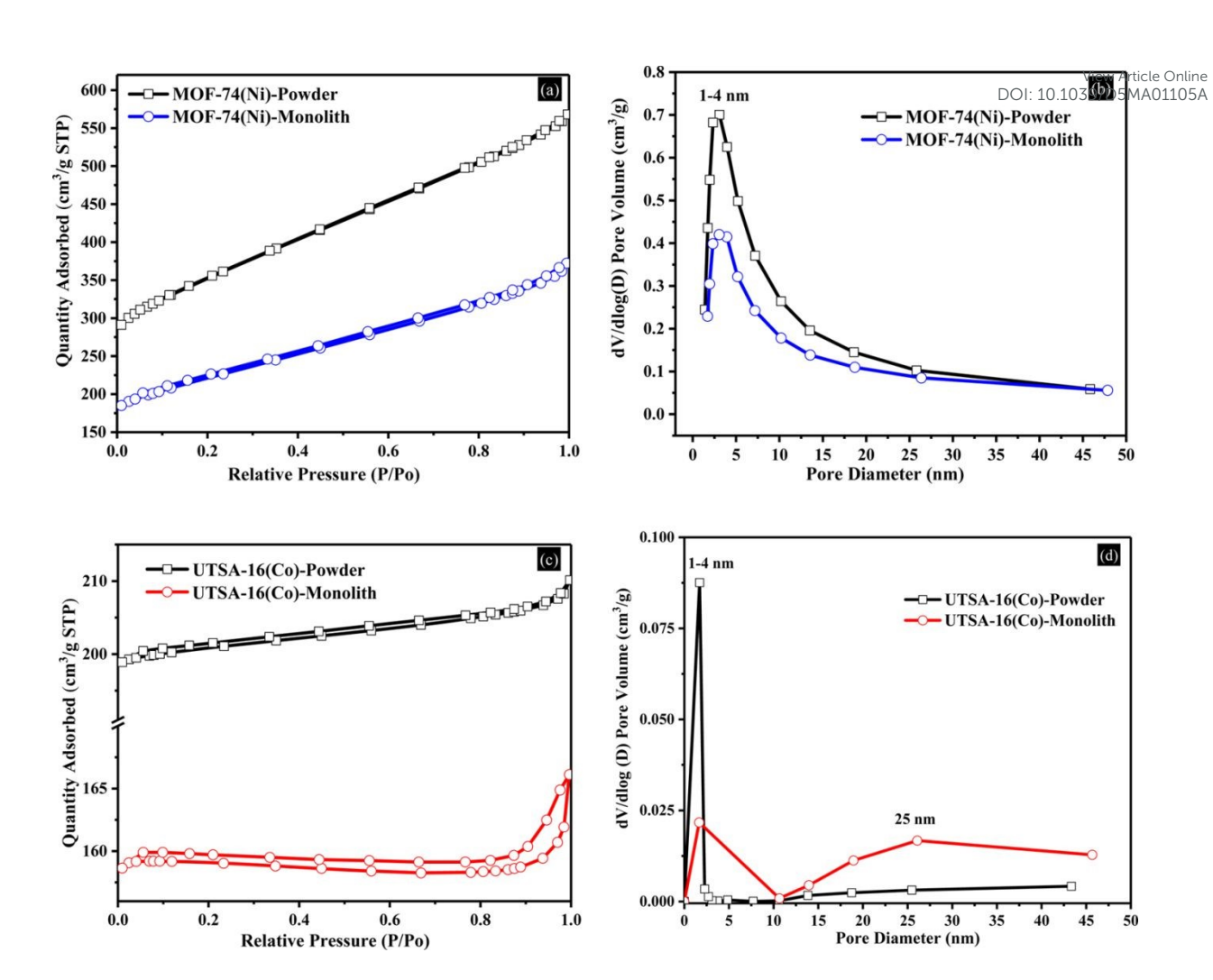


**Figure 17.** Nitrogen physisorption isotherms and pore size distribution curves for 3D-printed MOF monoliths (a, b) MOF-74(Ni) and (c, d) UTSA-16(Co) and their corresponding powders.<sup>47</sup> Reproduced with permission from reference **47**, Copyright (2017) American Chemical Society.

The data showed that the structured monoliths retained 79–87% of the powder's CO<sub>2</sub> capacity. Furthermore, the intentionally introduced mesoporosity facilitated dramatically improved mass transfer kinetics, evidenced by a sharper breakthrough curve (10 minutes for the monolith vs. 15 minutes for the powder). This demonstrates that the 3D-printed form factor mitigates kinetic limitations without sacrificing core adsorption capacity, thereby validating this monolithic approach for practical CO<sub>2</sub> capture.

View Article Online

DOI: 10.1039/D5MA01105A

This article is licensed under a Creative Commons Attribution 3.0 Unported Licence.

Open Access Article. Published on 08 listopadu 2025. Downloaded on 13.11.2025 7:46:18.

Powdered MOFs are characterised by poor mechanical strength compared to their monolithic counterparts.<sup>94</sup> The majority of research examining the mechanical properties of MOFs has primarily relied on nano indentation techniques. This technique involves pressing a hard indenter tip (often diamond) into a material's surface while precisely measuring the applied load and the resulting displacement, as illustrated in Figure 18. In this representative molecular dynamics simulation model, a conical diamond indenter is pressed into a single-crystal specimen. The substrate is typically divided into layers: a fixed boundary layer to prevent slippage, a thermostatic layer to maintain the target temperature, and a Newtonian layer where the indentation occurs, and atomic motion is calculated. This approach, which was established by Oliver and Pharr, is mainly used to determine two key properties: Young's modulus (E), which measures elasticity, and hardness (H).<sup>95</sup>

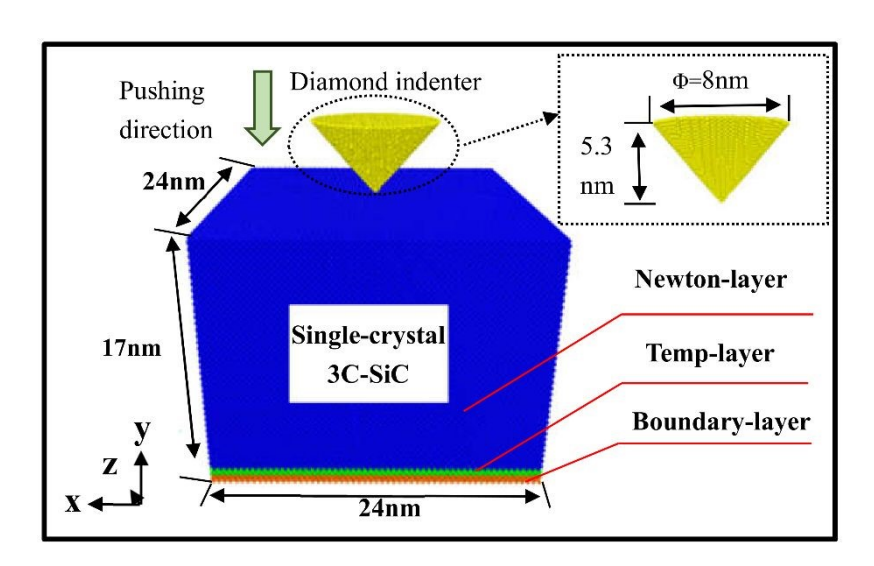


Figure 18: Schematic of a molecular dynamics simulation model for nanoindentation a single crystal, showing the indenter and the different atomic layers of substrate. 96 Reproduced from reference 96, under the terms of the Creative Commons (CC BY) license.

The monolithic samples are first made cylindrical by cold mounting, then they are polish the continuous minimize roughness. A diamond indenter tip is then used to indent the smooth surface to a certain depth whilst the continuous stiffness measurement will be measuring the elastic modulus and hardness. 97,98 Young's modulus (E) represents the material's elastic stiffness, that is, its ability to resist elastic (reversible) deformation under applied stress. A high E value indicates that the material is rigid and can retain its shape under mechanical load, which is crucial for maintaining structural integrity in applications involving pressure, vibration, or mechanical agitation. This is particularly important for monolithic MOFs used in gas separation, flow reactors, or packed bed systems, where structural deformation could lead to channel blockage, pressure drops, or even framework collapse.

Hardness (H), on the other hand, measures a material's resistance to permanent (plastic) deformation, such as scratching or indentation. A high hardness value suggests that the material can withstand localized mechanical stresses without sustaining damage. In MOFs, higher hardness is advantageous for resisting wear and abrasion during processing, handling, or operation in dynamic environments, such as catalytic beds or adsorption columns. Monolithic MOFs preserve their structural integrity under conditions of cyclic loading, including repetitive compression and decompression, as encountered in gas storage systems. Their stability without the inclusion of binders, coupled with a hierarchical porous structure, significantly enhances their mechanical properties and overall performance in practical applications. A notable example is that of ZIF-67 powder which was transformed into a monolith by the compression of the powder at 25MPa for 5 mins yielding a monolith after calcinating at 800 °C. The resulting monolith could withstand cyclic loadings of pressure up to 3MPa.<sup>99</sup>

Tricarico *et al.*, <sup>100</sup> used nanoindentation method to evaluate the mechanical properties of four MOF monoliths: ZIF-8, HKUST-1, MIL-68, and MOF-808. **Figure 19** illustrates the load-

depth curves from nanoindentation tests (**Figure 19A**) and the relationship between elacticle online recovery and the H/E ratio (**Figure 19B**), highlighting the distinct mechanical behaviour of each monolith. The results revealed a clear distinction in their mechanical responses, governed by their unique nanostructures. HKUST-1 exhibited the highest hardness (0.46 GPa) and an intermediate elastic recovery, contributing to its exceptional indentation fracture toughness (Kc =  $0.80 \pm 0.45$  MPa $\sqrt{m}$ ), the highest reported for any MOF material.

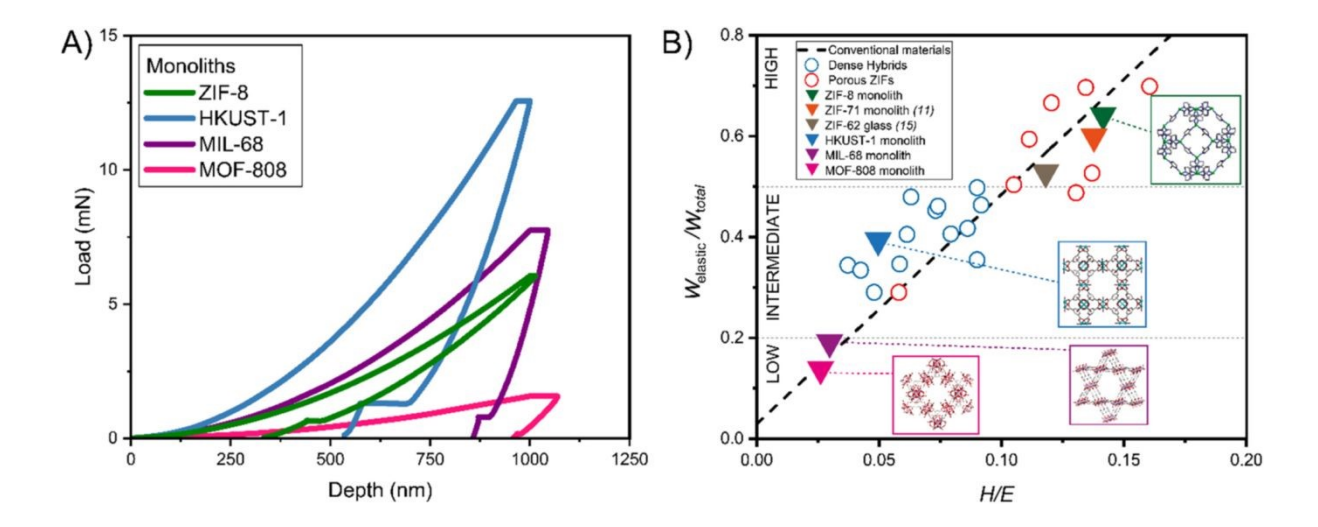


**Figure 19:** Mechanical Properties of monolithic MOFs, (A)Nanoindentation Load-Depth Curves and (B) Elastic Recovery versus Hardness/Modulus Ratio. Reproduced from reference **100**, under the terms of the Creative Commons (CC BY).

In contrast, ZIF-8 showed a high elastic recovery but intermediate hardness, making it more prone to radial cracking. Meanwhile, MIL-68 and MOF-808, characterized by smaller nanograins and a higher density of grain boundaries, displayed lower hardness and significantly reduced elastic recovery. This nanostructure promotes grain boundary sliding, which enhances ductility and energy dissipation, thereby providing remarkable resistance to crack propagation despite their lower inherent strength. These findings underscore how nanostructural features such as grain size, porosity, and framework topology directly influence both elastic and plastic

deformation mechanisms. The superior hardness and fracture toughness of HKUST<sub>1</sub>:1<sub>1</sub> make Michael Madillosa highly suitable for industrial applications requiring durability under mechanical stress.

Recent upgrades to the nanoindentation technique have seen the emergence of two advanced mechanical testing methods: flat punch nanoindentation and micropillar compression. Flat punch nanoindentation uses a cylindrical indenter with a flat end to compress a relatively large, flat area of a monolith. This technique is ideal for probing the bulk-like mechanical behaviour of porous monoliths since it minimizes localized densification that occurs with sharp tips usually used in conventional nanoindentation. As applied in the study of MOF monoliths, it enables the estimation of stress-strain relationships, providing insight into yielding and plastic flow under a constrained, triaxial stress state. It is commonly used to measure Young's modulus, yield strength, and to monitor fracture initiation under uniaxial loading. It helps in evaluating the structural stiffness and pore collapse behaviour in a more distributed stress field compared to standard indentation.

**Figure 20 (a, b)** shows the resulting load–depth (P–h) and stress–strain (σ-ε) curves from flat punch nanoindentation tests on ZIF-8 and MIL-68 monoliths, using a flat punch indenter with a diameter of 10.64 μm. The data, summarized in **Table 3**, reveal that both monoliths exhibit similar yield stresses (ZIF-8: 88.2 ± 16.4 MPa; MIL-68: 90.0 ± 10.5 MPa), but differ in their strain hardening behaviour, with ZIF-8 showing a higher strain hardening exponent (n ≈ 0.20) compared to MIL-68 (n ≈ 0.11). It was observed that MIL-68 exhibited an initial stiff response followed by softening for depths > 200 nm (as visible in the derivative dP/dh in **Figure 20 (c**). This was contrary to the case of ZIF-8, which exhibited a softer response, without a drastic change in its slope. The authors attributed the initial stiff response of MIL-68 to its higher elastic modulus, prior to the onset of grain boundary sliding.

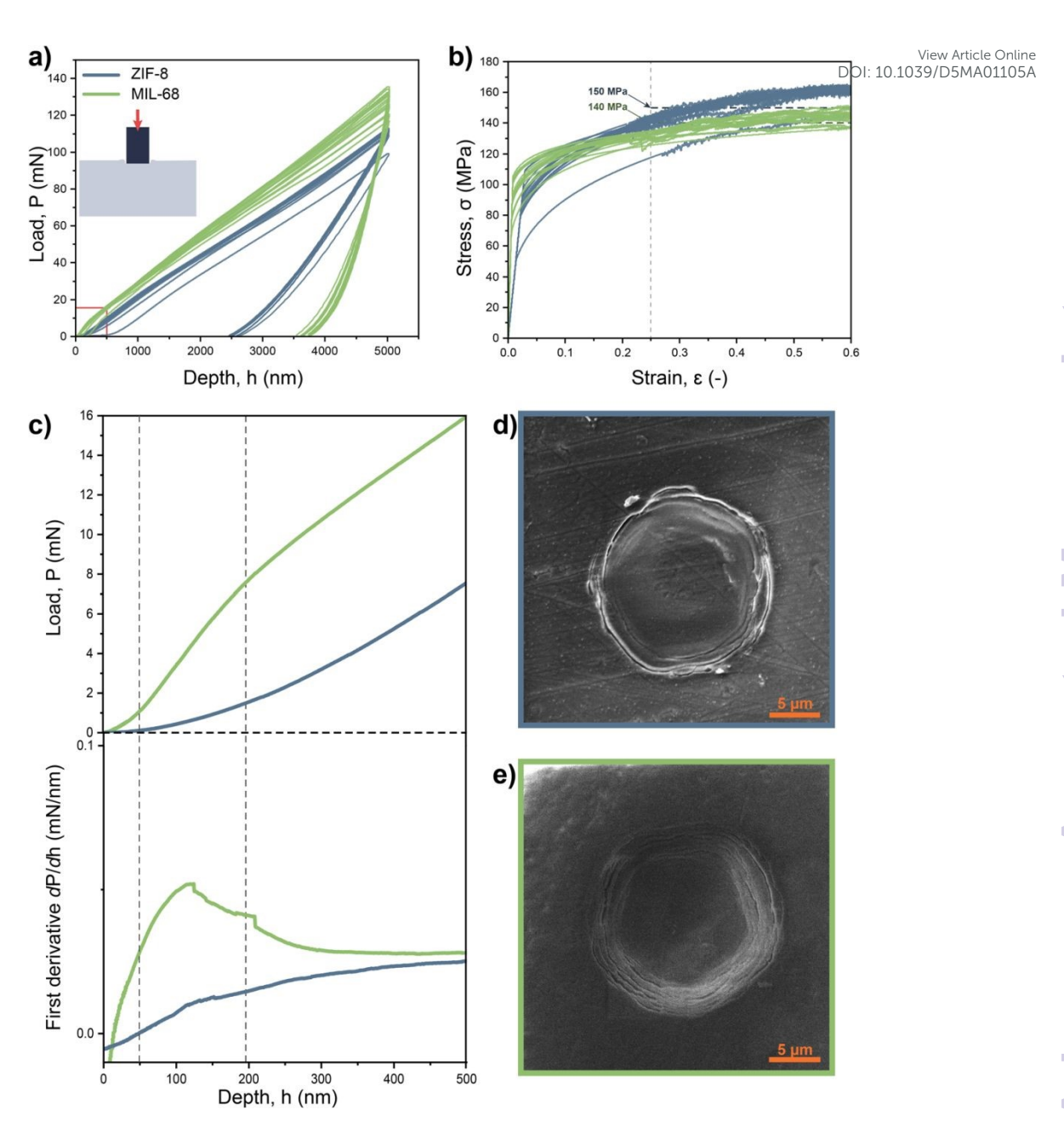


**Figure 20**: Flat punch tests on ZIF-8 and MIL-68 monoliths (a) load-depth curves, (b) stress-strain curves, (c) load-depth curves in the 0-500 nm range, (d) SEM image for flat punched ZIF-8, and (e) SEM image for flat punched for MIL-68.<sup>94</sup> Reproduced with permission from reference **94**, under the terms of the Creative Commons Attribution License (CC BY).

This article is licensed under a Creative Commons Attribution 3.0 Unported Licence

Open Access Article. Published on 08 listopadu 2025. Downloaded on 13.11.2025 7:46:18.

**Table 3:** Mechanical properties of ZIF-8 and MIL-68 monolith extrapolated from the strain obtained by flat punch nanoindentation.

Material	Number	Yield	Yield strain (-)	K(MPa)	(n-)	Average	Hardness
	of tests	stress				flow	(MPa)
		(MPa)				stress	
						(MPa)	
ZIF-8	18	88.2±16.4	0.00238±0.0033	184.1±9.5	0.1976±0.0405	140 ± 10	452 ± 20
MIL-68	16	90.0±10.5	0.0072±0.0008	154.0±6.6	0.1093±0.029	150±16	402±13

It was concluded that these MOF monoliths consists of stepwise microcracking, accommodating excessive build-up of stress, likely taking place at the grain boundaries between the nanocrystals. This mechanism is supported by the appearance of concentric ringshaped cracks around the residual imprints (**Figure 20 (d, e))**, resembling shear faults, and the absence of pop-ins in the load–depth curves, indicating contained damage without catastrophic crack propagation.

Micropillar compression involves fabricating tiny cylindrical or square pillars (usually via focused ion beam milling) from a monolith and compressing them using a flat punch. This technique provides data on uniaxial compressive strength, yielding, and failure modes at the microscale. It is particularly useful for studying anisotropic mechanical responses, brittle-to-ductile transitions, or the effects of defects in monolithic frameworks. For MOFs and other fragile porous materials, it enables controlled study of plastic deformation or fracture mechanisms without bulk sample limitations. This technique has been used for studying the stress–strain relationships of ZIF-8 and MIL-68 monoliths, obtained by a sol-gel synthesis route. 94 The stress-strain curves obtained and the micropillar compression images are shown in

Figure 21 and they show distinctly different plastic behaviour of the two monoliths. From Machines study, it was concluded that ZIF-8 exhibited elastic crack propagation failure as shown in Figure 21d, whereas MIL-68 had some plastic flow before failure (Figure 21e). 94 The difference in failure modes is attributed to the distinct framework architectures and nanostructures: ZIF-8 fails by longitudinal splitting due to its brittle nature, while MIL-68 shows ductile flow and transverse cracking, enhanced by its finer nanoparticle size and stiffer framework.

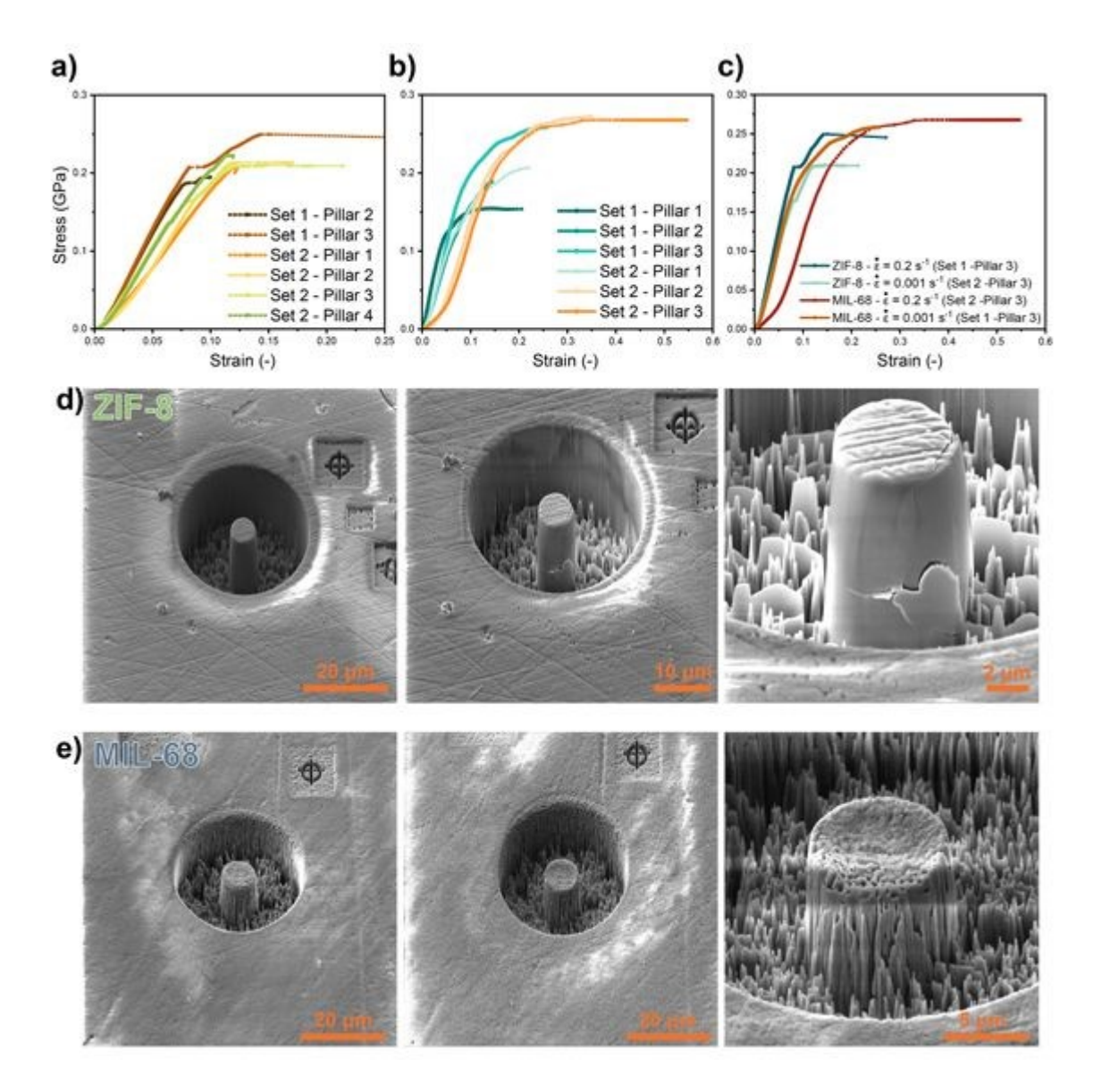


Figure 21: (a,b,c) Stress-strain curves of ZIF-8 and MIL-68 micropillars compression samples,

(d,e) Micropillars compression representative images.<sup>94</sup> Reproduced with permission from Additional Reproduced with Permission Reproduced Rep

Nanoindentation has been employed to evaluate the mechanical performance of a wide range of monolithic MOFs, as summarized in **Table 4.** These studies reveal that monolithic MOFs exhibit significantly enhanced mechanical durability compared to their powdered forms, making them suitable for high-pressure applications. Furthermore, their properties are not merely intrinsic but can be deliberately engineered. For instance, creating defects via thermolysis (e.g., in monoUiO-66-NH-30%-A) results in a predictable decrease in hardness and elasticity. Conversely, the encapsulation of guest molecules presents a exciting strategy for enhancing mechanical integrity. Recent work has shown that embedding rigid, planar dyes within monolithic UiO-66 frameworks increases both Young's modulus and hardness, suggesting a pore-filling stiffening effect. This enhanced resistance to fracture and wear is critical for the sustained utilization of monolithic MOFs in demanding applications like catalysis and gas storage.

**Table 4**: The Nanoindentation data for selected monoliths.

Monolith	Max depth (nm)	Indentation	Hardness (MPa)
	- , , ,	modulus (GPa)	, , ,
ZIF-8 <sup>94</sup>	2000	$3.18 \pm 0.04$	$452 \pm 20$
ZIF-71 <sup>35, 94</sup>	2000	$1.67 \pm 0.38$	$227 \pm 47$
MIL-68 <sup>94</sup>	2000	$13.24 \pm 0.52$	$402 \pm 13$
UiO-66-30%-B <sup>71</sup>	1000	$6.01 \pm 0.2$	$185 \pm 10$
	2000	$6.0 \pm 0.2$	$180 \pm 14$
UiO-66-30%-A <sup>71</sup>	1000	$4.8 \pm 0.3$	$169 \pm 16$
	2000	$4.6 \pm 0.2$	$155 \pm 13$
HKUST-1 <sup>100</sup>	1000	$15.25 \pm 0.61$	$761 \pm 53$
MOF-808 <sup>100</sup>	1000	$4.61 \pm 0.32$	$122 \pm 14$
UiO-66-COOH <sup>101</sup>	3000	$15.471 \pm 0.25$	$589 \pm 18$
UiO-66-NH <sub>2</sub> <sup>101</sup>	3000	$11.959 \pm 0.243$	$334 \pm 9$
UiO-66-(OH) <sub>2</sub> <sup>101</sup>	3000	$10.251 \pm 0.142$	$331 \pm 2$
HKUST-1 <sup>32</sup>	2000	$9.3 \pm 0.3$	$460 \pm 30$
UiO-66 <sup>98</sup>	2000	$2.06 \pm 0.2$	$72 \pm 12$
RhB@UiO-6698	2000	$3.02 \pm 1.59$	$145 \pm 101$
FI@UiO-66 <sup>98</sup>	2000	$3.79 \pm 0.42$	$151 \pm 27$
7MC@UiO-66 <sup>98</sup>	2000	$5.91 \pm 1.38$	$263 \pm 114$

View Article Online

DOI: 10.1039/D5MA01105A

# Open Access Article. Published on 08 listopadu 2025. Downloaded on 13.11.2025 7:46:18. [66] BY This article is licensed under a Creative Commons Attribution 3.0 Unported Licence.

## While conventional techniques such as powder X-ray diffraction (PXRD), gas sorption analysis, and electron microscopy provide essential information on the structure, porosity, and morphology of MOF monoliths, they often fall short of revealing the nanoscale features that dictate macroscopic mechanical and functional properties. The complex, often heterogeneous architecture of monoliths, comprising nanoparticles, grain boundaries, potential amorphous phases, and in composites, guest molecules-demands characterisation tools with superior spatial resolution and multifunctional capabilities.<sup>38</sup> Recently, a suite of advanced nanocharacterisation techniques has been leveraged to provide these critical, mechanistic insights, moving beyond bulk averaging to probe local phenomena. Atomic Force Microscopy (AFM) has emerged as a pivotal technique for visualising the results of mechanical interaction at the nanoscale. Its primary advantage lies in its ability to generate high-resolution, three-dimensional topographical maps of a surface after testing, offering unambiguous evidence of

This was demonstrated by Tian et al.  $^{32}$  in their study of a sol-gel derived HKUST-1 monolith for methane storage. The mechanical robustness of the monoHKUST-1 monolith, a critical property for its application in high-pressure gas storage, was comprehensively characterized via nanoindentation and Atomic Force Microscopy (AFM), as summarized in **Figure 22**. The nanoindentation results (**Figure 22a,b**) quantified the bulk mechanical properties, showing that the monolith possessed a Young's modulus of  $9.3 \pm 0.3$  GPa and, most notably, a hardness of  $460 \pm 30$  MPa. This hardness value was more than double that of any conventional HKUST-1 material reported previously, a fact highlighted in the inset of Figure 4b. An optical micrograph (**Figure 22c**) of the sample surface showed an array of these indents, providing a macroscopic

deformation behaviour that complements quantitative data from nanoindentation.

This article is licensed under a Creative Commons Attribution 3.0 Unported Licence

Open Access Article. Published on 08 listopadu 2025. Downloaded on 13.11.2025 7:46:18.

view that confirmed the tests were performed successfully and repeatedly across the material problem of the tests were performed successfully and repeatedly across the material problem of the tests were performed successfully and repeatedly across the material problem of the tests were performed successfully and repeatedly across the material problem of the tests were performed successfully and repeatedly across the material problem of the tests were performed successfully and repeatedly across the material problem of the tests were performed successfully and repeatedly across the material problem of the tests were performed successfully and repeatedly across the material problem of the tests were performed successfully and repeatedly across the material problem of the tests were performed successfully and repeatedly across the material problem of the tests were performed successfully and repeatedly across the material problem of the tests were performed by the test of the te

Crucially, AFM imaging of the residual indents (Figure 22d) was employed to move beyond numerical values and visualize the nanoscale quality of the deformation. The primary advantage of AFM here was its ability to provide a high-resolution, three-dimensional topographical map of the impression left by the indenter. The profile revealed a well-defined pit with smooth walls and, most importantly, a complete absence of surface cracking or radial fractures emanating from the edges. This evidence was the definitive visual proof of the monolith's superior mechanical resilience. It demonstrated that under intense local stress, the material underwent plastic deformation rather than brittle fracture. This finding directly correlated with the high hardness values, confirming that the sol-gel process had successfully created a dense, monolithic structure capable of resisting permanent deformation and mechanical damage, a vital requirement for any material destined for practical, industrial use.

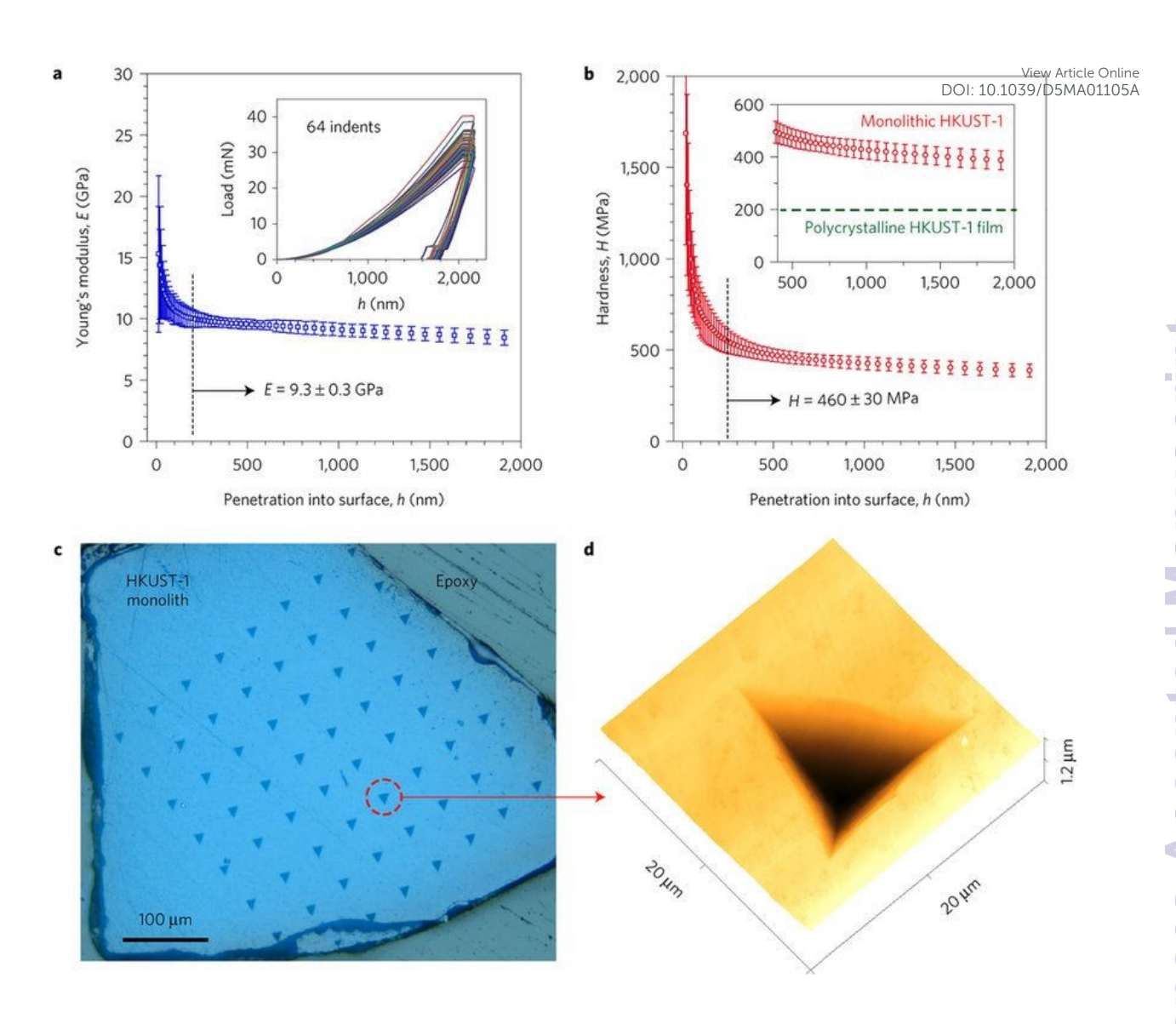


**Figure 22**: Nanoindentation on monoHKUST-1. (a,b) Young's modulus and hardness, respectively, as a function of indentation depth. (c) Optical micrograph showing the array of residual indents. (d) AFM profile depicting the 3D topography of a representative indent. <sup>32</sup> Reproduced with permission from reference **32**, under the terms of the Creative Commons Attribution License (CC BY).

Tricarico *et al.*<sup>35</sup> combined nano-FTIR spectroscopy with AFM-based methods (Tip Force Microscopy) to deconvolute the deformation mechanisms of ZIF-8 and ZIF-71 monoliths. The AFM topographical images and cross-sectional profiles, as illustrated in **Figure 23**, showed that the residual indents from Berkovich, cube corner, and spherical tips exhibited quite an insignificant pile-up at their edges. This observation is a critical signature of a material that undergoes plastic deformation with negligible work hardening. Furthermore, the images

cube corner tip designed to initiate fractures. These AFM findings provided direct visual evidence that supported the authors' proposed deformation mechanism: grain boundary sliding (GBS). In the nanocrystalline structure of the monoliths, plastic flow is accommodated by nanograins sliding past one another, a process that does not lead to the dislocation accumulation that causes work hardening and pile-up. Thus, the AFM data served as the crucial visual proof linking the monoliths' unique sol-gel-derived nanostructure to their ductile, plastic mechanical behaviour under compressive load. The corresponding cross-sectional profiles show the depth of the indent and the minimal material pile-up at the edges, indicating ductile deformation with negligible work hardening.

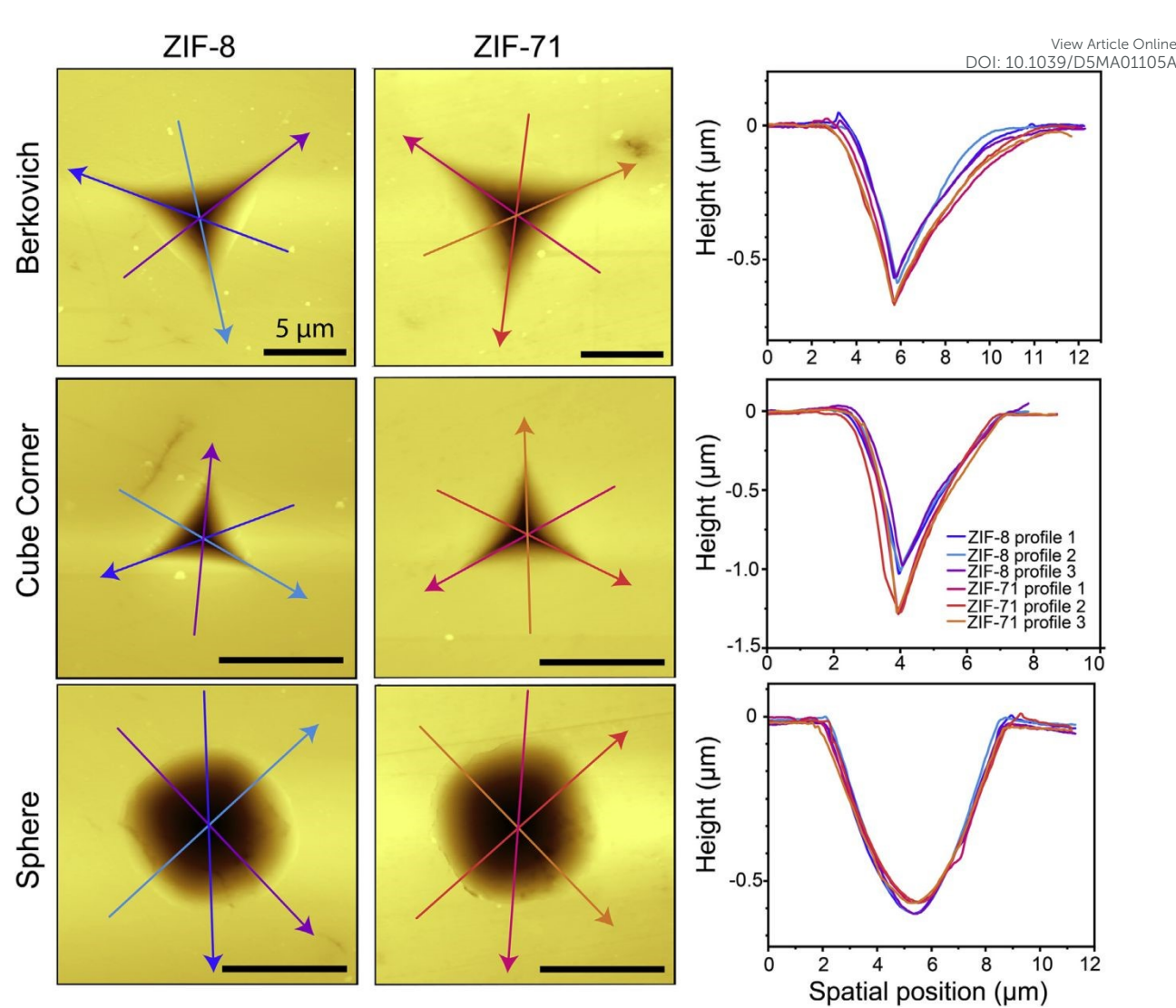
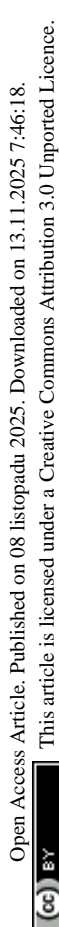


**Figure 23:** AFM height topography of the residual indents of Berkovich, cube corner, and spherical indentations for ZIF-8 and ZIF-71 monoliths. <sup>35</sup>Reproduced with permission from reference **35**, Copyright (2022) Elsevier B. V.

Later, Tricarico *et al.*<sup>98</sup> further advanced this approach by applying nano-FTIR to composite monoliths, using its nanochemical sensitivity to rule out framework alteration and prove that mechanical heterogeneity originated from physical guest distribution rather than chemical change. In their study, on luminescent monolithic MOFs, they employed an emerging nanoscale characterization tool known as near-field infrared nanospectroscopy (nano-FTIR) to unravel the complex structure-property relationships within their materials (**Figure 24**) This advanced technique bypasses the diffraction limit of conventional infrared spectroscopy by

utilizing a metallic atomic force microscope tip to act as an optical antenna, enabling Maditlo Antenna, enabling Maditlo

The authors leveraged this powerful tool to investigate the origin of the significant scatter in mechanical properties observed across their monoliths. Analysis was performed on the two distinct morphological phases identified-"smooth" and "porous". The key finding was that the local IR spectra from both phases across all composites were virtually identical and matched the bulk spectrum of pristine UiO-66, as illustrated in Figure 24d. This confirmed the preservation of the MOF's chemical framework integrity throughout the monolith despite the mechanical heterogeneity. However, the exquisite sensitivity of nano-FTIR did reveal a subtle yet crucial detail in the RhB@UiO-66 composite, the spectra from the mechanically softer "porous" phase showed a slight merging of the characteristic UiO-66 peak at ~1390 cm<sup>-1</sup> with peaks attributable to the rhodamine B dye. This indicated the presence of aggregated dye molecules residing in the intergranular macropores between MOF nanoparticles, rather than being neatly confined within the framework's nanopores. This finding directly explained the reduced stiffness of the "porous' phase, as these aggregate-rich regions created mechanically weaker zones, while the "smooth" phase, with its well-confined guests, exhibited superior mechanical performance. Thus, by providing nanoscale chemical evidence, nano-FTIR was instrumental in correlating the physical location of the guest molecules with the macroscopic mechanical behaviour of the monolithic composites.



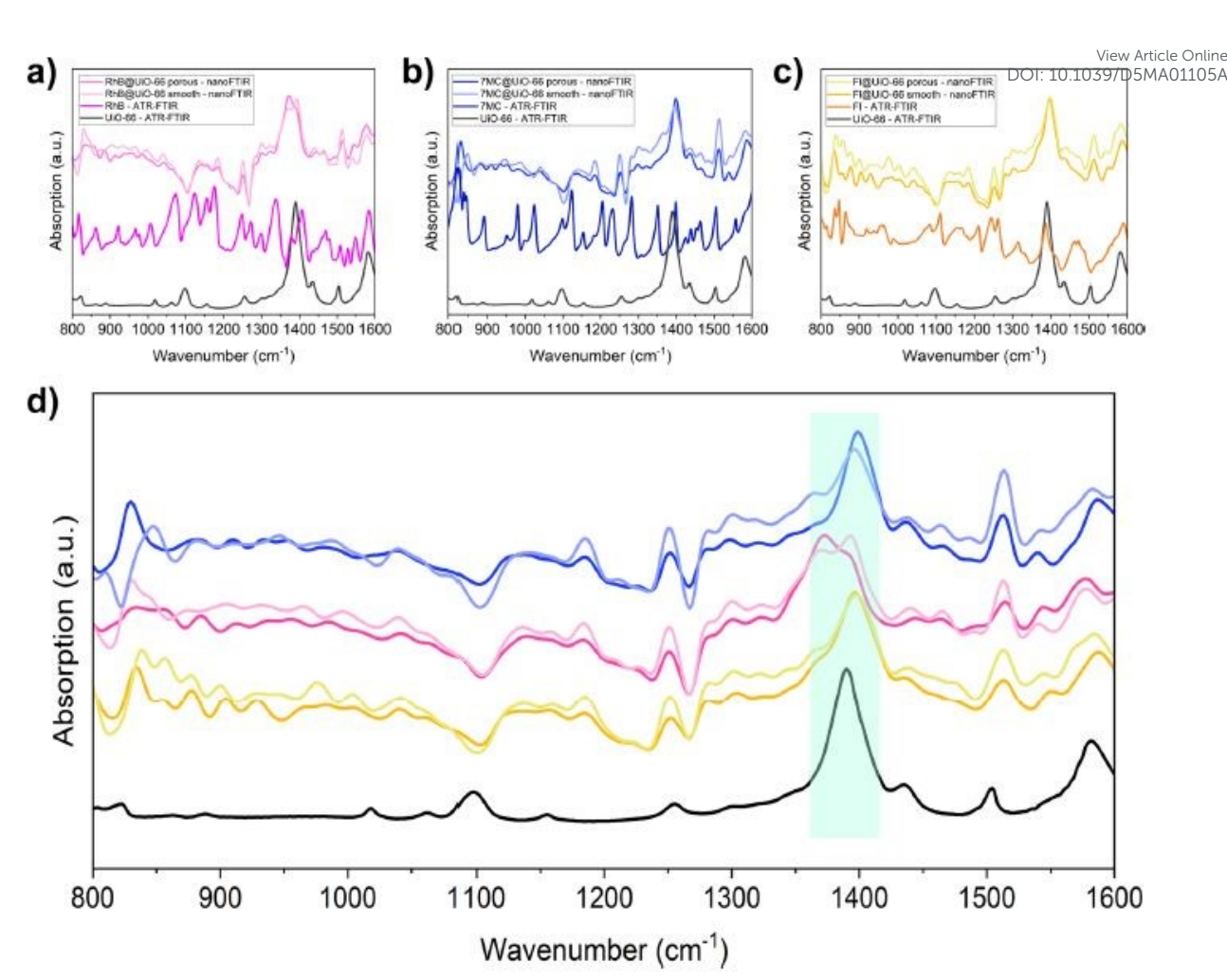


**Figure 24:** Far-field ATR-FTIR and nearfield nano-FTIR spectra of (a) RhB@monoUiO-66, (b) 7MC@monoUiO-66, and (c) Fl@monoUiO-66. (d)Comparison of the nano-FTIR (local) spectra of the porous and smooth phase of the three composites and the ATR-FTIR (bulk) spectrum of the pristine UiO-66 monolith (black trace). Characteristic vibrational mode of UiO-66 at 1390 cm<sup>-1</sup> is highlighted in green. <sup>98</sup> Reproduced with permission from reference **98**, Copyright (2024). America Chemical Society.

The adoption of these advanced techniques is transforming understanding of structure-property relationships in monolithic MOFs. Looking forward, the integration of techniques like nanoindentation mapping (e.g., NanoBlitz 3D) to quantitatively spatialise mechanical properties, and in situ mechanical testing within electron microscopes to observe deformation in real-time, will provide the next level of insight. These emerging tools are not merely for characterisation; they are essential guides for the rational design of next-generation monoliths with bespoke mechanical and functional properties for targeted applications.

This article is licensed under a Creative Commons Attribution 3.0 Unported Licence

Open Access Article. Published on 08 listopadu 2025. Downloaded on 13.11.2025 7:46:18.

APPLICATION OF MONOLITHIC MOFS

View Article Online DOI: 10.1039/D5MA01105A

**Catalysis** 

Monolithic MOFs offer significant advantages over their powdered counterparts in catalytic

applications due to their structural integrity, enhanced mass transfer properties, and ease of

handling. 25-27 Their high surface area provides a large number of active sites while also

facilitating efficient substrate diffusion, which is crucial for improving catalytic performance.

The interconnected hierarchical pore network typical of many monoliths combines

microporosity, for size and shape selectivity, with meso- and macroporosity, which function as

transport arteries to drastically reduce mass transfer limitations and prevent pore clogging. This

enhanced mass transfer is less prone to clogging when applied in flow reactors, making them

ideal for continuous processes. Additionally, their open porosity and interconnected networks

enhance reactant accessibility to active sites, ensuring efficient conversion rates in both gas

and liquid-phase reactions<sup>102</sup>

The mechanical robustness of monolithic structures allows for easy integration into catalytic

reactors, simplifying catalyst packing, recovery, and reuse, which is a critical advantage for

industrial application <sup>103</sup>. Furthermore, the monolithic format provides a versatile platform for

creating multi-functional systems, where the MOF itself can be the catalyst, or it can serve as

a high-surface-area support for other catalytic species (e.g., metal nanoparticles) distributed

throughout the 3D framework <sup>104,103</sup>

A study by Mehta et al. 103 demonstrated the advantage of monolithic MOFs in catalyst

recovery and reuse. The authors developed a sol-gel method to synthesize a robust, monolithic

ZIF-8 framework (monoZIF-8) and encapsulated SnO<sub>2</sub> nanoparticles (NPs) within it in situ to

create a SnO<sub>2</sub>@monoZIF-8 composite. This approach directly addressed the critical challenges

This article is licensed under a Creative Commons Attribution 3.0 Unported Licence

Open Access Article. Published on 08 listopadu 2025. Downloaded on 13.11.2025 7:46:18.

of using powdered NP@MOF composites such as difficult handling, NP agglomeration Viguration Additional NP agglomeration Viguration Viguration Additional NP agglomeration Viguration Vigura catalyst loss. The monolithic MOF provided a rigid, high-density scaffold that prevented NP leaching and allowed for incredibly facile catalyst recovery after reaction cycles via simple gravity filtration (Figure 25).

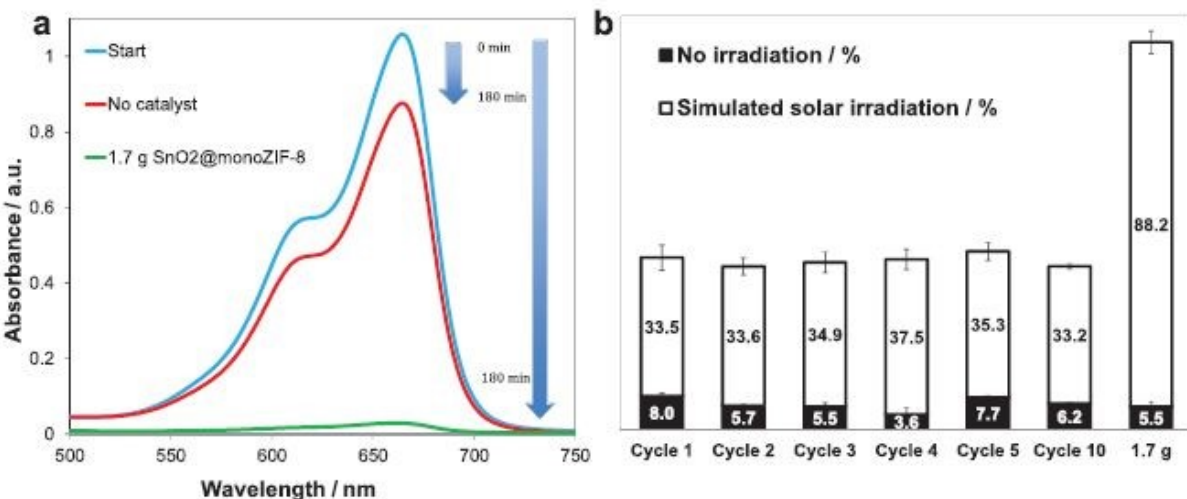
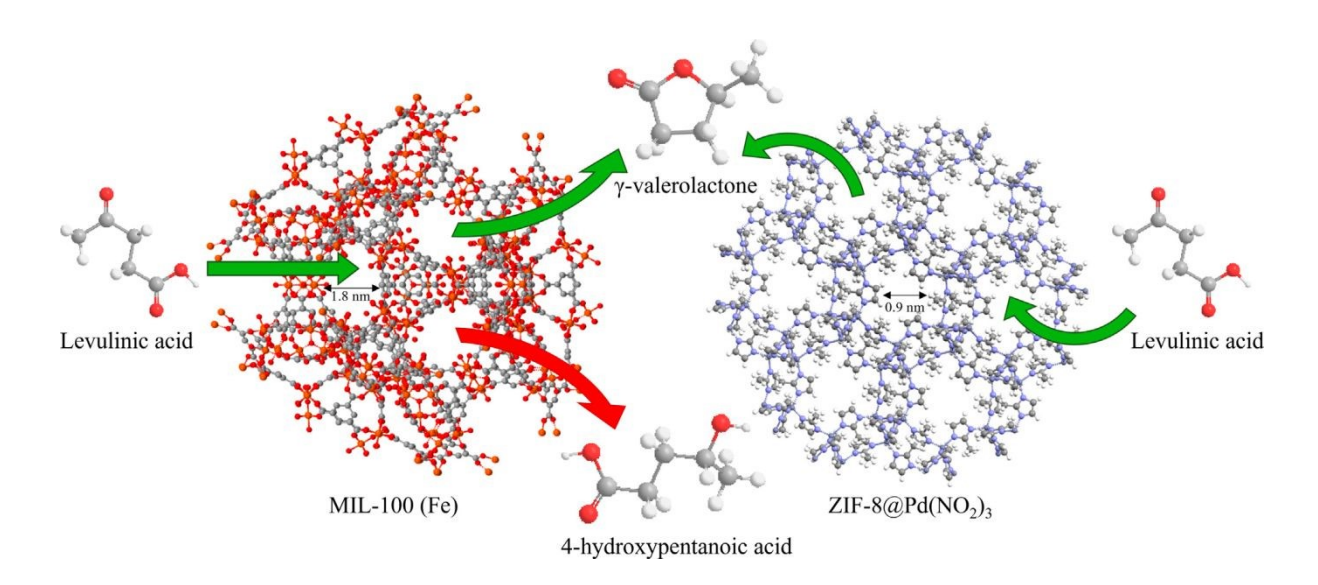


Figure 25. a) Photocatalytically induced spectral changes to aqueous MB dye  $(1.55 \times 10^{-5} \text{ M})$ highlighting degradation of the absorption maximum at 664 nm in the absence of composite (red) and presence of 1.7 g SnO<sub>2</sub>@<sub>mono</sub>ZIF-8 (green) after 3 h of simulated solar irradiation. b) Degradation of MB in the presence of 0.4 g (cycles 1–5 and 10) and 1.7 g of SnO<sub>2</sub>@<sub>mono</sub>ZIF-8. 103 Reproduced with permission from reference 103, under Creative Attribution Licence (CC BY).

McIntyre et al. 102 investigated the use of monolithic MOFs, specifically MIL-88B, MIL-100, and ZIF-8@Pd(NO<sub>3</sub>)<sub>2</sub> as catalysts for the transfer hydrogenation of levulinic acid (LA) to γvalerolactone (GVL), a valuable green solvent and fuel precursor. The study highlights the critical role of mass transport and diffusion limitations in determining catalytic selectivity and stability, particularly under basic aqueous conditions.

The monolithic forms of these MOFs were synthesized via modulated sol-gel methods, providing structural integrity, and facilitating handling compared to powdered analogues. As illustrated in Figure 26, the reaction involves the conversion of LA over different monolithic MOF catalysts. The authors demonstrated that despite having lower noble metal contents Machines More and MIL-100 catalysts achieved comparable conversion rates to the Pddoped ZIF-8 catalyst. However, the hydrophilic nature of the iron-based MOFs led to hydrolytic degradation over multiple cycles, reducing their long-term stability.



**Figure 26:** Schematic representation of levulinic acid conversion over monolithic MOF catalysts. <sup>102</sup> Reproduced with permission from reference **102**, under Creative Attribution Licence (CC BY)

A key finding was the role of pore architecture in product selectivity. The smaller pore apertures of ZIF-8@Pd(NO<sub>3</sub>)<sub>2</sub> (**Figure 27 C**) restricted side reactions, consistently yielding GVL selectivity above 80%, whereas the larger-pore MIL frameworks (**Figures 27 A, B**) showed decreased selectivity due to substrate accumulation and pore blockage.

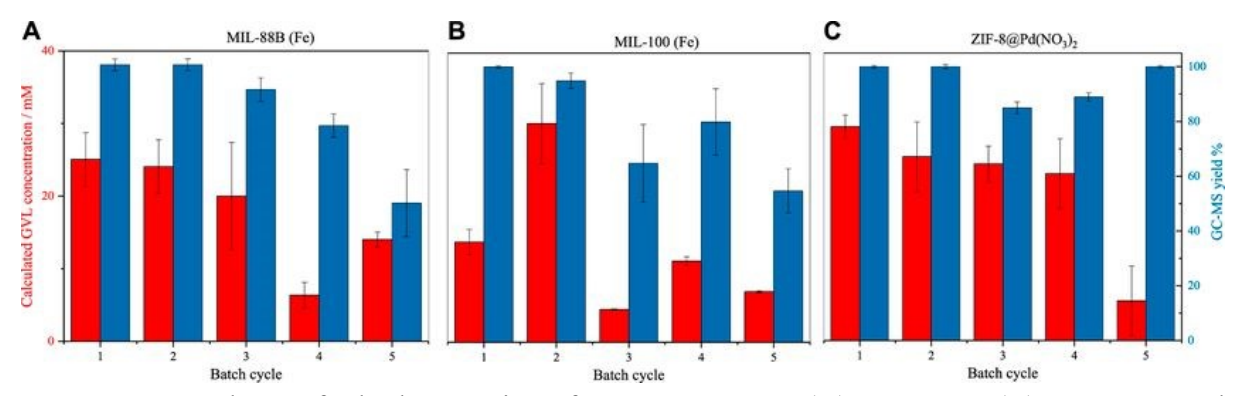


Figure 27: Batch transfer hydrogenation of LA to GVL over (A) MIL-88B, (B) MIL-100, and

(C) ZIF-8@Pd(NO<sub>3</sub>)<sub>2</sub>, showing conversion and selectivity over time.<sup>102</sup> Reproduced Virgidial Conline permission from reference **102**, under Creative Attribution Licence (CC BY).

Using zero-length column (ZLC) methods, the authors quantified diffusion constants and mass transfer coefficients, revealing that ZIF-8 exhibited superior mass transfer properties due to its hydrophobic nature and hierarchical porosity. This enhanced transport contributed to higher selectivity and reduced fouling. In contrast, the hydrophilic MIL frameworks suffered from slower diffusion and eventual structural collapse under basic conditions. This study underscores the importance of monolithic MOF design, combining micro- and mesoporosity-to optimize mass transfer and catalytic performance in liquid-phase biomass conversion reactions. It also highlights the trade-offs between activity, selectivity, and stability when selecting MOF platforms for sustainable catalytic processes.

Structuring MOFs into monolithic forms transcends mere shaping for practical handling; it is a critical strategy that fundamentally enhances their catalytic efficacy and viability. By integrating microporosity for molecular selectivity with meso- and macroporous networks that serve as transport arteries, monolithic MOFs drastically mitigate mass transfer limitations inherent to powdered counterparts, leading to improved reaction rates and selectivity. Furthermore, their macroscopic integrity facilitates seamless integration into continuous-flow reactors, eliminates issues of pressure drop and particle clogging, and enables effortless catalyst recovery and reuse, thereby addressing key barriers to the industrial adoption of MOF-based catalysts. This unique synergy of enhanced molecular-level performance and superior process-level operation solidifies monolithic MOFs as a transformative platform for advancing sustainable catalytic processes. Monolith MOFs that have been used for catalysis are presented in **Table 5**.

Open Access Article. Published on 08 listopadu 2025. Downloaded on 13.11.2025 7:46:18.

This article is licensed under a Creative Commons Attribution 3.0 Unported Licence.

**Table 5**: A summary of selected Monolith MOFs used in catalysis.

View Article Online DOI: 10.1039/D5MA01105A

mono MOF	Catalytic Activity	Comparison with powder		
		counterpart		
MIL -88B	Transfer hydrogenation of	Improved conversion ratio		
	Levulinic acid to γ-valerolactone			
MIL- 100	Transfer hydrogenation of	Showed similar initial activity but		
	Levulinic acid to γ-	had the poorest stability, with severe		
	valerolactone 102	permanent deactivation after just 2		
		cycles caused by rapid framework collapse.		
ZIF-8 @ Pd(NO <sub>3</sub> ) <sub>2</sub>	Transfer hydrogenation of	Displayed superior hydrolytic		
	Levulinic acid to γ-valerolactone	stability over 5 cycles due to its		
	102	hydrophobic framework. Activity		
		decline was attributed to pore		
		blockage rather than structural		
		degradation. Exhibited micropore		
M ZIE 0		diffusion limitations.		
M-ZIF 8	Catalytic condensation of	Presence of large mesopores in M-		
	malononitrile and benzaldehyde	ZIF8 contributed to improved rate of		
	into benzylidenemalononitrile	catalytic activity compared to that of a general ZIF-8 MOF <sup>105</sup>		
ZIF -8	Knoevenagel reaction between	Enhanced reaction kinetics due to		
	benzaldehyde and <sup>20</sup>	hierarchical macroporosity enabling		
		efficient flow-through catalysis. The		
		ZIF-8 monolith achieved 100%		
		conversion in under 130 seconds, far		
		surpassing the catalytic performance		
		of ZIF-8 powder, which took ~3		
11.0 ((		hours to complete the same reaction.		
monoUiO-66	Catalytic hydrolysis of methyl	Turnover frequency for mono UiO <sub>66</sub>		
	paraoxon to 4- nitrophenol	was 0.48 s <sup>-1</sup> while that of powder UiO <sub>66</sub> 0.94 s <sup>-1</sup> . This suggests the		
		monolith may have introduced		
		diffusion limitations or reduce		
		accessibility of active sites compared		
		to the powdered form. <sup>51</sup>		
SnO <sub>2</sub> @ <sub>mono</sub> ZIF-8	Photocatalytic degradation of	Improved photocatalytic activity and		
_	methylene blue	reusability, up to 10 times with no		
		loss of activity. 103		
Cu-BTC silica monolith	Catalytic oxidation of	Excellent yield with reduced reaction		
	alkylbenzene to ketones	time. <sup>104</sup>		

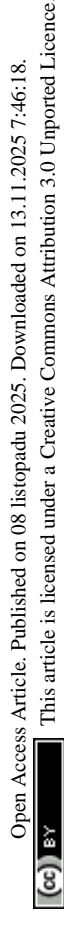
## Gas storage and adsorption

The environmental benefits of cleaner gaseous fuels like natural gas and hydrogen are well-documented, yet their widespread adoption is hindered by limitations in current gas storage

tunable pore sizes, and engineered geometries, making them ideal for gas storage applications.

Their porous structure facilitates rapid gas diffusion, enabling faster adsorption/desorption cycles which are critical for practical storage systems. Unlike powdered MOFs, monoliths exhibit minimal pressure loss during adsorption, superior heat and mass transfer, and attrition resistance, owing to their uniform flow channels and dense, stable architectures. 49

Madden et al.,31 demonstrated that the exceptionally high-density structure of monoHKUST-1 enables record-breaking hydrogen storage performance. The unique synthesis mechanism preserves porosity after shaping and yields benchmark volumetric BET areas, resulting in outstanding H<sub>2</sub> sorption characteristics. As illustrated in Figure 28, monoHKUST-1 displays a hydrogen adsorption capacity of 10.1 g L-1 at 25 °C and 100 bar, represents the highest measured H<sub>2</sub> capacity of a densified MOF using its true density under these conditions. At 100 bar, mono HKUST-1 stores more hydrogen than compressed gas or powdered HKUST-1, owing to its compact morphology and minimized interparticle voids. Under cryogenic temperaturepressure swing conditions from 100 bar at 77 K to 5 bar at 160 K, it delivers a greater usable hydrogen amount, highlighting its excellent adsorption-desorption reversibility and structural integrity. At 77 K across varying pressures, monoHKUST-1 consistently outperforms powdered MOF and even an empty tank in deliverable capacity. Notably, it achieves H<sub>2</sub> working capacities at 25 bars under cryogenic conditions, performance previously only possible by compressing hydrogen to 700 bars at ambient temperature. This reduction in required operating pressures holds promise for lowering engineering demands and costs while enhancing the safety of onboard hydrogen storage systems for vehicular applications. Furthermore, the monolithic structure reduces material degradation typically seen in HKUST-1 powders, as an oxidized surface layer shields the internal particles from moisture, preserving high performance even after extended atmospheric exposure.



a ----HKUST-1 20 H<sub>2</sub> Uptake (g L<sup>-1</sup>) H<sub>2</sub> Uptake (g L<sup>-1</sup>) 50 0 Temperature (°C) 50 100 Pressure (bar) d C 60 Empty Tank 7.50 "HKUST-1 Uptake (g L<sup>-1</sup>) 940 Ē20 77 K £ 10 10

50 10 Pressure (bar)

100

View Article Online DOI: 10.1039/D5MA01105A

Figure 283: a) H<sub>2</sub> uptake of monoHKUST-1at different temperatures b) Volumetric storage of monoHKUST-1 compared to compressed gas at 100 bars c) H<sub>2</sub> delivery under cryogenic conditions and d) Deliverable H<sub>2</sub> capacity of monoHKUST-1 compared to HKUST-1 powder and an empty tank at various adsorption pressures at 77 K. <sup>31</sup> Reproduced with permission from reference **31**. Copyright (2022) American Chemical Society.

25

50 Pressure (bar)

100

The same architectural advantages translate to methane storage, where mono HKUST-1 approaches the US Department of Energy (DOE) target of 263 cm<sup>3</sup>(STP)/cm<sup>3</sup>, a 30-50% improvement over pelletized/powdered forms.<sup>32,106</sup> The volumetric adsorption isotherms illustrated in Figure 29 demonstrate mono HKUST-1's superior capacity, approaching the target of 263 cm<sup>3</sup>(STP)/cm<sup>3</sup> at high pressure, while pelletized forms show reduced uptake due to pore collapse from compression. Kinetic analysis reveals faster methane adsorption in the monolith across all pressures, attributed to its hierarchical pore structure enhancing gas diffusion. Pressure decay measurements further confirm the monolith's stability, exhibiting slower pressure drop at 40 bar due to better heat dissipation and stronger gas-framework interactions. Together, these results establish monolithic HKUST-1 as technologically advantageous for

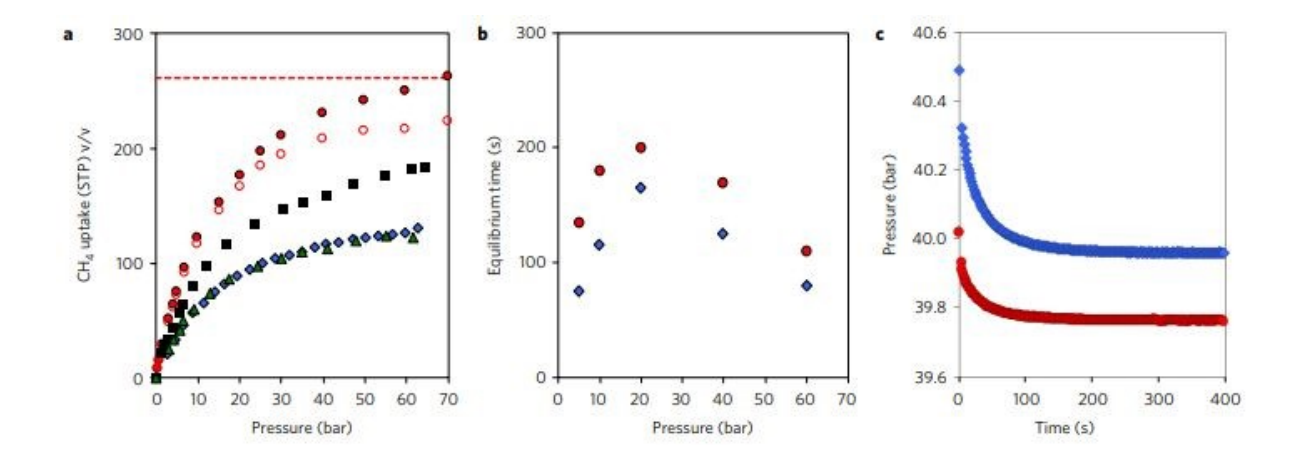


**Figure 294:** Gas adsorption in HKUST-1. a) Comparison of absolute volumetric methane adsorption isotherms at 298 K on monoHKUST-1 (red filled circles), excess volumetric uptake on monoHKUST-1 (red open circles), HKUST-1 pellets under hand packing (blue diamonds), HKUST-1 pellets packed under 27.6MPa (black squares), and HKUST-1 pellets under 68.9MPa (green triangles). b) Equilibrium time of methane adsorption at 298 K as a function of equilibrium pressure, and c) decay of pressure with time at 40 bar for monoHKUST-1 (blue diamonds) and powdHKUST-1 (red circles). <sup>32</sup> Reproduced with permission from reference **32**. Copyright (2017) Springer Nature Limited.

This article is licensed under a Creative Commons Attribution 3.0 Unported Licence

Open Access Article. Published on 08 listopadu 2025. Downloaded on 13.11.2025 7:46:18.

Lawson *et al.*<sup>56</sup> prepared polyethyleneimine (PEI) and tetraethylenepentamine (TEPA) impregnated MIL-101monoliths MOFs using 3D printing technique, through pre- and post-functionalization approaches, and evaluated their CO<sub>2</sub> capture performances. The adsorption analysis results indicated that all impregnated monoliths showed improved CO<sub>2</sub> capacities from the pristine monolith at dilute concentrations, and pre-impregnation yielded higher CO<sub>2</sub> uptakes than post-impregnation. Specifically, the pre-impregnated TEPA and pre-impregnated PEI monoliths, with 3.5 and 5.5 mmol N/g amine content, respectively, displayed a capture capacity of 1.6 and 1.4 mmol/g, respectively, at 3000 ppm and 25 °C.

**Figure 30** compares the CO<sub>2</sub> adsorption performance of powdered and monolithic forms of HKUST-1, UiO-66, and UiO-66-NH<sub>2</sub> through gravimetric and volumetric isotherms at 298

K. 85 While powdered MOFs exhibit higher gravimetric uptake due to their greater sufficie online area, 33 monolithic MOFs address a critical challenge in industrial deployment by combining high bulk density 32 with preserved sorption performance, enabling superior volumetric separation efficiency in applications like carbon capture and gas purification. 34

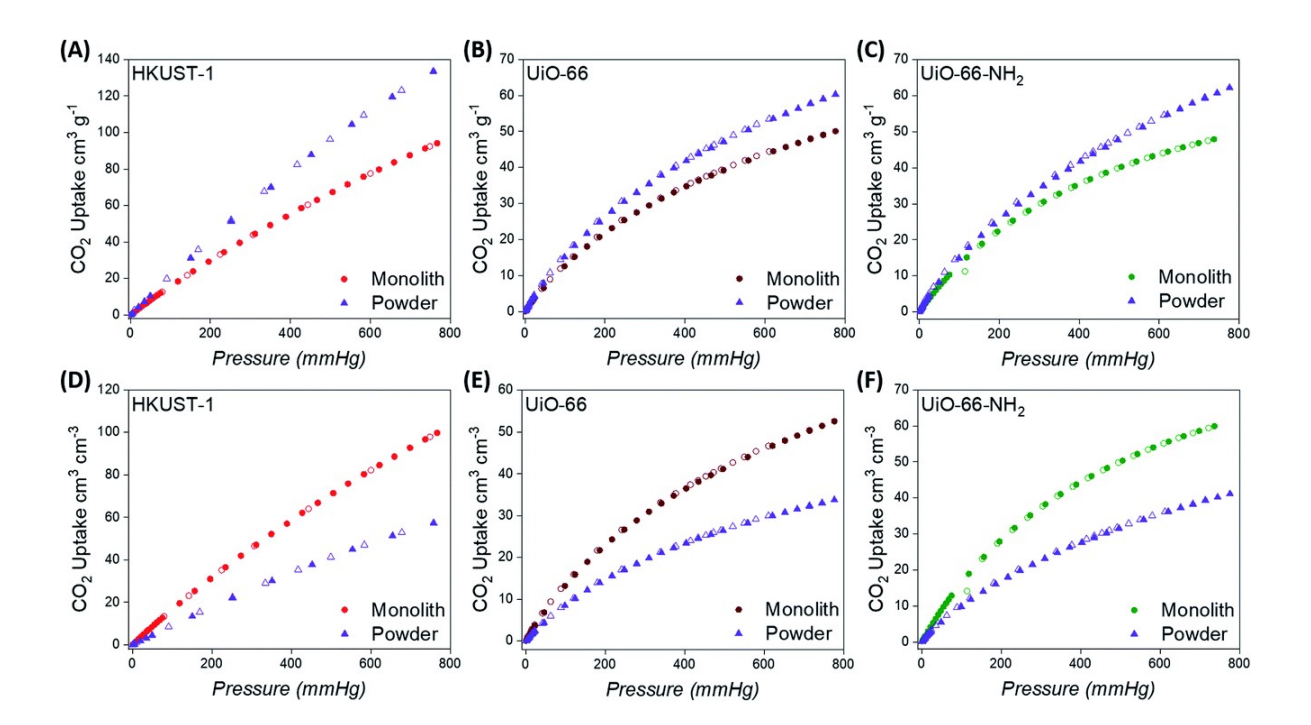


**Figure 305**: Gravimetric (A–C) and volumetric (D–F) CO<sub>2</sub> adsorption isotherms at 298 K for monolithic and powdered HKUST-1, UiO-66 and UiO-66-NH<sub>2</sub> materials. Closed symbols represent adsorption while open symbols represent desorption. <sup>85</sup> Reproduced from Reference **85**, with permission from the Royal Society of Chemistry.

### **Energy storage**

MOFs have gained considerable attention for energy storage applications due to their tunable porosity, high surface areas, and chemical versatility. However, conventional MOF powders often suffer from poor electrical conductivity and mechanical instability, limiting their performance in devices such as superconductors and batteries. The development of monolithic MOFs offers a promising route to overcome these challenges by creating robust, continuous structure with enhanced electrical properties.<sup>34, 57, 107</sup> The tunable architecture of monolithic

MOFs provides high strength while maintaining lightweight, making them portable entergyticle online storage systems. Additionally, the use of MOF precursors allows the resulting derivatives to possess numerous active sites, thereby improving the utilisation of the intrinsic active sites. The structural advantage translates to impressive performances across a range of energy-related applications, including batteries, supercapacitors, and electrocatalysis. 109

One innovative approach involves the fabrication of monolithic composites of MOFs and conductive additives like graphene. A particularly notable study<sup>107</sup> demonstrated the synthesis of a composite material based on HKUST-1 and commercial, non-modified graphene. In this method, a one-pot synthesis strategy was employed to produce a moldable composite without the need for graphene oxidation or chemical functionalization, which can otherwise degrade the electrical properties of graphene. By carefully controlling the graphene loading during synthesis, researchers were able to tune the porosity and achieve high surface areas ranging between 1078 and 1156  $m^2g^{-1}$ . Furthermore, the electrical conductivity of the resulting monolithic coatings showed a significant dependence on graphene content, reaching values from  $7.6 \times 10^{-6}$  S  $m^{-1}$  up to  $6.4 \times 10^{-1}$  S  $m^{-1}$  (Figure 31).

Moving forward, further research is needed to optimize the structural stability, conductivity, and scalability of monolithic MOFs for commercial energy storage applications. Strategies such as composite formation with conductive materials (e.g., graphene, carbon nanotubes), doping with transition metals, and hybridizing with other porous materials could significantly enhance their electrochemical properties. With continued innovation, monolithic MOFs are poised to play a critical role in the development of next-generation energy storage systems.

View Article Online

DOI: 10.1039/D5MA01105A

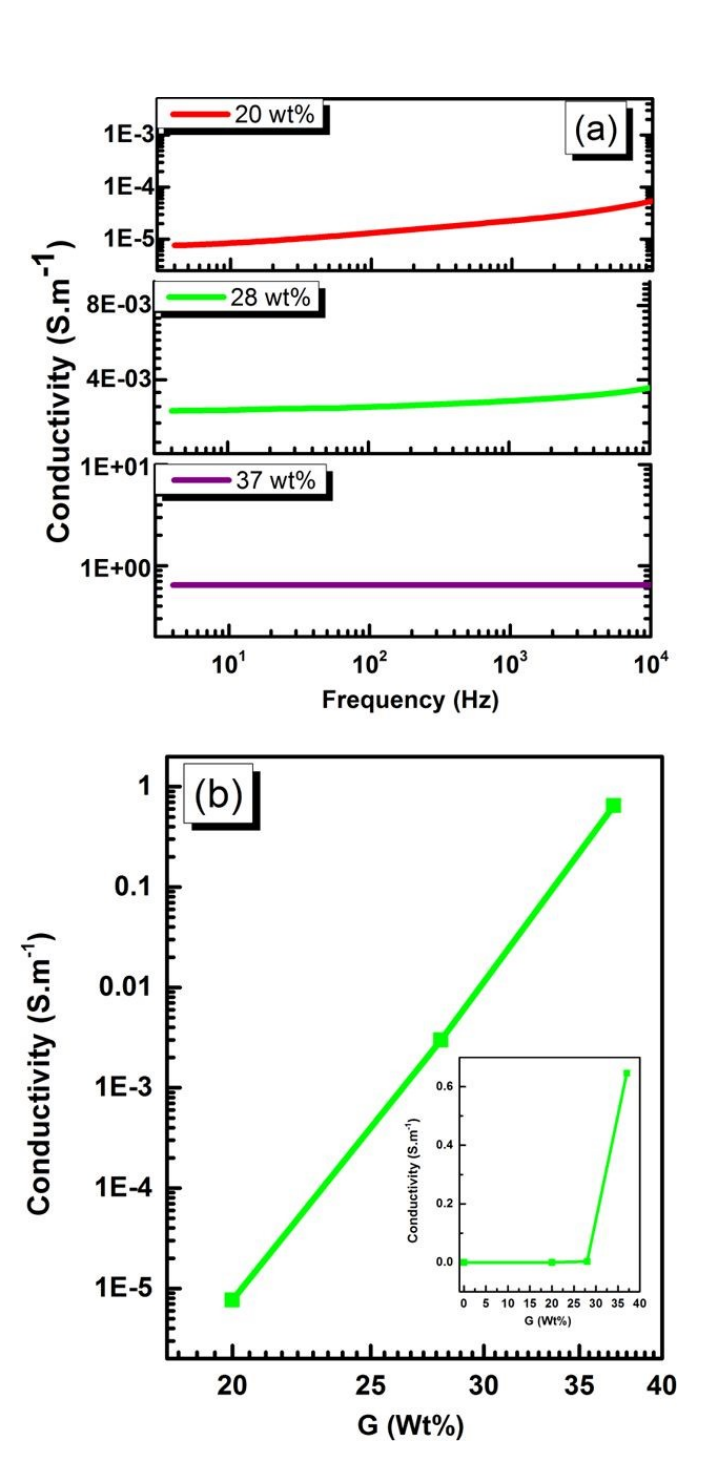


**Figure 31:** a) Conductivity measurements for several monoliths of HKUST-1 containing increasing loadings of G, and (b) electrical conductivity measured at 4 Hz for the three monolith composites. <sup>107</sup> Reproduced with permission from reference **107**. Copyright (2019) American Chemical Society.

Open Access Article. Published on 08 listopadu 2025. Downloaded on 13.11.2025 7:46:18.

[6c] BY This article is licensed under a Creative Commons Attribution 3.0 Unported Licence.

View Article Online DOI: 10.1039/D5MA01105A

Monolithic MOFs excel in adsorption, catalytic degradation, and membrane-based separation of contaminants. Their interconnected porosity facilitates rapid diffusion of water pollutants such as heavy metals, organic dyes, pesticides and pharmaceuticals with uptake capacities rivalling powdered MOFs. <sup>111, 112, 45</sup> These contaminants are often challenging to eliminate through conventional water treatment methods such as filtration, sedimentation, membrane bioreactors, and even advanced oxidation processes. To overcome these limitations, studies have demonstrated that monolith MOFs can be dispersed in wastewater to adsorb pollutants after which they can be recovered by filtration. Subsequently, the monolith MOFs can then be regenerated via solvent extraction, making them reusable and cost effective. <sup>90</sup>

For instance, Wang *et al.* developed a monolithic, hydrophobic ZIF-8 material (IPD-mesoMOF-12) by packing sufficiently small nanocrystals to create interparticle mesopores. The monolith exhibited a high BET surface area (1732 m²/g) and mesopore volume (up to 1.70 cm³/g). When tested for toluene removal from aqueous solution, it achieved a high Langmuir adsorption capacity of 242 mg/g, surpassing typical activated carbons, and reached equilibrium within 30 minutes. Critically, the monolith demonstrated excellent regenerability and the framework's structural integrity was maintained after recycling. <sup>45</sup>

Parsazadeh *et al.* <sup>111</sup> prepared an HKUST-1 monolith MOF and used it as an adsorbent for the removal of eosin yellow and malachite green dyes. The study concluded that the HKUST-1 monolith MOF exhibited high efficiency for dye removal, highlighting its potential as an effective adsorbent material. Similarly, Yao *et al.*, <sup>113</sup> applied a freeze casting procedure in liquid nitrogen to prepare Ti- MOF monolith /polymer composites. Dye adsorption experiments were conducted on methylene blue, methyl orange and indigo carmine. It was observed that efficient adsorption occurred across pH range of 3-9. This work successfully

demonstrated an alternative strategy for synthesising monolithic MOFs / polymer composite Molitobal offering a promising route for wastewater treatment application beyond the traditional use of powders. The results of the tests are shown in **Figure 32**, where the monolithic composite displays superior activity in wastewater treatment coupled to easier separation from solution.



**Figure 32:** Comparison of NH<sub>2</sub>-MIL-125(Ti) powder and monolith Ti-MOF@PEG10 composite in dye absorption. <sup>113</sup> Reproduced with permission from reference **113**. Copyright (2025), Elsevier B. V.

UiO-66-NH<sub>2</sub>-CS aerogel monolith synthesised by Liu *et al.* through covalent cross linking was used to investigate the adsorption of Pb<sup>2+</sup> from aqueous solutions. The success of this study shows that such synthesis methods may offer an effective route for transforming MOF powder particles into more flexible and mouldable forms, facilitating easier application in pollution treatment fields.<sup>114</sup> Similarly, Cu–BTC/NFC aerogel composites were synthesised using a direct mixing method, followed by gelation and freeze drying. Adsorption studies were carried out targeting the organic dye congo red and a heavy metal Mn<sup>7+</sup>. The Cu-BTC/ NFC monolith showed exceptional adsorption capacity for congo red and also acted as a reducing agent,

removing permanganate ions by reducing them to manganese dioxide as illustrated in Figure addition and a substrated in Figure 2011 and 115 and 115 are a substrated in Figure 2011 and 115 are a substrated in

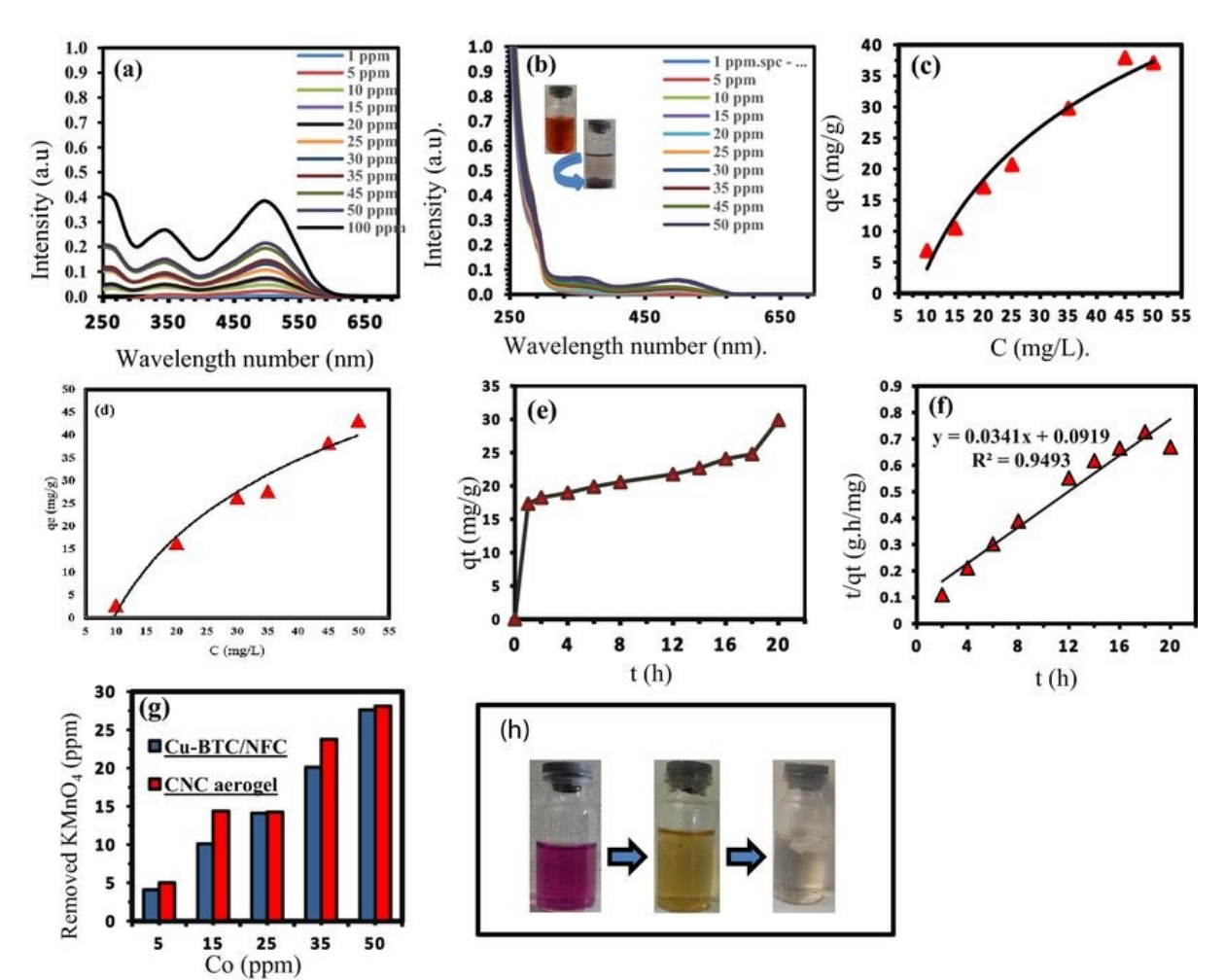


**Figure 33:** a) The UV–Vis spectra of aqueous solutions of congo red before adsorption, b) after exposing to Cu-BTC/NFC for 18 h, c) adsorption isotherm of Cu-BTC/NFC aerogel composite for various concentrations of Congo Red,, (d) adsorption isotherm for different concentrations of Congo Red in Cu-BTC/CNC aerogel composite, (e) The time dependency of the adsorption, (f) The pseudo-second-order model for the kinetics of the reaction, (g) The CNC aerogel and Cu-BTC/NFC aerogel composite adsorption isotherm for various concentrations of KMnO<sub>4</sub>. (h) The colour change process during the reduction of KMnO4. <sup>115</sup> Reproduced with permission from reference **115**. Copyright (2025) Springer Nature Limited.

Monolithic MOFs with large surface areas, tuneable wettabilities and good water resistance have been shown to play an important role in oil–water separations. In a recent study, a superhydrophobic (water contact angle of above 170°), water-stable MOF containing Cu<sup>2+</sup> and hexafluorinated dicarboxylate linkers was prepared. After coating on a porous support, the

This article is licensed under a Creative Commons Attribution 3.0 Unported Licence

Open Access Article. Published on 08 listopadu 2025. Downloaded on 13.11.2025 7:46:18.

monolithic MOF film exhibits excellent oil absorption capacities and reusability during Madillosa separation of hexadecane, biodiesel, toluene and crude oil from water. 90

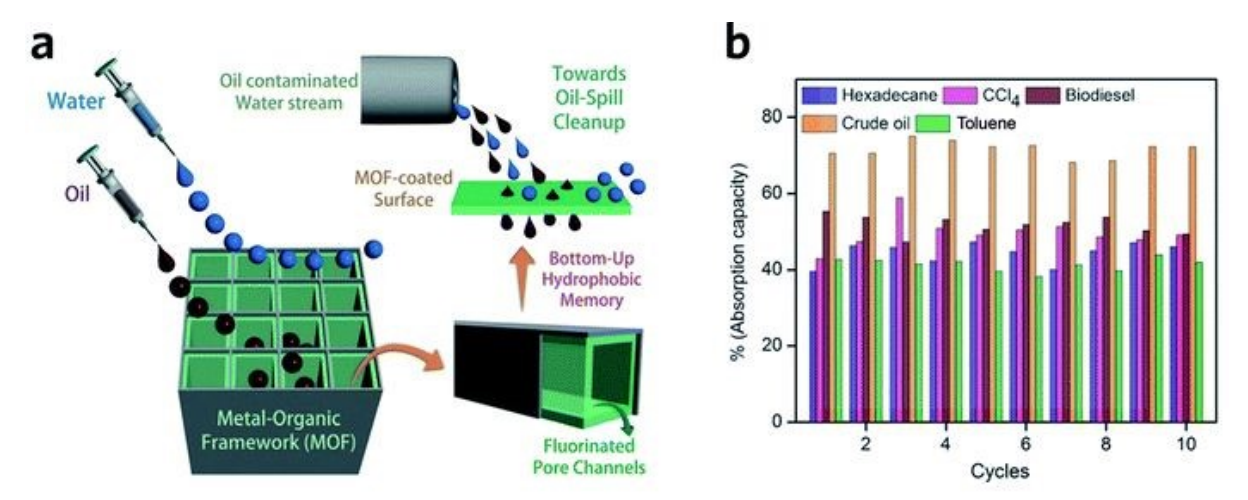


**Figure. 34** Oil-water separation using monolithic MOF materials. (a) Schematic diagram of oil-water separation with the monolith MOF containing fluorinated linkers. (b) Oil absorption capacities of the monolithic MOF containing fluorinated linkers. <sup>90</sup> Reproduced with permission from reference **90**. Copyright (2020) Royal Society of Chemistry

### **Sensing**

Detection is a critical process across many sectors of the chemical industry, driving essential operations such as pollution monitoring, industrial safety and medical diagnostics. In this context, monolithic materials have gained significant attention, offering unique advantages over traditional sensing materials. <sup>32</sup> A variety of sensing techniques have been developed utilising monoliths, particularly the electrical/chemi-resistive method. <sup>116, 117</sup>

A unique monolithic chemiresistor sensor was utilised for detection of formaldehyde, a probable carcinogen (**Figure 35**). TiO<sub>2</sub> was coated with monoZIF-7 providing a distinctive and selective pathway formaldehyde detection. The key innovation lies in the synergistic combination of two mechanisms: UV light activation of the TiO<sub>2</sub> layer at room temperature, which selectively enhances sensitivity to highly reactive gases like formaldehyde and ethanol while ignoring other interferents, and the molecular sieving effect of the ZIF-7/PEBA MMM

overlayer. The precisely tuned pore aperture of ZIF-7 (~0.3 nm) allows the small effective online formaldehyde molecules (0.373 nm) to diffuse through to the sensor surface while effectively blocking larger interfering gases such as ethanol (0.45 nm), benzene, and toluene (0.585 nm). This strategy resulted in exclusive, ultrasensitive detection of formaldehyde down to 25 ppb with an ultrahigh selectivity ratio (>50) over ethanol at room temperature. This monolithic design led to improved sensitivity and stability compared to conventional sensor coatings.

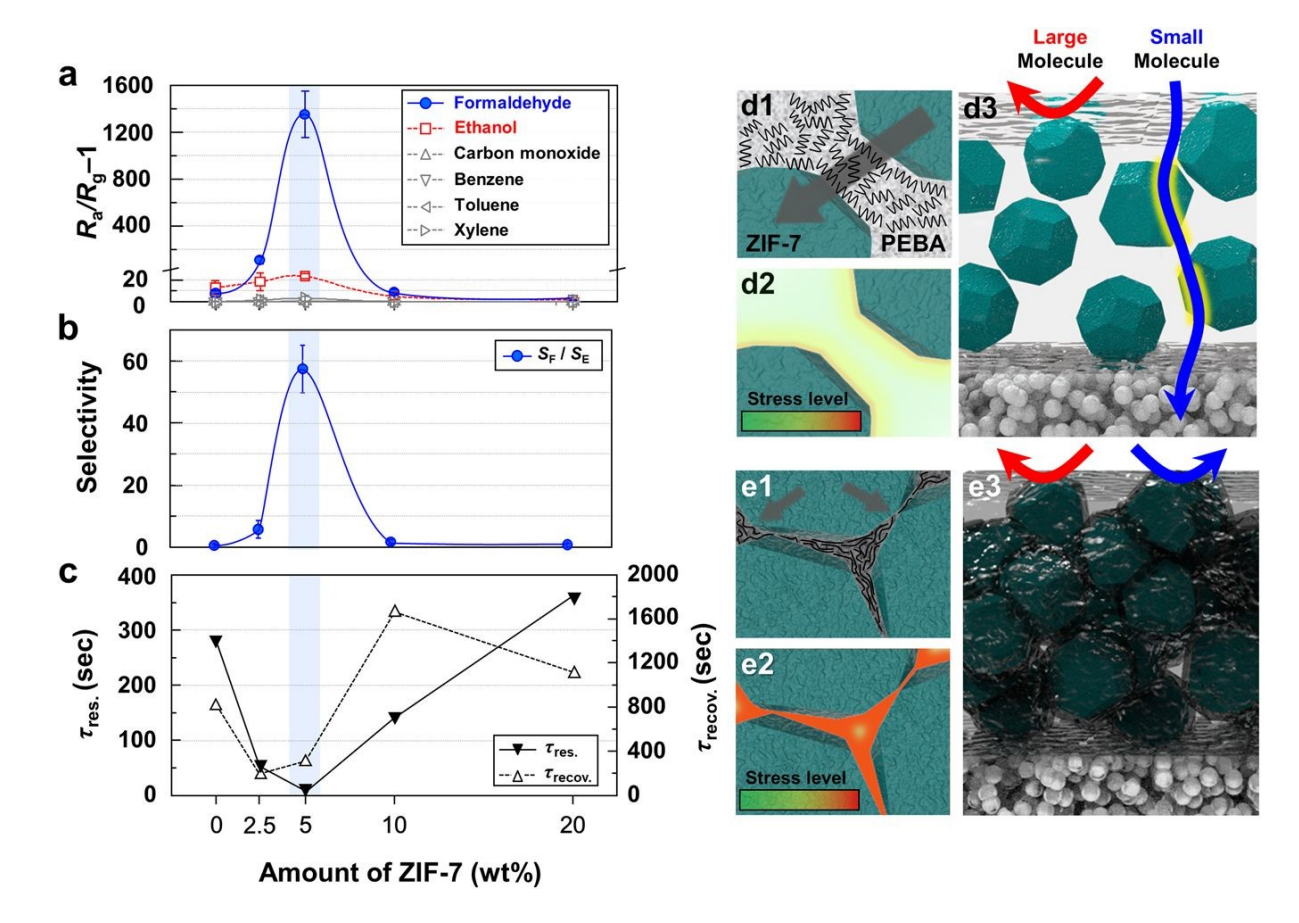


**Figure 35:** Gas response, formaldehyde selectivity, response/recovery times, and gas-sensing mechanism. (a) Gas response of pure PEBA/TiO<sub>2</sub>, 2.5MMM/TiO<sub>2</sub>, 5MMM/TiO<sub>2</sub>, 10MMM/TiO<sub>2</sub>, 20MMM/TiO<sub>2</sub> sensors (temperature: 23 °C). (b) Formaldehyde selectivity to ethanol of pure PEBA/TiO<sub>2</sub>, 2.5MMM/TiO<sub>2</sub>, 5MMM/TiO<sub>2</sub>, 10MMM/TiO<sub>2</sub>, 20MMM/TiO<sub>2</sub> sensors. (c) 90% response time ( $\tau_{res}$ ., left) and 90% recovery times ( $\tau_{recov}$ ., right) of pure PEBA/TiO<sub>2</sub>, 2.5MMM/TiO<sub>2</sub>, 5MMM/TiO<sub>2</sub>, 10MMM/TiO<sub>2</sub>, and 20MMM/TiO<sub>2</sub> sensors. (d, e) Schematic illustration of gas penetration model, stress level, and polymer configuration when mild amount of ZIF-7 loading in PEBA (d) and excessively high amount of ZIF-7 loading in PEBA (e). <sup>116</sup> Reproduced with permission from reference **116**, Copyright (2024) American Chemical Society.

In a related study, MOF(Tb) xerogel presented its application as chemosensor for the selectivided of of the selectivided detection of nitroaromatics such as 2,4-dinitrophenol (2,4-DNT) and 2,6-dinitrophenol (2,6-DNT). Further experiments demonstrated excellent selectivity and recyclability, maintaining its performance across multiple sensing cycles. Its ZIF-8 monolithic membranes have been applied in humidity sensing, taking advantage of their hydrophobic/hydrophilic balance, although improvements are needed to address water stability challenges. Its Humidity sensing is another area where monoliths have shown potential. However, challenges remain, particularly regarding the fragility of many materials in aqueous conditions, which necessitates further research and development to improve their stability and durability. Its International Control of the control of the

In a recent study by Li *et al.*,<sup>117</sup> a monolithic MOF-based metal-insulator-metal (MIM) resonator was developed for high-performance optical chemical sensing. The device was constructed by sandwiching a monolithic HKUST-1 surface-mounted metal-organic framework (SURMOF) film between two gold layers, fabricated via a layer-by-layer deposition method. The structure exhibited high reflectivity (>95%) and tunable coloration across the visible spectrum by varying the MOF thickness. To overcome the diffusion limitation imposed by the top metal layer, femtosecond laser-processing was used to create microwell arrays on the surface, which significantly enhanced the adsorption and diffusion of analyte molecules into the porous MOF layer without compromising optical performance.

The optimized device with a microwell period of 40 µm and height of 220 nm demonstrated rapid response (5.2 s) and high sensitivity to xylene vapours, with a detection limit of 17.39 ppm, as shown in **Figure 36 (a-c)**. The real-time reflectance response, detailed in **Figure 36 (d-f)**, further confirmed the fast kinetics and high dynamic range of the sensor. The integration of monolithic MOFs into MIM resonators represents a significant advancement in optical

sensing platforms, combining high structural integrity with enhanced analyte accessibility and integrity with enhanced analyte accessibility.

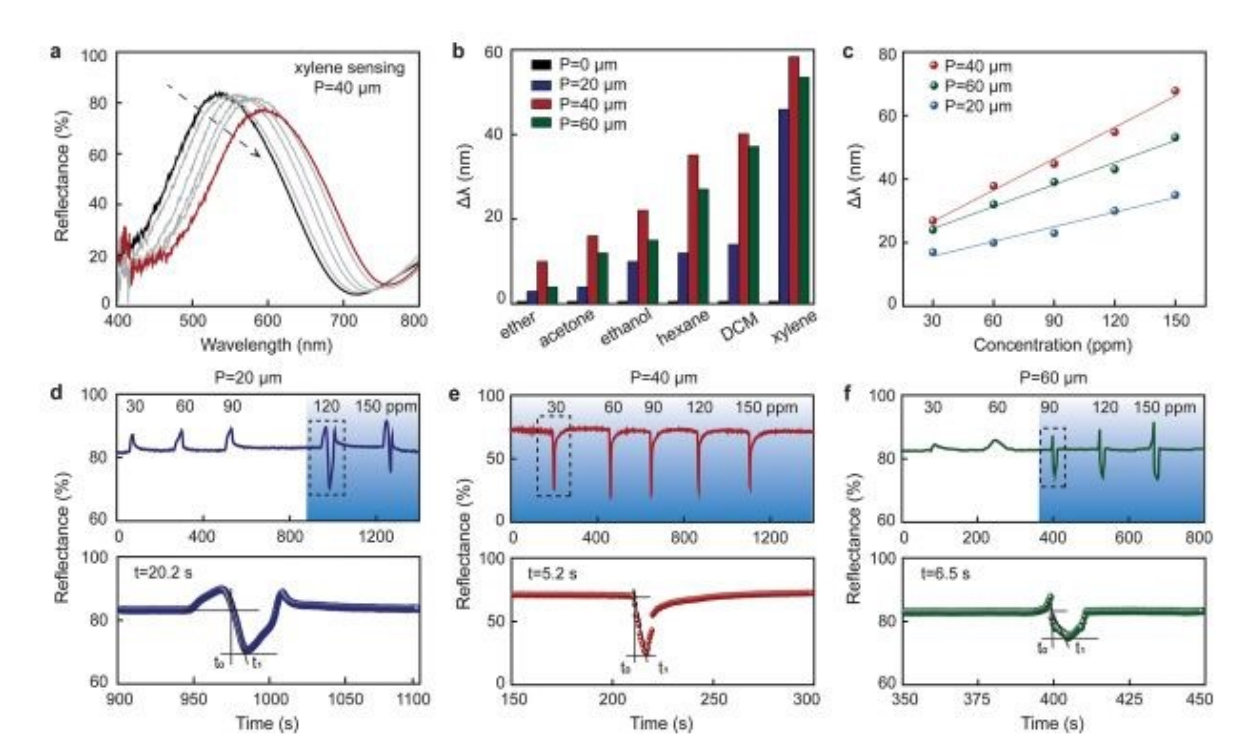


**Figure 36.** Chemical sensing on the monolithic MOF-based MIM resonator with different periods of the microwell arrays. (a) Reflection spectral shifts of the MOF-based MIM resonator with microwell arrays during xylene sensing. (b) Reflection band shifts upon exposure to various saturated chemical vapours. (c) Concentration-dependent sensing performance and (d–f) time-dependent reflectance changes for different microwell periods. Adapted with permission from reference **117**. Copyright (2023) American Chemical Society.

### MULTIFUNCTIONAL COMPOSITES AND EMERGING APPLICATIONS

This article is licensed under a Creative Commons Attribution 3.0 Unported Licence

Open Access Article. Published on 08 listopadu 2025. Downloaded on 13.11.2025 7:46:18.

The integration of monolithic MOFs with other functional materials represents a frontier in designing advanced composites that leverage synergetic effects. By moving beyond pure MOF monoliths, these composites address limitations such as poor electrical conductivity, limited stability, or lack of specific functionality, opening doors to emerging applications.

A significant direction involves the combination of MOFs with ionic liquids (ILs). ILs, known for their high ionic conductivity, thermal stability, and tunable chemistry, can be encapsulated

within MOF pores or used to form composite monoliths. For example, as highlighted in reviews, IL/MOF composites are being explored as advanced solid electrolytes in energy storage devices, highly selective membranes for gas separation, supported catalysts for CO<sub>2</sub> conversion, <sup>122</sup> and as specialized stationary phases for chromatographic separations. <sup>123</sup> The monolithic form of such composites ensures ease of handling and integration into devices while the IL enhances host-guest interactions and ionic transport.

Similarly, the incorporation of two-dimensional materials like MXenes or molybdenum disulfide (MoS<sub>2</sub>) with MOFs into monolithic structures has garnered interest. MXenes offer high electrical conductivity and rich surface chemistry, while MoS<sub>2</sub> is a renowned semiconductor catalyst. <sup>124,125</sup> A monolithic MOF-MXene composite could synergize the high surface area and selectivity of the MOF with the excellent electrical conductivity of MXenes, creating ideal electrodes for supercapacitors or electrocatalysis. Likewise, combining photoactive MoS<sub>2</sub> with MOFs in a monolithic scaffold can facilitate efficient charge separation and mass transport, significantly enhancing photocatalytic performance for reactions like water splitting or pollutant degradation. <sup>126,127</sup>

Beyond integrating other materials into MOF monoliths, a powerful strategy is the functionalization of the MOF's external surface to impart new properties to the entire monolithic structure. A recent pioneering study by Bogdanova *et al.* <sup>128</sup> demonstrates this by grafting long-chain hydrocarbons (C18) onto the surface of highly oriented UiO-66-NH<sub>2</sub> MOF thin films. The key innovation lies in the well-defined, large spacing (~0.8 nm) between grafting sites on the monolith MOF lattice. These spacing forces the hydrocarbon chains to adopt a coiled, brush-like conformation with high conformational entropy. When a water droplet contacts this surface, the chains must stretch to accommodate it, incurring a large entropic penalty that effectively pushes the water away, resulting in a superhydrophobic surface

with water contact angles exceeding 160°, as illustrated in **Figure 37.** Counterintuitively in the control of t

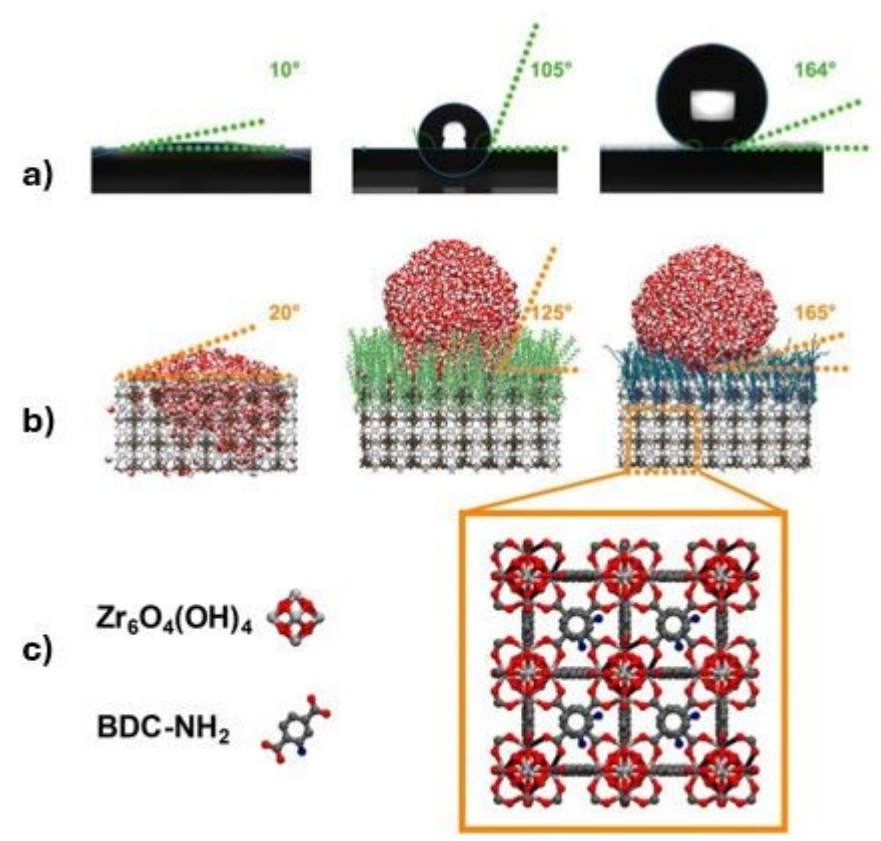


**Figure 37**: Engineered super hydrophobicity showing the transition from a hydrophilic pristine monolith MOF surface to a super hydrophobic surface after entropy-driven functionalization with C18 hydrocarbon chains. a) Experimental b) Simulated and c) monolith MOF structure. <sup>128</sup> Reproduced from reference **128** Copyright (2025) Royal Society of Chemistry.

A highly impactful emerging application for these advanced materials is in atmospheric water harvesting (AWH), where the inherent powdery nature and poor mechanical stability of pure MOFs are major obstacles to practical implementation. Research is advancing on two key fronts: the creation of pure MOF monoliths and the integration of MOFs into composite

matrices. The review by Panahi-Sarmad *et al.*<sup>23</sup> details how integrating MOFs with Continuous macroporous monoliths like aerogels, cryogels, or foams creates a hierarchical structure that combines the nanoscale adsorption properties of MOFs with the mechanical integrity and rapid mass transport of the monolith scaffold. The paper highlights a composite where MOF-801 particles are integrated into a cross-linked calcium alginate (CA) matrix with polypyrrole (PPy) to form a porous monolith (denoted as PMC). This composite leverages the MOF's high-water affinity at low humidity, the alginate's structural support and hydrophilicity, and the polypyrrole's photothermal properties for efficient solar-driven desorption. The results showed a water uptake capacity of 1.106 g/g at 60% RH (relative humidity) and a remarkable daily water harvesting rate of 1.081 kg of water per kg of sorbent in field tests, demonstrating the practical viability of such composites for arid regions. The synthesis, structure, and performance of this specific composite are illustrated in Figure 38.

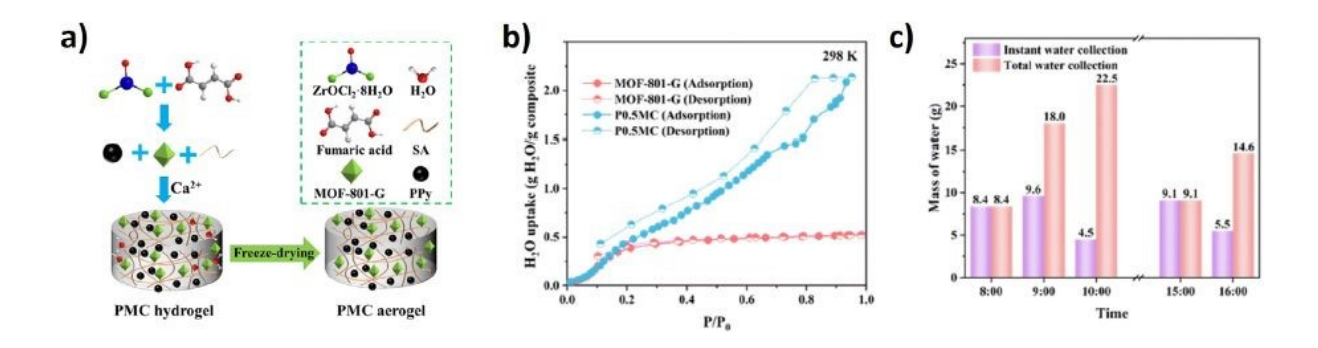


**Figure 38:** a) Schematic of the PMC monolith synthesis via freeze-drying. b) Water adsorption isotherm of the P0.5MC composite showing high capacity. c) Real-world AWH performance data demonstrating high daily water yield.<sup>23</sup> Reproduced with permission from reference **23**, under Creative Commons Attribution Licence (CC BY)

Furthermore, the authors discussed advanced fabrication techniques like 3D printing to create monolithic structures with optimized millimetre-scale grids for enhanced air circulation and water vapor interaction. This approach, combined with the encapsulation of hygroscopic salts

like LiCl within the MOF-monolith matrix, preventing leakage and agglomeration is structured associated with pure salts while significantly boosting water uptake capacity under low-humidity conditions.

In a parallel, complementary approach, the synthesis of pure, robust monolithic MOFs, such as the hierarchically porous MOF-801 monolith prepared via sol-gel phase separation (as previously discussed and shown in **Figure 3**),<sup>39</sup> directly addresses the critical barriers of poor mass transfer and high pressure drop inherent in packed powder beds. The performance of this binder free monolith is compelling: it achieves excellent water uptake at 30% RH even at a 4g scale, providing a viable pathway for industrial-scale water harvesting devices by avoiding the pore blockage and reduced capacity typical of composite sorbents. Quantitatively, the material demonstrated a superior water vapor sorption capacity, exceeding that of conventional MOF-801 powder by 1.2 times in small batches and outperforming compressed tablets by 1.4 times in large-scale tests at 30% RH. Furthermore, the structure showed excellent cyclic stability. Crucially, for scale-up, the monolith possessed remarkable mechanical robustness, with a compressive Young's modulus of up to 61.3 MPa, enabling it to withstand practical handling, as comprehensively illustrated in **Figure 39**.

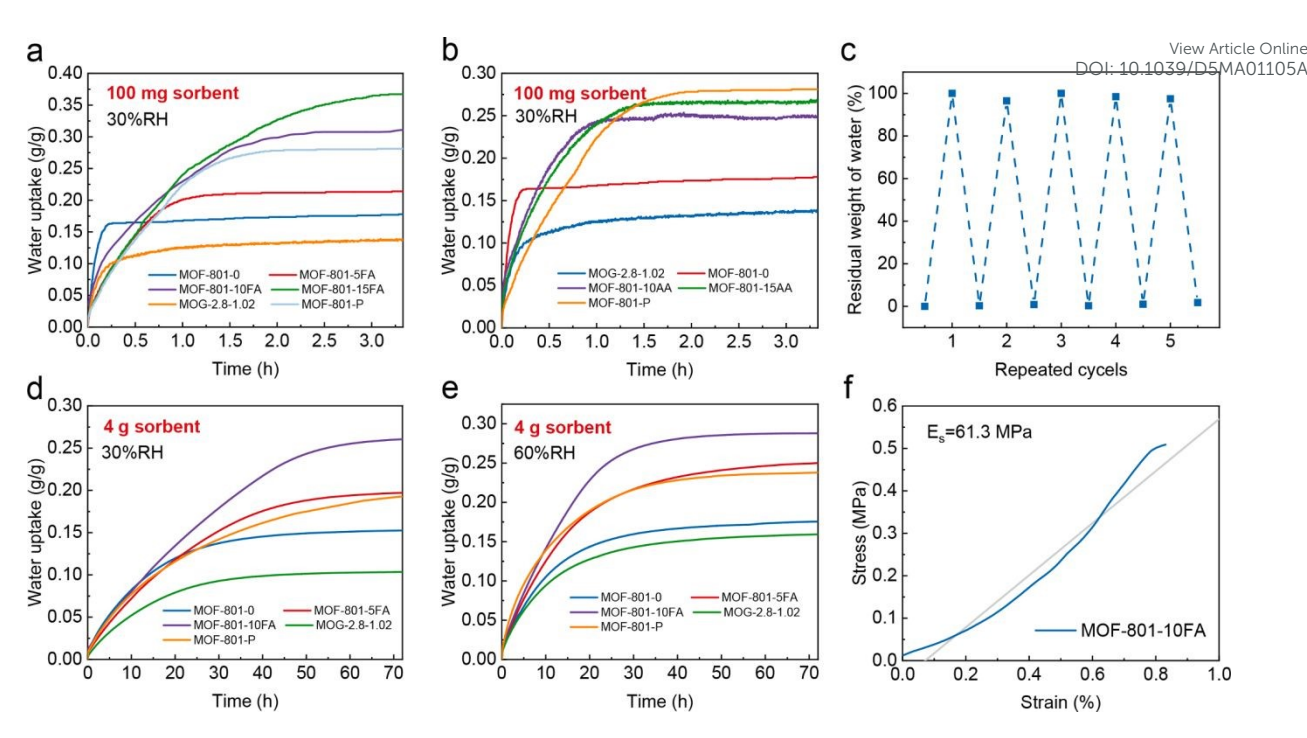


**Figure 39:** Water vapor sorption kinetics at 30% RH and 25 °C of the sorbents (all in powder form) treated by formic acid (FA) (a) and acetic acid (AA) (b) with a mass of 100 mg. The repeated sorption and desorption performance of MOF-801-10FA (c). Water vapor sorption kinetics at 30% RH (d) and 60% RH (e) and at 25 °C of the sorbents (all in monolithic form) with a mass of 4g. The stress–strain curve of MOF-801-10FA with a slope equal to compressive Young's modulus (f). <sup>39</sup> Reproduced with permission from reference **39**. Copyright (2023) Elsevier B. V.

Together, these studies underscore a major trend in the field: the move beyond powder synthesis towards engineering monolithic structures, whether pure or composite, with tailored hierarchies that are essential for real-world applications requiring efficient fluid transport, rapid sorption kinetics, and mechanical durability.

Beyond compositing, monolithic MOFs represent a promising class of precursors for the synthesis of shaped, derived functional materials. The thermal decomposition of MOFs under controlled atmospheres (a process known as calcination) is a well-established route to transform powdered MOFs into functional derivatives like metal oxides, carbon-based

composites, or single-atom catalysts. This concept of using MOFs as sacrificial templates and selection of materials demonstrated in the literature for powdered systems, yielding a wide range of materials for applications in catalysis and sensing. For instance, a zeolitic imidazolate framework (ZIF) can be converted into nitrogen-doped porous carbon with high electrical conductivity for electrocatalysis <sup>129</sup>, and sophisticated materials like CuO/Cu<sub>2</sub>O can be derived from HKUST-1<sup>130</sup>, exhibiting excellent performance in applications such as pollutant degradation.

In a related study, cobalt-based zeolitic imidazolate frameworks (ZIF-67) was converted into hollow cobalt sulphide (Co<sub>3</sub>S<sub>4</sub>) nanopolyhedrons through a solvothermal sulphidation process.<sup>131</sup> The resulting material inherits the high surface area and porous morphology of the ZIF-67 precursor but gains significantly enhanced electrochemical activity due to the formation of a metal sulphide. When applied as an electrode material, these hollow Co<sub>3</sub>S<sub>4</sub> structures demonstrate excellent supercapacitive performance, highlighting the potential of this top-down synthesis route for creating advanced energy storage materials.

The exciting potential for monolithic MOFs lies in applying this same principle to a pre-formed macroscopic structure. While the current literature on the direct calcination of pre-formed, macroscopic MOF monoliths into shaped derivatives is more limited, the work on powders provides a strong foundational proof-of-concept. It indicates that the calcination pathway could be effectively transferred to monolithic MOFs to create robust, structured functional materials with retained macroscopic integrity. This potential is underscored by research that utilizes structured MOF precursors. A compelling example is the work by Zhang et al. <sup>132</sup>, who used a solvothermal method to synthesize a terephthalate-based MOF precursor, which was then calcined in air at 400 °C for 3 h to yield (Ni, Cu)O@C derivatives with a hierarchical porous composite structure containing macropores (Figure 40). This pathway from a structured MOF

to a structured derivative effectively demonstrates how the advantages of a monolithic for fide online can be transferred to a new class of materials with distinct properties, highlighting the viability of this approach for future monolithic systems.

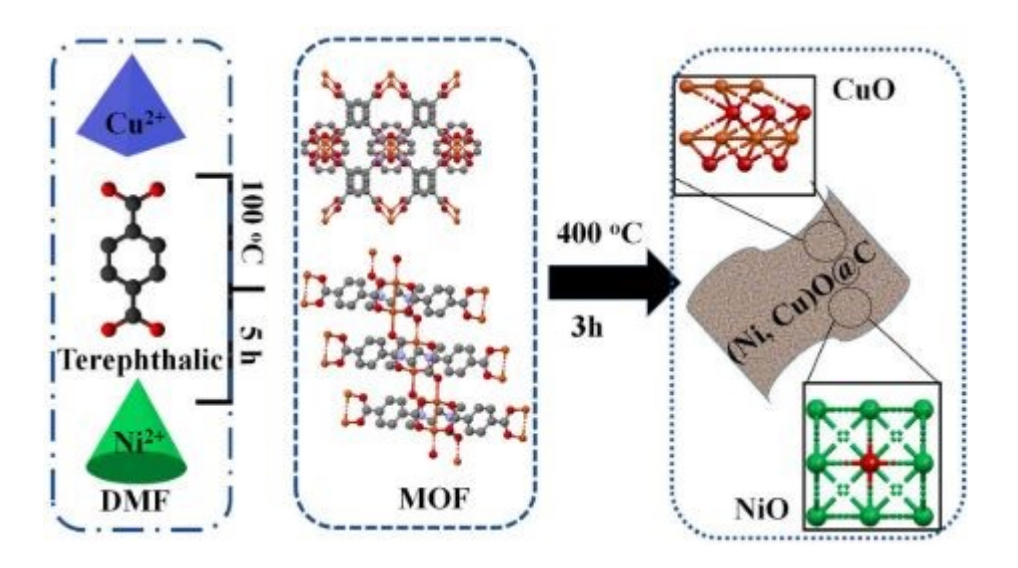


**Figure 40:** Schematic illustration of the synthesis of hierarchical (Ni,Cu)O@C derivatives via calcination of a terephthalate-based MOF precursor. <sup>132</sup> Reproduce with permission reference **132**, under the terms of Creative Commons Attribution Licence (CC BC)

## **Challenges and Future Perspectives**

Monolithic MOFs represent a significant advancement in porous materials engineering, offering a unique combination of hierarchical porosity, mechanical stability, and enhanced processability into integrated structures. Although these attributes position them as strong candidates for advanced applications, the technology is still in its early stages. Several critical challenges must be addressed to fully unlock the potential of monolithic MOFs.

According to Lorignon *et al*,<sup>57</sup> during 3D printing of monolith MOFs there is a possible loss of key properties, particularly porosity and crystallinity. Such loses can restrict the final shape and architecture of the monolith, ultimately limiting its applicability in practical systems. Another significant challenge relates to the workability of monolithic MOFs, largely due to

Open Access Article. Published on 08 listopadu 2025. Downloaded on 13.11.2025 7:46:18.

This article is licensed under a Creative Commons Attribution 3.0 Unported Licence.

that the synthesis mechanisms of monolith MOFs are still unclear. Additionally, for monolithic MOFs to be viable across a wide range of applications, large-scale production is essential; however, current synthetic strategies often require long reaction times.<sup>34</sup> For example, as highlighted in the synthesis sections, certain sol-gel processes require extended aging times of up to 120 hours,<sup>71</sup> and DIW ink preparation can be a multi-step process taking 1-2 days,<sup>51, 52</sup> directly impacting production throughput.

While monolithic MOFs hold great potential for diverse applications, several environmental concerns must also be addressed. In particular, there is need to explore fabrication methods that enable the mass production of complex monolithic structures, preferably through solvent-free techniques or employing environmentally benign solvents in the synthesis process.<sup>90</sup>

Combining MOFs with other materials, such as polymers and nanoparticles, presents and effective strategy for creating multifunctional composites that leverage the strengths of each component, resulting in materials well-suited for a variety of applications. Although this concept remains under active investigation, several researchers have already explored its potential. <sup>23,128</sup> For instance, Tian *et al.*<sup>133</sup> encapsulated polyvinylpyrrolidone (PVP) -stabilized gold nanoparticles (Au NPs) within ZIF-67 particles to form monolithic Au@ZIF-67 composites. The composites combine the benefits of both constituents, retaining the characteristic porosity and high bulk density from monoZIF-67 along with the localized surface plasmonic resonance (LSPR) properties from Au NPs. This results in an enhanced CO<sub>2</sub> photoreduction rate as compared to pristine ZIF-67. Under visible irradiation, the optimal monolithic Au@ZIF-67, 8mLAu@ZIF-67, achieved a volumetric CO production rate 1.5 and 3 times higher than monoZIF-67 and powZIF-67, respectively. Additionally, the monolithic

Open Access Article. Published on 08 listopadu 2025. Downloaded on 13.11.2025 7:46:18.

composite exhibits excellent mechanical stability, as indicated by their high elastic modification of the composite exhibits excellent mechanical stability, as indicated by their high elastic modification of the composite exhibits excellent mechanical stability, as indicated by their high elastic modification of the composite exhibits excellent mechanical stability, as indicated by their high elastic modification of the composite exhibits excellent mechanical stability, as indicated by their high elastic modification of the composite exhibits excellent mechanical stability.

In another notable study, Avila et al<sup>134</sup> synthesised a perovskite@ MOF monolith composite, which demonstrated exceptional stability against humidity, temperature variations, and exposure to different solvents (**Figure 21**). Overally, the integration of nanoparticles with monolithic MOFs offers exciting opportunities for enhancing functionality and broadening the range of potential applications.

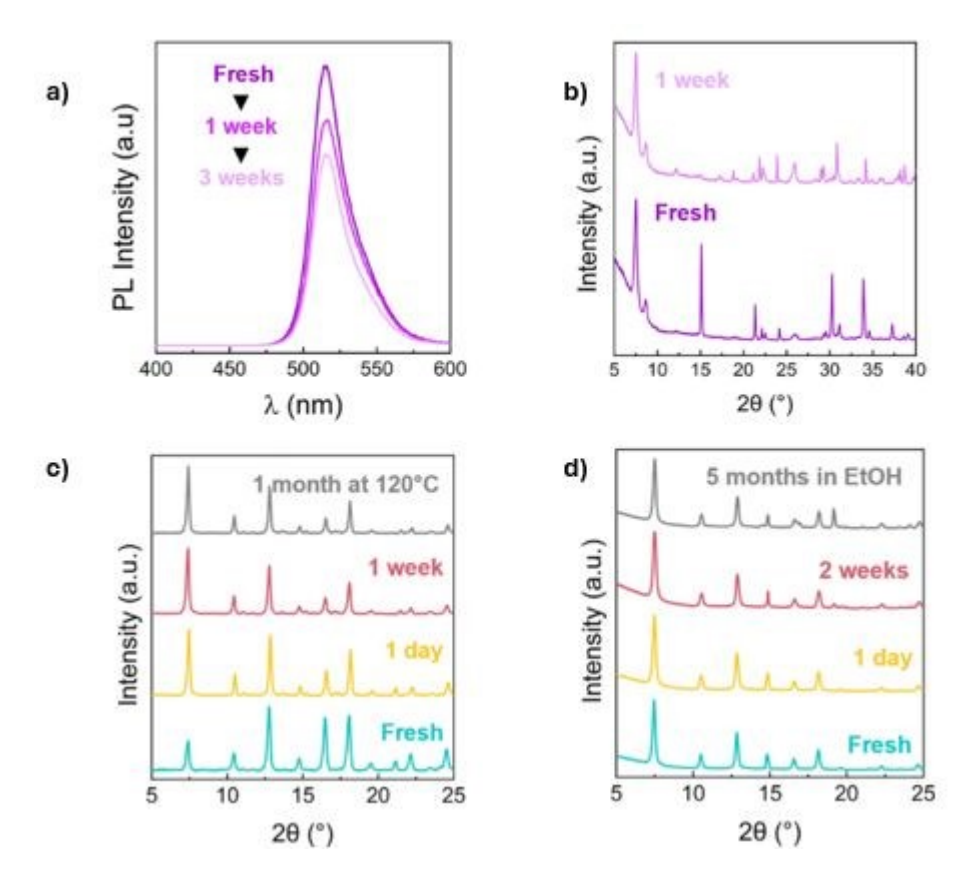


**Figure 21:** (a) Temporal evolution of the photoluminescence spectrum of a MAPbBr<sub>3</sub>@UiO-66 monolith over 3 weeks at 75% relative humidity, (b) PXRD patterns of the MAPbBr<sub>3</sub>@UiO-66 monolith before (dark purple) and after (light purple) immersion in water for 1 week, (c) Evolution of PXRD patterns of the MAPbBr<sub>3</sub>@ZIF-8 monolith when thermally stressed at 120 °C for 1 month, and d) when immersed in EtOH for 5 months. <sup>134</sup> Reproduced with permission from reference **134**, under the terms of the Creative Commons CC-BY.

View Article Online

DOI: 10.1039/D5MA01105A

When assessing sustainability and environmental footprint of MOFs, several factors come into

play. Typically, the materials are composed of metal ions and organic linkers. Metals like iron,

zinc, and copper are relatively benign, whereas rare, energy-intensive to extract, or toxic metals

like cadmium carry a higher environmental cost. Similarly, the choice of organic linkers and

their synthetic origin (petrochemical, bio-based, etc.) also matters. 135

A major determinant of impact is the synthesis route, including solvents, energy inputs, and

purification. Traditional synthesis often relies on toxic solvents like dimethylformamide

(DMF), <sup>136</sup> raising concerns about waste and safety, alongside energy-intensive processes.

Recent life cycle assessment (LCA) studies (Ntouros et al., 2021) highlight that solvent use

(e.g., DMF and methanol) can constitute over 80% of the total environmental burden, with

post-synthetic washing sometimes costing more than the MOF formation itself. This context

has driven interest in solvent-free approaches for synthesizing monolithic MOFs.

Several alternative strategies have been explored to minimize solvent usage and reduce

environmental impact. Mechanochemical synthesis and freeze casting are among the most

promising solvent-free or low-solvent methods. For instance, a reusable NH<sub>2</sub>-MIL-

125(Ti)@polymer monolith fabricated via freeze casting exhibited an impressive adsorption

capacity of 747.4 mg/g for wastewater dyes, outperforming pure MOF powders and

demonstrating mechanical integrity for multiple reuses 113. Mechanochemical synthesis, in

particular, offers high space-time yields with lower energy and solvent consumption. 137

Reactive extrusion, another emerging approach, allows for continuous processing and

significantly lowers the environmental impact compared to conventional solvothermal

synthesis. 138

Although some MOF synthesis processes still demand considerable energy, contributing Moff and their overall environmental footprint, the production of monolithic MOFs represents a more sustainable alternative. Their enhanced mechanical strength not only facilitates easier handling and recycling but also helps reduce material waste, further aligning with the principles of green chemistry. It is important to emphasize, however, that shaping methods such as freeze casting or extrusion only contribute to sustainability when the MOF synthesis itself is green. Simply structuring a monolith using a sustainable technique does not offset the environmental burden of an upstream solvent-intensive MOF synthesis. Full sustainability must be evaluated across the entire lifecycle, from raw material sourcing, synthesis, purification, shaping, to end-of-life disposal or reuse.

# **Emerging Trends And Future Directions**

As the applications of monolithic MOFs continue to grow, there is increasing emphasis on enhancing functionality, scalability and sustainability.<sup>22</sup> This shift is evident in recent innovations in synthesis methods, which increasingly adopt green approaches such as solvent-free or aqueous-phase techniques, to minimize environmental impact.<sup>139</sup> Techniques like solgel and hydrothermal synthesis have been refined to support these goals, offering more environmentally friendly pathways while preserving material quality.<sup>90,140</sup> These methods also help reduce pollutant generation and often incorporate bio-based precursors.

In parallel, additive manufacturing techniques, particularly 3D printing, have emerged as powerful tools for engineering the hierarchical structure of monoliths. These approaches enable the creation of complex architectures with improved functionality. Looking forward, strategies such as roll-to-roll production and biomimetic design are gaining traction. These aim to bridge the gap between laboratory-scale research and industrial-scale production by enhancing cost-effectiveness and mechanical robustness under harsh operating conditions.

Another key development is the creation of hybrid composites through the incorporation was arcter online nanoparticles, polymers, ionic liquids or MXenes into monolithic MOFs. 126,127,133,134 These composites enhance multifunctionality, making them highly suitable for catalysis, sensing, and environmental remediation. For instance, hierarchical porous monoliths are increasingly used in water treatment and catalysis due to their superior mass transfer, catalytic activity, and separation efficiency, which are benefits arising from their integrated macro-, meso-, and microporous structures.

Recent advances in nanocharacterization techniques have been essential in supporting these developments. While Scanning Electron Microscopy (SEM) and Transmission Electron Microscopy (TEM)<sup>142</sup> provide detailed analyses of pore architectures and phase distributions, and nanoparticle arrangements, a suite of newer tools is providing critical, mechanistic insights. Atomic Force Microscopy (AFM) is now pivotal for visualizing nanoscale deformation and damage resilience after mechanical testing, providing unambiguous evidence to complement quantitative data. <sup>30</sup>Furthermore, techniques like nano-FTIR spectroscopy offer nanochemical mapping with ~20 nm resolution, enabling the correlation of local chemical environments (e.g., guest molecule distribution) with macroscopic mechanical and functional properties. <sup>98</sup> The integration of these methods with established techniques like nanoindentation is transforming the understanding of structure-property relationships in monolithic MOFs, guiding the rational design of next-generation materials with tailored properties. Mechanical and thermal testing further ensure that monolithic materials can withstand elevated pressures and temperatures.

## Conclusion

The synthesis methods for monolithic MOFs are moving towards more green and efficient pathways, while their applications are also evolving into a wide range of fields including biomedical, energy and environmental sectors. Continued research in synthesis and application

Open Access Article. Published on 08 listopadu 2025. Downloaded on 13.11.2025 7:46:18.

is expected to generate novel multifunctional composites, further broadening the practical was additional composites. of these materials. Inherent challenges traditionally associated with conventional MOFs, such as poor mechanical stability, difficult handling and processing, have been significantly mitigated through the development of monolithic MOFs. Their enhanced structural integrity, ease of handling, and tunable properties position them as strong candidates for industrial applications including gas storage, catalysis, separation and drug delivery. Key methods for synthesis of monolith MOFs particularly sol-gel techniques and 3D printing, have shown significant potential in producing monolithic MOFs with tailored architectures and functionalities while offering routes to greener synthesis methods. As research progresses, overcoming issues related to scalability, reproducibility, mass transport limitations, and optimization of both physical and chemical properties will be crucial. Prospective work should focus on refining synthesis approaches, developing advanced nanocharacterisation tools, exploring innovative fabrication methods, and expanding the scope of applications into areas like atmospheric water harvesting and advanced sensing. With the rapid pace of advancements in this field, monolithic MOFs are on the verge of playing a pivotal role in addressing complex scientific and industrial challenges, ultimately contributing to the development of more efficient, sustainable technologies.

## **Author contributions**

Donald Muringaniza - investigation, writing, original draft preparation; Laurencia Zulu - investigation, writing, original draft preparation; Linia Gedi Marazani- reviewing and editing; Piwai Tshuma -supervision, reviewing and editing; Gift Mehlana- conceptualization, supervision, resources, reviewing and editing.

#### Acknowledgements

This document has been produced with the financial assistance of the European Union (Commission no. DCI-PANAF/2020/420-028), through the African Research Initiative for Scientific Excellence (ARISE), pilot programme. ARISE is implemented by the African Academy of Sciences with support from the European Commission and the African Union Commission.

The contents of this document are the sole responsibility of the author(s) and can under no circumstances be regarded as reflecting the position of the European Union, the African Academy of Sciences, and the African Union Commission."

#### **Conflict of interest**

The authors declare no conflict of interest.

## **REFERENCES**

- (1) Kaushal, S.; Kaur, G.; Kaur, J.; Singh, P. P. First Transition Series Metal-Organic Frameworks: Synthesis, Properties and Applications. *Mater. Adv.* 2021, 2 (22), 7308–7335. https://doi.org/10.1039/d1ma00719j.
- (2) Xiang, W.; Zhang, Y.; Chen, Y.; Liu, C. J.; Tu, X. Synthesis, Characterization and Application of Defective Metal-Organic Frameworks: Current Status and Perspectives. *J. Mater. Chem. A* **2020**, *8* (41), 21526–21546. https://doi.org/10.1039/d0ta08009h.
- (3) Furukawa, H.; Ko, N.; Go, Y. B.; Aratani, N.; Choi, S. B.; Choi, E.; Yazaydin, A. Ö.; Snurr, R. Q.; O'Keeffe, M.; Kim, J.; Yaghi, O. M. Ultrahigh Porosity in Metal-Organic Frameworks. *Science (80-.).* **2010**, *329* (5990), 424–428. https://doi.org/10.1126/science.1192160.
- (4) Alhumaimess, M. S. Metal–Organic Frameworks and Their Catalytic Applications. *J. Saudi Chem. Soc.* **2020**, *24* (6), 461–473. https://doi.org/https://doi.org/10.1016/j.jscs.2020.04.002.

- (5) Xu, C.; Fang, R.; Luque, R.; Chen, L.; Li, Y. Functional Metal–Organic Frameworks Shaotilosal for Catalytic Applications. *Coord. Chem. Rev.* **2019**, *388*, 268–292. https://doi.org/10.1016/j.ccr.2019.03.005.
- (6) Singh, S.; Sivaram, N.; Nath, B.; Khan, N. A.; Singh, J.; Ramamurthy, P. C. Metal Organic Frameworks for Wastewater Treatment, Renewable Energy and Circular Economy Contributions. *npj Clean Water* 2024, 7 (1), 124. https://doi.org/10.1038/s41545-024-00408-4.
- (7) Gao, F.; Yan, R.; Shu, Y.; Cao, Q.; Zhang, L. Strategies for the Application of Metal-Organic Frameworks in Catalytic Reactions. *RSC Adv.* **2022**, *12* (16), 10114–10125. https://doi.org/10.1039/d2ra01175a.
- (8) Linnane, E.; Haddad, S.; Melle, F.; Mei, Z.; Fairen-Jimenez, D. The Uptake of Metal-Organic Frameworks: A Journey into the Cell. *Chem. Soc. Rev.* **2022**, *51* (14), 6065–6086. https://doi.org/10.1039/d0cs01414a.
- (9) Zhan, F.; Wang, H.; He, Q.; Xu, W.; Chen, J.; Ren, X.; Wang, H.; Liu, S.; Han, M.; Yamauchi, Y.; Chen, L. Metal-Organic Frameworks and Their Derivatives for Metal-Ion (Li, Na, K and Zn) Hybrid Capacitors. *Chem. Sci.* 2022, *13* (41), 11981–12015. https://doi.org/10.1039/d2sc04012c.
- (10) Sonowal, K.; Saikia, L. Metal-Organic Frameworks and Their Composites for Fuel and Chemical Production via CO2 Conversion and Water Splitting. *RSC Adv.* 2022, *12* (19), 11686–11707. https://doi.org/10.1039/d1ra09063a.
- (11) Adil, H. I.; Thalji, M. R.; Yasin, S. A.; Saeed, I. A.; Assiri, M. A.; Chong, K. F.; Ali, G. A. M. Metal-Organic Frameworks (MOFs) Based Nanofiber Architectures for the Removal of Heavy Metal Ions. *RSC Adv.* 2022, *12* (3), 1433–1450. https://doi.org/10.1039/d1ra07034g.

- (13) Sai Bhargava Reddy, M.; Ponnamma, D.; Sadasivuni, K. K.; Kumar, B.; Abdullah, A.
   M. Carbon Dioxide Adsorption Based on Porous Materials. *RSC Adv.* 2021, 11 (21), 12658–12681. https://doi.org/10.1039/d0ra10902a.
- (14) Li, D.; Yadav, A.; Zhou, H.; Roy, K.; Thanasekaran, P.; Lee, C. Advances and Applications of Metal-Organic Frameworks (MOFs) in Emerging Technologies: A Comprehensive Review. *Glob. challenges (Hoboken, NJ)* 2024, 8 (2), 2300244. https://doi.org/10.1002/gch2.202300244.

- (15) Ghasempour, H.; Wang, K.; Powell, J. A.; Zarekarizi, F.; Lv, X.; Morsa-, A. Metal Organic Frameworks Based on Multicarboxylate Linkers. **2020**.
- (16) Yeskendir, B.; Dacquin, J. P.; Lorgouilloux, Y.; Courtois, C.; Royer, S.; Dhainaut, J. From Metal-Organic Framework Powders to Shaped Solids: Recent Developments and Challenges. *Mater. Adv.* 2021, 2 (22), 7139–7186.
  https://doi.org/10.1039/d1ma00630d.
- (17) Fonseca, J.; Gong, T. Fabrication of Metal-Organic Framework Architectures with Macroscopic Size: A Review. *Coord. Chem. Rev.* 2022, 462, 214520. https://doi.org/https://doi.org/10.1016/j.ccr.2022.214520.
- (18) Bazer-Bachi, D.; Assié, L.; Lecocq, V.; Harbuzaru, B.; Falk, V. Towards Industrial Use of Metal-Organic Framework: Impact of Shaping on the MOF Properties. *Powder Technol.* **2013**, *255* (2014), 52–59. https://doi.org/10.1016/j.powtec.2013.09.013.
- (19) Morris, R. E.; Brammer, L. Coordination Change, Lability and Hemilability in Metal-

Open Access Article. Published on 08 listopadu 2025. Downloaded on 13.11.2025 7:46:18.

View Article Online

DOI: 10.1039/D5MA01105A

Organic Frameworks. Chem. Soc. Rev. 2017, 46 (17), 5444–5462.

https://doi.org/10.1039/c7cs00187h.

- (20) Sun, Y.; Zhu, Y.; Zhang, S.; Binks, B. P. Fabrication of Hierarchical Macroporous ZIF-8 Monoliths Using High Internal Phase Pickering Emulsion Templates. *Langmuir* **2021**, *37* (28), 8435–8444. https://doi.org/10.1021/acs.langmuir.1c00757.
- (21) Lee, Y. R.; Jang, M. S.; Cho, H. Y.; Kwon, H. J.; Kim, S.; Ahn, W. S. ZIF-8: A Comparison of Synthesis Methods. *Chem. Eng. J.* 2015, 271, 276–280. https://doi.org/10.1016/j.cej.2015.02.094.
- (22) Yu, X.; Li, B.; Wu, L.; Shi, D.; Han, S. Review and Perspectives of Monolithic Metal–Organic Frameworks: Toward Industrial Applications. *Energy & Fuels* **2023**, *37*. https://doi.org/10.1021/acs.energyfuels.3c00858.
- (23) Panahi-Sarmad, M.; Guo, T.; Hashemi, S. A.; Ghaffarkhah, A.; Wuttke, S.; Rojas, O.; Jiang, F. Hierarchically MOF-Based Porous Monolith Composites for Atmospheric Water Harvesting. *Adv. Mater.* 2025, e2413353.
  https://doi.org/10.1002/adma.202413353.
- Vilela, S.; Salcedo-Abraira, P.; Micheron, L.; Solla, E.; Yot, P.; Horcajada, P. Robust
   Monolithic Metal-Organic Framework with Hierarchical Porosity. *Chem. Commun.* 2018, 54. https://doi.org/10.1039/C8CC07252C.
- (25) Chaparro-Garnica, C. Y.; Bailón-García, E.; Lozano-Castelló, D.; Bueno-López, A. Design and Fabrication of Integral Carbon Monoliths Combining 3D Printing and Sol-Gel Polymerization: Effects of the Channel Morphology on the CO-PROX Reaction.
  Catal. Sci. Technol. 2021, 11 (19), 6490–6497. https://doi.org/10.1039/d1cy01104a.
- (26) Cao, Y.; Han, W.; Pu, Z.; Wang, X.; Wang, B.; Liu, C.; Uyama, H.; Shen, C.

- (27) Spilstead, K. B.; Haswell, S. J.; Barnett, N. W.; Conlan, X. A.; Stevenson, P. G.; Francis, P. S. Development of a Resin Based Silica Monolithic Column Encapsulation. *Anal. Methods* 2015, 7 (12), 4908–4911. https://doi.org/10.1039/c5ay00722d.
- (28) Hinamoto, Y.; Sugawara, A.; Asoh, T.-A.; Nandi, M.; Uyama, H. Functionalized Cellulose Monolith Based Affinity Chromatography Columns for Efficient Separation of Protein Molecules. *RSC Appl. Polym.* 2023, *1* (1), 82–96. https://doi.org/10.1039/d3lp00041a.

- (29) Lambarska, A.; Szymańska, K.; Hanefeld, U. Monoliths Enabling Biocatalysis in Flow Chemistry. *Green Chem.* **2024**, 10718–10738. https://doi.org/10.1039/d4gc03535f.
- (30) Tian, T.; Zeng, Z.; Vulpe, D.; Casco, M. E.; Divitini, G.; Midgley, P. A.; Silvestre-Albero, J.; Tan, J. C.; Moghadam, P. Z.; Fairen-Jimenez, D. A Sol-Gel Monolithic Metal-Organic Framework with Enhanced Methane Uptake. *Nat. Mater.* **2018**, *17* (2), 174–179. https://doi.org/10.1038/NMAT5050.
- (31) Madden, D. G.; O'Nolan, D.; Rampal, N.; Babu, R.; Çamur, C.; Al Shakhs, A. N.;
  Zhang, S. Y.; Rance, G. A.; Perez, J.; Maria Casati, N. Pietro; Cuadrado-Collados, C.;
  O'Sullivan, D.; Rice, N. P.; Gennett, T.; Parilla, P.; Shulda, S.; Hurst, K. E.; Stavila,
  V.; Allendorf, M. D.; Silvestre-Albero, J.; Forse, A. C.; Champness, N. R.; Chapman,
  K. W.; Fairen-Jimenez, D. Densified HKUST-1 Monoliths as a Route to High
  Volumetric and Gravimetric Hydrogen Storage Capacity. J. Am. Chem. Soc. 2022, 144
  (30), 13729–13739. https://doi.org/10.1021/jacs.2c04608.
- (32) Tian, T.; Zeng, Z.; Vulpe, D.; Casco, M. E.; Divitini, G.; Midgley, P. A.; Silvestre-

- Albero, J.; Tan, J. C.; Moghadam, P. Z.; Fairen-Jimenez, D. A Sol-Gel Monolithic View Article Online Metal-Organic Framework with Enhanced Methane Uptake. *Nat. Mater.* **2018**, *17* (2), 174–179. https://doi.org/10.1038/NMAT5050.
- (33) Connolly, B. M.; Aragones-Anglada, M.; Gandara-Loe, J.; Danaf, N. A.; Lamb, D. C.;
  Mehta, J. P.; Vulpe, D.; Wuttke, S.; Silvestre-Albero, J.; Moghadam, P. Z.; Wheatley,
  A. E. H.; Fairen-Jimenez, D. Tuning Porosity in Macroscopic Monolithic MetalOrganic Frameworks for Exceptional Natural Gas Storage. *Nat. Commun.* 2019, *10*(1), 1–11. https://doi.org/10.1038/s41467-019-10185-1.
- (34) Duan, C.; Yu, Y.; Li, J.; Li, L.; Huang, B.; Chen, D.; Xi, H. Recent Advances in the Synthesis of Monolithic Metal-Organic Frameworks. *Sci. China Mater.* **2021**, *64* (6), 1305–1319. https://doi.org/10.1007/s40843-020-1585-1.
- (35) Tricarico, M.; Tan, J. C. Mechanical Properties and Nanostructure of Monolithic Zeolitic Imidazolate Frameworks: A Nanoindentation, Nanospectroscopy, and Finite Element Study. *Mater. Today Nano* 2022, 17 (Mmc). https://doi.org/10.1016/j.mtnano.2021.100166.
- (36) Ploner, K.; Delir Kheyrollahi Nezhad, P.; Gili, A.; Kamutzki, F.; Gurlo, A.; Doran, A.; Cao, P.; Heggen, M.; Köwitsch, N.; Armbrüster, M.; Watschinger, M.; Klötzer, B.; Penner, S. The Sol-Gel Autocombustion as a Route towards Highly CO2-Selective, Active and Long-Term Stable Cu/ZrO2methanol Steam Reforming Catalysts. *Mater. Chem. Front.* **2021**, *5* (13), 5093–5105. https://doi.org/10.1039/d1qm00641j.
- (37) Pattadar, D. K.; Zamborini, F. P. Effect of Size, Coverage, and Dispersity on the Potential-Controlled Ostwald Ripening of Metal Nanoparticles. *Langmuir* **2019**, *35* (50), 16416–16426. https://doi.org/10.1021/acs.langmuir.9b02421.
- (38) Tricarico, M.; Besnard, C.; Cinque, G.; Korsunsky, A. M.; Tan, J. C. Stress–Strain

- Relationships and Yielding of Metal-Organic Framework Monoliths. *Commun* Metal-Organic Framework Monoliths.
- (39) He, Y.; Fu, T.; Wang, L.; Liu, J.; Liu, G.; Zhao, H. Self-Assembly of MOF-801 into Robust Hierarchically Porous Monoliths for Scale-up Atmospheric Water Harvesting. *Chem. Eng. J.* **2023**, *472* (July), 144786. https://doi.org/10.1016/j.cej.2023.144786.
- (40) Holey, S. A.; Nayak, R. R. Harnessing Glycolipids for Supramolecular Gelation: A Contemporary Review. ACS Omega 2024, 9 (24), 25513–25538. https://doi.org/10.1021/acsomega.4c00958.
- Hunter-Sellars, E.; Saenz-Cavazos, P. A.; Houghton, A. R.; McIntyre, S. R.; Parkin, I. P.; Williams, D. R. Sol-Gel Synthesis of High-Density Zeolitic Imidazolate
  Framework Monoliths via Ligand Assisted Methods: Exceptional Porosity,
  Hydrophobicity, and Applications in Vapor Adsorption. *Adv. Funct. Mater.* 2021, 31
  (5), 2008357 (1-10). https://doi.org/10.1002/adfm.202008357.

- (42) Borlaf, M.; Moreno, R. Colloidal Sol-Gel: A Powerful Low-Temperature Aqueous Synthesis Route of Nanosized Powders and Suspensions. *Open Ceram.* **2021**, *8* (November), 100200. https://doi.org/10.1016/j.oceram.2021.100200.
- Hunter-Sellars, E.; Saenz-Cavazos, P. A.; Houghton, A. R.; McIntyre, S. R.; Parkin, I.
  P.; Williams, D. R. Sol-Gel Synthesis of High-Density Zeolitic Imidazolate
  Framework Monoliths via Ligand Assisted Methods: Exceptional Porosity,
  Hydrophobicity, and Applications in Vapor Adsorption (Advanced Functional
  Materials, (2021), 31, 5, (2008357), 10.1002/Adfm.20200. *Advanced Functional Materials*. 2021, pp 12–14. https://doi.org/10.1002/adfm.202102716.
- (44) Pathak, A.; Alghamdi, L. A.; Fernández-Catalá, J.; Tricarico, M.; Cazorla-Amorós, D.; Tan, J. C.; Berenguer-Murcia, Á.; Mehlana, G.; Wheatley, A. E. H. Understanding

- Metal–Organic Framework Densification: Solvent Effects and the Growth of College Anticle Online Primary Nanoparticles in Monolithic ZIF-8. *Small* **2025**, *21* (21), 1–27. https://doi.org/10.1002/smll.202500510.
- (45) Wang, A.; Jin, M.; Li, N.; Ma, Y.; Chen, L.; Ma, D.; Chen, B. X.; Gao, F.; Tian, Y. Q.; Shi, Y. K. Zeolitic Imidazolate Framework Monoliths with High Mesoporosity and Effective Adsorption of Toluene from Aqueous Solution. *New J. Chem.* **2017**, *41* (16), 8031–8035. https://doi.org/10.1039/c7nj02024d.
- (46) Hong, W. Y.; Perera, S. P.; Burrows, A. D. Manufacturing of Metal-Organic Framework Monoliths and Their Application in CO2 Adsorption. *Microporous Mesoporous Mater.* 2015, 214, 149–155. https://doi.org/10.1016/j.micromeso.2015.05.014.
- (47) Thakkar, H.; Eastman, S.; Al-Naddaf, Q.; Rezaei, F. 3D-Printed Metal-Organic Framework Monoliths for Gas Adsorption Processes. *ACS Appl. Mater. Interfaces* **2017**, *9* (41), 36908–35916. https://doi.org/10.1021/acsami.7b11626.
- (48) Lim, G. J. H.; Wu, Y.; Shah, B. B.; Koh, J. J.; Liu, C. K.; Zhao, D.; Cheetham, A. K.; Wang, J.; Ding, J. 3D-Printing of Pure Metal-Organic Framework Monoliths. *ACS Mater. Lett.* **2019**, *1* (1), 147–153. https://doi.org/10.1021/acsmaterialslett.9b00069.
- (49) Molavi, H.; Mirzaei, K.; Barjasteh, M.; Rahnamaee, S. Y.; Saeedi, S.;
  Hassanpouryouzband, A.; Rezakazemi, M. 3D-Printed MOF Monoliths: Fabrication
  Strategies and Environmental Applications; Springer Nature Singapore, 2024; Vol. 16.
  https://doi.org/10.1007/s40820-024-01487-1.
- (50) Truby, R. L.; Lewis, J. A. Printing Soft Matter in Three Dimensions. *Nature* 2016, *540* (7633), 371–378. https://doi.org/10.1038/nature21003.

- Young, A. J.; Guillet-Nicolas, R.; Marshall, E. S.; Kleitz, F.; Goodhand, A. D.; View Article Online Glanville, L. B. L.; Reithofer, M. R.; Chin, J. M. Direct Ink Writing of Catalytically Active UiO-66 Polymer Composites. *Chem. Commun.* **2019**, *55* (15), 2190–2193. https://doi.org/10.1039/c8cc10018g.
- (52) Pei, R.; Fan, L.; Zhao, F.; Xiao, J.; Yang, Y.; Lai, A.; Zhou, S. F.; Zhan, G. 3D-Printed Metal-Organic Frameworks within Biocompatible Polymers as Excellent Adsorbents for Organic Dyes Removal. *J. Hazard. Mater.* 2020, 384, 121418.
  https://doi.org/10.1016/j.jhazmat.2019.121418.
- (53) Verougstraete, B.; Schuddinck, D.; Lefevere, J.; Baron, G. V.; Denayer, J. F. M. A 3D-Printed Zeolitic Imidazolate Framework-8 Monolith For Flue- and Biogas Separations by Adsorption: Influence of Flow Distribution and Process Parameters. *Front. Chem. Eng.* 2020, 2. https://doi.org/10.3389/fceng.2020.589686.

- Claessens, B.; Dubois, N.; Lefevere, J.; Mullens, S.; Cousin-Saint-Remi, J.; Denayer, J. F. M. 3D-Printed ZIF-8 Monoliths for Biobutanol Recovery. *Ind. Eng. Chem. Res.*2020, 59 (18), 8813–8824. https://doi.org/10.1021/acs.iecr.0c00453.
- (55) Grande, C. A.; Blom, R.; Middelkoop, V.; Matras, D.; Vamvakeros, A.; Jacques, S. D.
  M.; Beale, A. M.; Di Michiel, M.; Anne Andreassen, K.; Bouzga, A. M. Multiscale
  Investigation of Adsorption Properties of Novel 3D Printed UTSA-16 Structures.
  Chem. Eng. J. 2020, 402 (May), 126166. https://doi.org/10.1016/j.cej.2020.126166.
- (56) Lawson, S.; Griffin, C.; Rapp, K.; Rownaghi, A. A.; Rezaei, F. Amine-Functionalized MIL-101 Monoliths for CO2 Removal from Enclosed Environments. *Energy and Fuels* 2019, 33 (3), 2399–2407. https://doi.org/10.1021/acs.energyfuels.8b04508.
- (57) Lorignon, F.; Gossard, A.; Carboni, M. Hierarchically Porous Monolithic MOFs: An Ongoing Challenge for Industrial-Scale Effluent Treatment. *Chem. Eng. J.* 2020, 393

View Article Online

DOI: 10.1039/D5MA01105A

- (March). https://doi.org/10.1016/j.cej.2020.124765.
- (58) Liu, X.; Zhao, D.; Wang, J. Challenges and Opportunities in Preserving Key Structural Features of 3D-Printed Metal/Covalent Organic Framework. *Nano-Micro Lett.* **2024**, *16* (1), 1–20. https://doi.org/10.1007/s40820-024-01373-w.
- (59) Do, X. D.; Hoang, V. T.; Kaliaguine, S. MIL-53(Al) Mesostructured Metal-Organic Frameworks. *Microporous Mesoporous Mater.* **2011**, *141* (1–3), 135–139. https://doi.org/10.1016/j.micromeso.2010.07.024.
- (60) Lawson, S.; Snarzyk, M.; Hanify, D.; Rownaghi, A. A.; Rezaei, F. Development of 3D-Printed Polymer-MOF Monoliths for CO2 Adsorption. *Ind. Eng. Chem. Res.* 2020, 59 (15), 7151–7160. https://doi.org/10.1021/acs.iecr.9b05445.
- (61) Kreider, M. C.; Sefa, M.; Fedchak, J. A.; Scherschligt, J.; Bible, M.; Natarajan, B.; Klimov, N. N.; Miller, A. E.; Ahmed, Z.; Hartings, M. R. Toward 3D Printed Hydrogen Storage Materials Made with ABS-MOF Composites. *Polym. Adv. Technol.* 2018, 29 (2), 867–873. https://doi.org/10.1002/pat.4197.
- (62) Li, R.; Yuan, S.; Zhang, W.; Zheng, H.; Zhu, W.; Li, B.; Zhou, M.; Wing-Keung Law, A.; Zhou, K. 3D Printing of Mixed Matrix Films Based on Metal-Organic Frameworks and Thermoplastic Polyamide 12 by Selective Laser Sintering for Water Applications. ACS Appl. Mater. Interfaces 2019, 11 (43), 40564–40574.
  https://doi.org/10.1021/acsami.9b11840.
- (63) Pustovarenko, A.; Seoane, B.; Abou-Hamad, E.; King, H. E.; Weckhuysen, B. M.; Kapteijn, F.; Gascon, J. Rapid Fabrication of MOF-Based Mixed Matrix Membranes through Digital Light Processing. *Mater. Adv.* 2021, 2 (8), 2739–2749. https://doi.org/10.1039/d1ma00023c.

- (64) Halevi, O.; Tan, J. M. R.; Lee, P. S.; Magdassi, S. Hydrolytically Stable MQF: in 3D/D5MA01105A

  Printed Structures. *Adv. Sustain. Syst.* **2018**, *2* (2), 1–5.

  https://doi.org/10.1002/adsu.201700150.
- (65) Lawson, S.; Rezaei, F. Effects of Process Parameters on CO2/H2Separation
  Performance of 3D-Printed MOF-74 Monoliths. ACS Sustain. Chem. Eng. 2021, 9
  (32), 10902–10912. https://doi.org/10.1021/acssuschemeng.1c03443.
- (66) Verougstraete, B.; Schuddinck, D.; Lefevere, J.; Baron, G. V.; Denayer, J. F. M. A 3D-Printed Zeolitic Imidazolate Framework-8 Monolith For Flue- and Biogas Separations by Adsorption: Influence of Flow Distribution and Process Parameters. *Front. Chem. Eng.* 2020, 2 (November), 1–8. https://doi.org/10.3389/fceng.2020.589686.
- (67) Figueroa–Quintero, L.; Ramos–Fernández, E. V.; Narciso, J. 3D-Printed Brass Monoliths for ZIF-8 Synthesis and CO2 Conversion: A Novel Approach Using Selective Laser Melting. *J. Environ. Chem. Eng.* 2025, *13* (2). https://doi.org/10.1016/j.jece.2025.115453.

- (68) Fu, Q.; Wen, L.; Zhang, L.; Chen, X.; Pun, D.; Ahmed, A.; Yang, Y.; Zhang, H.
  Preparation of Ice-Templated MOF-Polymer Composite Monoliths and Their
  Application for Wastewater Treatment with High Capacity and Easy Recycling. ACS
  Appl. Mater. Interfaces 2017, 9 (39), 33979–33988.
  https://doi.org/10.1021/acsami.7b10872.
- (69) Herrmann, M.; Kempa, P. B.; Fietzek, H.; Altenburg, T.; Polyzoidis, A.; Piscopo, C. G.; Löbbecke, S. Characterization of Metal-Organic Frameworks Using X-Ray Diffraction. *Chemie-Ingenieur-Technik* 2016, 88 (7), 967–970. https://doi.org/10.1002/cite.201500123.
- (70) Alberoni, C.; Barroso-Martin, I.; Infantes-Molina, A.; Rodriguez-Castellon, E.; Talon,

- A.; Zhao, H.; You, S.; Vomiero, A.; Moretti, E. Ceria Doping Boosts Methylene Bine Article Online Photodegradation in Titania Nanostructures. *Mater. Chem. Front.* **2021**, *5* (11), 4138–4152. https://doi.org/10.1039/d1qm00068c.
- (71) Marazani, L. G.; Gascon-Perez, V.; Pathak, A.; Tricarico, M.; Tan, J. C.; Zaworotko, M. J.; Wheatley, A. E. H.; Makhubela, B. C. E.; Mehlana, G. Water Sorption Studies with Mesoporous Multivariate Monoliths Based on UiO-66. *Mater. Adv.* 2024, 5 (19), 7679–7689. https://doi.org/10.1039/d4ma00522h.
- (72) Rivera-Torrente, M.; Mandemaker, L. D. B.; Filez, M.; Delen, G.; Seoane, B.; Meirer, F.; Weckhuysen, B. M. Spectroscopy, Microscopy, Diffraction and Scattering of Archetypal MOFs: Formation, Metal Sites in Catalysis and Thin Films. *Chem. Soc. Rev.* 2020, 49 (18), 6694–6732. https://doi.org/10.1039/d0cs00635a.
- (73) Zhu, J.; Usov, P. M.; Xu, W.; Celis-Salazar, P. J.; Lin, S.; Kessinger, M. C.; Landaverde-Alvarado, C.; Cai, M.; May, A. M.; Slebodnick, C.; Zhu, D.; Senanayake, S. D.; Morris, A. J. A New Class of Metal-Cyclam-Based Zirconium Metal-Organic Frameworks for CO2 Adsorption and Chemical Fixation. *J. Am. Chem. Soc.* 2018, *140* (3), 993–1003. https://doi.org/10.1021/jacs.7b10643.
- (74) Zheng, Y.; Kasai, H.; Kobayashi, S.; Kawaguchi, S.; Nishibori, E. In Situ Observation of a Mechanically Induced Self-Sustaining Reaction for Synthesis of Silver. *Mater*.
  Adv. 2022, 4 (4), 1005–1010. https://doi.org/10.1039/d2ma00903j.
- (75) Nguyen, H. L. Reticular Design and Crystal Structure Determination of Covalent Organic Frameworks. *Chem. Sci.* 2021, 12 (25), 8632–8647.
  https://doi.org/10.1039/d1sc00738f.
- (76) Bourda, L.; Krishnaraj, C.; Van Der Voort, P.; Van Hecke, K. Conquering the Crystallinity Conundrum: Efforts to Increase Quality of Covalent Organic

View Article Online

DOI: 10.1039/D5MA01105A

Frameworks. *Mater. Adv.* **2021**, *2* (9), 2811–2845. https://doi.org/10.1039/d1ma00008j.

- (77) Odling, G.; Logan, H.; Chan, A.; Bissel, A. J.; Pulham, C. R.; Oliver, D. E. Large Scale Recyclable Monolithic Methyltrimethoxysilane Aerogels Formed by Self-Reinforcement. *Mater. Adv.* 2023, 4 (17), 3724–3732.
  https://doi.org/10.1039/d3ma00085k.
- (78) Khan, M.; Ali, F.; Ramzan, S.; AlOthman, Z. A. N-Phenyl Acrylamide-Incorporated Porous Silica-Bound Graphene Oxide Sheets with Excellent Removal Capacity for Cr(Iii) and Cr(vi) from Wastewater. *RSC Adv.* **2023**, *13* (24), 16047–16066. https://doi.org/10.1039/d3ra02568c.
- (79) Wang, Y.; Zhang, L.; Asoh, T. A.; Uyama, H. Hydrophobic and Hydrophilic Modification of Hierarchically Porous Monolithic Polyimide Derivatives as Functional Liquid Absorbers. *Mater. Adv.* 2021, 2 (11), 3560–3568. https://doi.org/10.1039/d1ma00185j.
- (80) Shekhar, S.; Chowdhury, C. Topological Data Analysis Enhanced Prediction of Hydrogen Storage in Metal-Organic Frameworks (MOFs). *Mater. Adv.* **2023**, *5* (2), 820–830. https://doi.org/10.1039/d3ma00591g.
- (81) Altintas, C.; Keskin, S. Role of Partial Charge Assignment Methods in High-Throughput Screening of MOF Adsorbents and Membranes for CO2/CH4 Separation. *Mol. Syst. Des. Eng.* **2020**, *5* (2), 532–543. https://doi.org/10.1039/c9me00163h.
- (82) Neville, G. M.; Jagpal, R.; Paul-Taylor, J.; Tian, M.; Burrows, A. D.; Bowen, C. R.; Mays, T. J. Freeze Casting of Porous Monolithic Composites for Hydrogen Storage.
  Mater. Adv. 2022, 414 (6861). https://doi.org/10.1039/d2ma00710j.

- (83) Toyao, T.; Liang, K.; Okada, K.; Ricco, R.; Styles, M. J.; Tokudome, Y.; Horiuchi<sup>Victo Article Online</sup> Hill, A. J.; Takahashi, M.; Matsuoka, M.; Falcaro, P. Positioning of the HKUST-1 Metal-Organic Framework (Cu3(BTC)2) through Conversion from Insoluble Cu-Based Precursors. *Inorg. Chem. Front.* 2015, 2 (5), 434–441. https://doi.org/10.1039/c4qi00215f.
- (84) Si, Y.; Li, X.; Yang, G.; Mie, X.; Ge, L. Fabrication of a Novel Core–Shell CQDs@ZIF-8 Composite with Enhanced Photocatalytic Activity. *J. Mater. Sci.* **2020**, 55 (27), 13049–13061. https://doi.org/10.1007/s10853-020-04909-8.
- (85) Madden, D. G.; Babu, R.; Çamur, C.; Rampal, N.; Silvestre-Albero, J.; Curtin, T.;
  Fairen-Jimenez, D. Monolithic Metal-Organic Frameworks for Carbon Dioxide
  Separation. Faraday Discuss. 2021, 231, 51–65. https://doi.org/10.1039/d1fd00017a.
- (86) Lovitt, J. I.; Gorai, T.; Cappello, E.; Delente, J. M.; Barwich, S. T.; Möbius, M. E.; Gunnlaugsson, T.; Hawes, C. S. Supramolecular Aggregation Properties of 4-(1-Morpholino)-1,8-Naphthalimide Based Fluorescent Materials. *Mater. Chem. Front.* 2021, 5 (8), 3458–3469. https://doi.org/10.1039/d1qm00091h.
- (87) Weber, S.; Schäfer, S.; Saccoccio, M.; Seidel, K.; Kohlmann, H.; Gläser, R.; Schunk, S. A. Mayenite-Based Electride C12A7e—: An Innovative Synthetic Methodviaplasma Arc Melting. *Mater. Chem. Front.* 2021, 5 (3), 1301–1314. https://doi.org/10.1039/d0qm00688b.
- (88) Noh, S.; Oh, H.; Kim, J.; Jung, S.; Shim, J. H. Cobalt-Copper-Embedded Nitrogen-Doped Carbon Nanostructures Derived from Zeolite Imidazolate Frameworks as Electrocatalysts for the Oxygen Reduction Reaction. *ACS Omega* **2024**, *9* (27), 29431–29441. https://doi.org/10.1021/acsomega.4c01667.
- (89) León-Alcaide, L.; López-Cabrelles, J.; Esteve-Rochina, M.; Ortí, E.; Calbo, J.;

- (90) Hou, J.; Sapnik, A. F.; Bennett, T. D. Metal-Organic Framework Gels and Monoliths. *Chemical Science*. Royal Society of Chemistry 2020, pp 310–323. https://doi.org/10.1039/c9sc04961d.
- (91) Furukawa, H.; Cordova, K. E.; O'Keeffe, M.; Yaghi, O. M. The Chemistry and Applications of Metal-Organic Frameworks. *Science (80-.).* **2013**, *341* (6149). https://doi.org/10.1126/science.1230444.

- (92) Thommes, M.; Kaneko, K.; Neimark, A. V.; Olivier, J. P.; Rodriguez-Reinoso, F.; Rouquerol, J.; Sing, K. S. W. Physisorption of Gases, with Special Reference to the Evaluation of Surface Area and Pore Size Distribution (IUPAC Technical Report). *Pure Appl. Chem.* 2015, 87 (9–10), 1051–1069. https://doi.org/10.1515/pac-2014-1117.
- (93) Wang, Z.; Liu, L.; Li, Z.; Goyal, N.; Du, T.; He, J.; Li, G. K. Shaping of Metal-Organic Frameworks: A Review. *Energy and Fuels* **2022**, *36* (6), 2927–2944. https://doi.org/10.1021/acs.energyfuels.1c03426.
- (94) Tricarico, M.; Besnard, C.; Cinque, G.; Korsunsky, A. M.; Tan, J. C. Stress–Strain
   Relationships and Yielding of Metal-Organic Framework Monoliths. *Commun. Mater.* 2023, 4 (1), 1–35. https://doi.org/10.1038/s43246-023-00412-0.
- (95) Bahr, D. F.; Reid, J. A.; Mook, W. M.; Bauer, C. A.; Stumpf, R.; Skulan, A. J.; Moody, N. R.; Simmons, B. A.; Shindel, M. M.; Allendorf, M. D. Mechanical Properties of Cubic Zinc Carboxylate IRMOF-1 Metal-Organic Framework Crystals.

- *Phys. Rev. B Condens. Matter Mater. Phys.* **2007**, *76* (18), 1–7.

  Niew Article Online DOI: 10.1039/D5MA01105A

  https://doi.org/10.1103/PhysRevB.76.184106.
- (96) Ning, X.; Wu, N.; Zhong, M.; Wen, Y.; Li, B.; Jiang, Y. Molecular Dynamics Simulation Analysis of Damage and Expansion Process of Nanoindentation Single-Crystal 3C-SiC Carbide Specimens at Different Temperature. *Nanomaterials* 2023, *13* (2), 235. https://doi.org/10.3390/nano13020235.
- (97) Tian, T.; Velazquez-Garcia, J.; Bennett, T. D.; Fairen-Jimenez, D. Mechanically and Chemically Robust ZIF-8 Monoliths with High Volumetric Adsorption Capacity. *J. Mater. Chem. A* **2015**, *3* (6), 2999–3005. https://doi.org/10.1039/c4ta05116e.
- (98) Tricarico, M.; Mollick, S.; Kachwal, V.; Sherman, D. A.; Tan, J. C. Exploring the Photophysical and Mechanical Behavior of Fluorescent Metal-Organic Framework Monoliths. *Chem. Mater.* 2024, 36 (17), 8247–8254. https://doi.org/10.1021/acs.chemmater.4c00963.
- (99) Le, Z.; Zhang, W.; Li, W.; Tan, J.; Li, R.; Wang, X.; Kaneti, Y. V.; Jiang, X.; Chu, J.; Yamauchi, Y.; Hu, M. Metal-Organic Powder Thermochemical Solid-Vapor Architectonics toward Gradient Hybrid Monolith with Combined Structure-Function Features. *Matter* **2020**, *3* (3), 879–891. https://doi.org/10.1016/j.matt.2020.07.002.
- (100) Tricarico, M.; Tan, J.-C. Nanostructure-Dependent Indentation Fracture Toughness of Metal-Organic Framework Monoliths. *Next Mater.* 2023, *1* (1), 100009. https://doi.org/10.1016/j.nxmate.2023.100009.
- (101) Duan, X.; Feng, L.; Wu, D.; Kong, Z.; Shi, D.; Zhang, L.; He, J. Tuning the Mechanical Properties of Sol-Gel Monolithic Metal-Organic Frameworks by Ligand Engineering. J. Colloid Interface Sci. 2024, 654, 1312–1319. https://doi.org/10.1016/j.jcis.2023.10.150.

- (102) McIntyre, S. R.; Saenz-Cavazos, P. A.; Hunter-Sellars, E.; Williams, D. R. Production Article Online (102) McIntyre, S. R.; Saenz-Cavazos, P. A.; Hunter-Sellars, E.; Williams, D. R. Production (102) McIntyre, S. R.; Saenz-Cavazos, P. A.; Hunter-Sellars, E.; Williams, D. R. Production (102) McIntyre, S. R.; Saenz-Cavazos, P. A.; Hunter-Sellars, E.; Williams, D. R. Production (102) McIntyre, S. R.; Saenz-Cavazos, P. A.; Hunter-Sellars, E.; Williams, D. R. Production (102) McIntyre, S. R.; Saenz-Cavazos, P. A.; Hunter-Sellars, E.; Williams, D. R. Production (102) McIntyre, S. R.; Saenz-Cavazos, P. A.; Hunter-Sellars, E.; Williams, D. R. Production (102) McIntyre, S. R.; Saenz-Cavazos, P. A.; Hunter-Sellars, E.; Williams, D. R. Production (102) McIntyre, S. R.; Saenz-Cavazos, P. A.; Hunter-Sellars, E.; Williams, D. R. Production (102) McIntyre, S. R.; Saenz-Cavazos, P. A.; Hunter-Sellars, E.; Williams, D. R. Production (102) McIntyre, S. R.; Saenz-Cavazos, P. A.; Hunter-Sellars, E.; Williams, D. R. Production (102) McIntyre, S. R.; Saenz-Cavazos, P. A.; McIntyre, S. R.; McInty Selectivity and Mass Transport in Levulinic Acid Transfer Hydrogenation by Monolithic MIL-100, MIL-88B and ZIF-8@Pd MOFs. Front. Chem. 2023, 10, 1–12. https://doi.org/10.3389/fchem.2022.1087939.
- (103) Mehta, J. P.; Tian, T.; Zeng, Z.; Divitini, G.; Connolly, B. M.; Midgley, P. A.; Tan, J. C.; Fairen-Jimenez, D.; Wheatley, A. E. H. Sol-Gel Synthesis of Robust Metal-Organic Frameworks for Nanoparticle Encapsulation. Adv. Funct. Mater. 2018, 28 (8), 1-7. https://doi.org/10.1002/adfm.201705588.
- (104) Song, G. Q.; Lu, Y. X.; Zhang, Q.; Wang, F.; Ma, X. K.; Huang, X. F.; Zhang, Z. H. Porous Cu-BTC Silica Monoliths as Efficient Heterogeneous Catalysts for the Selective Oxidation of Alkylbenzenes. RSC Adv. 2014, 4 (57), 30221–30224. https://doi.org/10.1039/c4ra04076g.
- (105) Ganesan, A.; Leisen, J.; Thyagarajan, R.; Sholl, D. S.; Nair, S. Product Selectivity and Mass Transport in Levulinic Acid Transfer Hydrogenation by Monolithic MIL-100, MIL-88B and ZIF-8@Pd MOFs. ACS Appl. Mater. Interfaces 2023, 15 (34), 40623-40632. https://doi.org/10.1021/acsami.3c08344.
- (106) Connolly, B. M.; Madden, D. G.; Wheatley, A. E. H.; Fairen-Jimenez, D. Shaping the Future of Fuel: Monolithic Metal-Organic Frameworks for High-Density Gas Storage. J. Am. Chem. Soc. 2020, 142 (19), 8541–8549, https://doi.org/10.1021/jacs.0c00270.
- (107) Hassan, M. H.; Haikal, R. R.; Hashem, T.; Rinck, J.; Koeniger, F.; Thissen, P.; Stefan Heißler, S.; Wöll, C.; Alkordi, M. H. Electrically Conductive, Monolithic Metal-Organic Framework-Graphene (MOF@G) Composite Coatings. ACS Appl. Mater. Interfaces 2019, 11 (6), 6442–6447. https://doi.org/10.1021/acsami.8b20951.
- (108) Heidarizadeh, F.; Jin, X.; Xu, Y. Significance of Copper Benzene 1,3,5-Tricarboxylate

- Metal Organic Framework: Environmental and Biomedical Applications. *Mater* View Article Online Chem. Horizons **2023**, *2* (2), 155–170.
- (109) Abubakar, A. J. A.; Canevesi, R. L. S.; Sanchez, D. A. L.; Grande, C. A. Monoliths for Gas Storage Manufactured with Precision Pore Engineering Using 3D-Printed Templates. *Chem. Eng. J.* 2024, 489 (January), 151450. https://doi.org/10.1016/j.cej.2024.151450.
- (110) Teffu, D. M.; Makgopa, K.; Somo, T. R.; Ratsoma, M. S.; Honey, S.; Makhado, E.; Modibane, K. D. Metal and Covalent Organic Frameworks (MOFs and COFs): A Comprehensive Overview of Their Synthesis, Characterization and Enhanced Supercapacitor Performance. *Coord. Chem. Rev.* 2025, *540* (January), 216798. https://doi.org/10.1016/j.ccr.2025.216798.
- (111) Parsazadeh, N.; Yousefi, F.; Ghaedi, M.; Dashtian, K.; Borousan, F. Preparation and Characterization of Monoliths HKUST-1 MOF: Via Straightforward Conversion of Cu(OH)2-Based Monoliths and Its Application for Wastewater Treatment: Artificial Neural Network and Central Composite Design Modeling. *New J. Chem.* 2018, 42 (12), 10327–10336. https://doi.org/10.1039/c8nj01067f.
- (112) Yao, P.; Liu, Y.; Tang, X.; Lu, S.; Li, Z.; Yao, Y. Green Chemical Engineering Synthesis of Reusable NH 2 -MIL-125 (Ti)@ Polymer Monolith as Ef Fi Cient Adsorbents for Dyes Wastewater Remediation Polyvinyl Alcohol. **2023**, *4* (May 2022), 439–447.
- (113) Yao, P.; Liu, Y.; Tang, X.; Lu, S.; Li, Z.; Yao, Y. Synthesis of Reusable NH2-MIL-125(Ti)@polymer Monolith as Efficient Adsorbents for Dyes Wastewater Remediation. *Green Chem. Eng.* **2023**, *4* (4), 439–447. https://doi.org/10.1016/j.gce.2022.06.004.

- (114) Liu, Q.; Li, S.; Yu, H.; Zeng, F.; Li, X.; Su, Z. Covalently Crosslinked Zirconium. View Article Online Based Metal-Organic Framework Aerogel Monolith with Ultralow-Density and Highly Efficient Pb(II) Removal. *J. Colloid Interface Sci.* **2020**, *561* (Ii), 211–219. https://doi.org/10.1016/j.jcis.2019.11.074.
- (115) Shaheed, N.; Javanshir, S.; Esmkhani, M.; Dekamin, M. G.; Naimi-Jamal, M. R. Synthesis of Nanocellulose Aerogels and Cu-BTC/Nanocellulose Aerogel Composites for Adsorption of Organic Dyes and Heavy Metal Ions. *Sci. Rep.* **2021**, *11* (1), 1–11. https://doi.org/10.1038/s41598-021-97861-9.
- (116) Jo, Y. K.; Jeong, S. Y.; Moon, Y. K.; Jo, Y. M.; Yoon, J. W.; Lee, J. H. Exclusive and Ultrasensitive Detection of Formaldehyde at Room Temperature Using a Flexible and Monolithic Chemiresistive Sensor. *Nat. Commun.* **2021**, *12* (1), 1–9. https://doi.org/10.1038/s41467-021-25290-3.

- (117) Li, Z.; Liu, J.; Feng, L.; Pan, Y.; Tang, J.; Li, H.; Cheng, G.; Li, Z.; Shi, J.; Xu, Y.; Liu, W. Monolithic MOF-Based Metal-Insulator-Metal Resonator for Filtering and Sensing. *Nano Lett.* **2023**, *23* (2), 637–644. https://doi.org/10.1021/acs.nanolett.2c04428.
- (118) Qin, Z. S.; Dong, W. W.; Zhao, J.; Wu, Y. P.; Zhang, Q.; Li, D. S. A Water-Stable Tb(III)-Based Metal-Organic Gel (MOG) for Detection of Antibiotics and Explosives. *Inorg. Chem. Front.* **2018**, *5* (1), 120–126. https://doi.org/10.1039/c7qi00495h.
- (119) Zhao, D.; Wang, Y.; Shao, J.; Zhang, P.; Chen, Y.; Fu, Z.; Wang, S.; Zhao, W.; Zhou, Z.; Yuan, Y.; Fu, D.; Zhu, Y. Temperature and Humidity Sensor Based on MEMS Technology. AIP Adv. 2021, 11 (8). https://doi.org/10.1063/5.0053342.
- (120) González-Gómez, M.; Martínez Medina, E.; Kovač, J.; Casals, O.; Martínez López,M.; Xuriguera-Martín, E.; Fàbrega, C. A Low-Cost Colorimetric HKUST-1 Sensor for

- Ppm-Level Humidity Detection. *Sensors Actuators B Chem.* **2025**, *441* (February) View Article Online https://doi.org/10.1016/j.snb.2025.137973.
- (121) Wu, K.; Fei, T.; Zhang, T. Humidity Sensors Based on Metal Organic Frameworks. **2022**.
- (122) Pandya, I.; El Seoud, O. A.; Assiri, M. A.; Kumar Kailasa, S.; Malek, N. I. Ionic Liquid/ Metal Organic Framework Composites as a New Class of Materials for CO2 Capture: Present Scenario and Future Perspective. *J. Mol. Liq.* 2024, 395, 123907. https://doi.org/https://doi.org/10.1016/j.molliq.2023.123907.
- (123) Han, Y.; Wang, S.; Liu, Y.; Bai, L.; Yan, H.; Liu, H. Preparation of Poly(Ionic Liquid@MOF) Composite Monolithic Column and Its Application in the Online Enrichment and Purification of Tectochrysin in Medicinal Plants. *Anal. Methods* 2022, 14 (4), 401–409. https://doi.org/10.1039/D1AY01954F.
- (124) Khosroshahi, N.; Bakhtian, M.; Asadi, A.; Safarifard, V. Revolutionizing Energy Storage: The Emergence of MOF/MXene Composites as Promising Supercapacitors.

  Nano Express 2023, 4. https://doi.org/10.1088/2632-959X/ad0446.
- (125) Mu, F.; Zhao, J.; Rong, Q.; Gu, C.; Zhao, Q. Co / Ni-MOF @ MXene Electrode Material for High-Performance Supercapacitor. **2025**, 117–124.
- (126) He, C.; Yin, W.; Li, X.; Zheng, J.; Tang, B.; Rui, Y. Molybdenum Disulfide Synthesized by Molybdenum-Based Metal Organic Framework with High Activity for Sodium Ion Battery. *Electrochim. Acta* 2021, 365, 137353. https://doi.org/10.1016/j.electacta.2020.137353.
- (127) Dourandish, Z.; Sheikhshoaie, I.; Maghsoudi, S. Molybdenum Disulfide/Nickel-Metal Organic Framework Hybrid Nanosheets Based Disposable Electrochemical Sensor for

- Determination of 4-Aminophenol in Presence of Acetaminophen. *Biosensors*, 2023, Sind Online (5), 524. https://doi.org/10.3390/bios13050524.
- (128) Bogdanova, E.; Liu, M.; Hodapp, P.; Borbora, A.; Wenzel, W.; Bräse, S.; Jung, A.; Dong, Z.; Levkin, P. A.; Manna, U.; Hashem, T.; Wöll, C. Functionalization of Monolithic MOF Thin Films with Hydrocarbon Chains to Achieve Superhydrophobic Surfaces with Tunable Water Adhesion Strength. *Mater. Horizons* 2024, *12* (4), 1274–1281. https://doi.org/10.1039/d4mh00899e.
- (129) Xu, J.; Sun, Z.; Li, F.; An, Q.; Bao, Y.; Han, D.; Niu, L. Nitrogen-Doped Porous Carbon Derived from Zeolitic Imidazolate Framework-67 Strung into Necklace with Carbon Nanotubes for the Detection of Calcium at Ultralow Level. *J. Electrochem.*Soc. 2020, 167. https://doi.org/10.1149/1945-7111/ab91cb.

- (130) Peng, B.; Feng, C.; Liu, S.; Zhang, R. Synthesis of CuO Catalyst Derived from HKUST-1 Temple for the Low-Temperature NH 3 -SCR Process. *Catal. Today* **2017**, *314*. https://doi.org/10.1016/j.cattod.2017.10.044.
- (131) Zhu, M.; Yang, Y.; Zhang, X.; Liang, Y.; Tang, J. Cobalt-Based Zeolitic Imidazole Framework Derived Hollow Co<sub>3</sub>S<sub>4</sub> Nanopolyhedrons for Supercapacitors. *Appl. Organomet. Chem. TA TT 2024*, *38* (8). https://doi.org/10.1002/aoc.7533 LK https://UnivofPretoria.on.worldcat.org/oclc/10581926218.
- (132) Zhang, Y.; Wang, R. Metal–Organic Framework (MOF)-Derived Metal Oxides for Selective Catalytic Reduction (SCR) of NOx. *Molecules* 2025, 30 (13), 2836. https://doi.org/10.3390/molecules30132836.
- (133) Tian, T.; Xu, J.; Abdolazizi, A.; Ji, C.; Hou, J.; Riley, D. J.; Yan, C.; Ryan, M. P.; Xie, F.; Petit, C. A Monolithic Gold Nanoparticle@metal-Organic Framework Composite as CO2 Photoreduction Catalyst. *Mater. Today Nano* **2023**, *21*.

View Article Online

DOI: 10.1039/D5MA01105A

https://doi.org/10.1016/j.mtnano.2022.100293.

- (134) Avila, E.; Salway, H.; Ruggeri, E.; Çamur, C.; Rampal, N.; Doherty, T. A. S.; Moseley, O. D. I.; Stranks, S. D.; Fairen-Jimenez, D.; Anaya, M. Better Together: Monolithic Halide Perovskite@metal-Organic Framework Composites. *Matter* 2024, 4319–4331. https://doi.org/10.1016/j.matt.2024.08.022.
- (135) Ntouros, V.; Kousis, I.; Papadaki, D.; Pisello, A. L.; Assimakopoulos, M. N. Life Cycle Assessment on Different Synthetic Routes of Zif-8 Nanomaterials. *Energies* 2021, 14 (16), 1–22. https://doi.org/10.3390/en14164998.
- (136) Escobar-Hernandez, H. U.; Shen, R.; Papadaki, M. I.; Powell, J. A.; Zhou, H.-C.; Wang, Q. Hazard Evaluation of Metal–Organic Framework Synthesis and Scale-up: A Laboratory Safety Perspective. ACS Chem. Heal. Saf. 2021, 28 (5), 358–368. https://doi.org/10.1021/acs.chas.1c00044.
- (137) Marrett, J. M.; Effaty, F.; Ottenwaelder, X.; Friščić, T. Mechanochemistry for Metal–Organic Frameworks and Covalent–Organic Frameworks (MOFs, COFs): Methods, Materials, and Mechanisms. *Adv. Mater.* 2025, 2418707.
  https://doi.org/10.1002/adma.202418707.
- (138) Al-Ghazzawi, F.; Conte, L.; Potts, M. W.; Richardson, C.; Wagner, P. Reactive Extrusion Printing of Zeolitic Imidazolate Framework Films. *ACS Appl. Mater. Interfaces* **2024**, *16* (33), 44270–44277. https://doi.org/10.1021/acsami.4c08609.
- (139) Sakai, M.; Hori, H.; Matsumoto, T.; Matsukata, M. One-Pot Synthesis Method of MIL-96 Monolith and Its CO2 Adsorption Performance. ACS Appl. Mater. Interfaces 2023, 15 (18), 22395–22402. https://doi.org/10.1021/acsami.2c22955.
- (140) Chen, Y.; Zhang, S.; Cao, S.; Li, S.; Chen, F.; Yuan, S.; Xu, C.; Zhou, J.; Feng, X.;

- Ma, X.; Wang, B. Roll-to-Roll Production of Metal-Organic Framework Coatings for Article Online Particulate Matter Removal. *Adv. Mater.* **2017**, *29* (15), 4–9. https://doi.org/10.1002/adma.201606221.
- (141) Li, Y.; Chen, S.; Cai, X.; Hong, J.; Wu, X.; Xu, Y.; Zou, J.; Chen, B. H. Rational Design and Preparation of Hierarchical Monoliths through 3D Printing for Syngas Methanation. *J. Mater. Chem. A* 2018, 6 (14), 5695–5702.
  https://doi.org/10.1039/c8ta01597j.
- (142) Hunter-Sellars, E.; Saenz-Cavazos, P. A.; Houghton, A. R.; McIntyre, S. R.; Parkin, I.
  P.; Williams, D. R. Sol-Gel Synthesis of High-Density Zeolitic Imidazolate
  Framework Monoliths via Ligand Assisted Methods: Exceptional Porosity,
  Hydrophobicity, and Applications in Vapor Adsorption. *Adv. Funct. Mater.* 2021, *31*(5). https://doi.org/10.1002/adfm.202008357.

## **Data Availability Statement**

View Article Online DOI: 10.1039/D5MA01105A

No primary research results, software or code have been included and no new data were generated or analysed as part of this review.